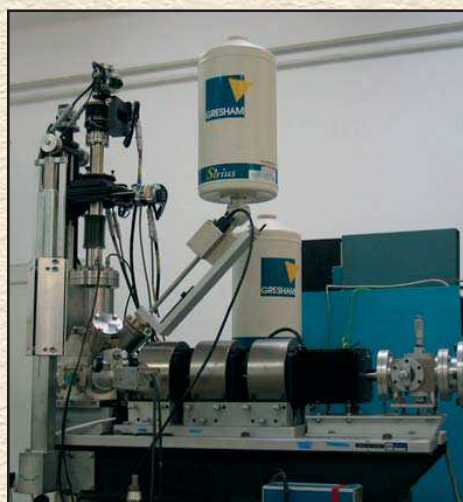


# ATOMKI

## ANNUAL REPORT

### 2008



INSTITUTE OF NUCLEAR RESEARCH  
OF THE HUNGARIAN ACADEMY OF SCIENCES  
DEBRECEN, HUNGARY

INSTITUTE OF NUCLEAR RESEARCH  
OF THE HUNGARIAN ACADEMY OF SCIENCES  
DEBRECEN, HUNGARY

ANNUAL REPORT  
2008



ATOMKI

*Postal address:*

P.O. Box 51  
H-4001 Debrecen,  
Hungary

*Editors:*

I. Rajta  
E. Leiter

HU ISSN0 0231-3596

## Preface

For the community of our institute, 2008 was a time of changes both inside and outside.

Professor Rezső G. Lovas decided to finish his term as a director of Atomki by the end of 2007. During his eleven-year-period as a director, he worked for our Institute and its scientific excellence very efficiently. From now, he focuses on his research work and the affairs of the Hungarian Academy of Sciences. On behalf of Atomki, I would like to thank him the continuous care and efforts during the last decade, and wish him a similarly fruitful future work in the Institute and at the Academy.

I was appointed by the General Secretary of the Hungarian Academy of Sciences (HAS) from January 1st to serve Atomki as its director for three years. From July 1st, a new term started for the section and division heads and the vice directors, too. The names can be found in the organization diagram of the present annual report.

The Hungarian Academy of Sciences elected a new President, József Pálinkás in May. He is a physicist, Professor of the University of Debrecen, and a former director of Atomki. He is active in organizing and promoting science; successfully accelerated the discussion of the modernization of the Law about the Hungarian Academy of Sciences. The Law has already been accepted by the Hungarian Parliament.

2008 proved to be an active year, with remarkable successes. We are very proud, that György Gyürky is one of the awardees of the ERC (European Research Council) Starting Grant scheme. The subject of his project is the experimental study of the astrophysical p-process in Debrecen. This very prestigious grant also started in 2008. Béla Sulik has been elected as Fellow of the American Physical Society, based on “his significant contributions, both theoretical and experimental, to the fundamental understanding of atomic and molecular collisions”.

In the spirit of forming an efficient European Research Area with active regional initiatives, Atomki and the Research Institute for Particle Nuclear Physics (RMKI, Budapest) established an open consortium (Hungarian Ion-beam Physics Platform, HIPP) for operating and developing the ion beam physics resources of the stakeholders as a unified distributed facility of common strategy and coordinated user access. Both Atomki and RMKI are legal entities belonging to the network of research institutions of HAS. I note here that the special report, included in the present volume covers the activity of our Laboratory of Ion Beam Applications.

Atomki made a wide range of contribution to the activity for the Debrecen bid hosting of the European Spallation Neutron Source (ESS). As a potential host institution in the starting phase of the project, we worked on preliminary plans for this phase. Committees, experts and advisory board members visited us for discussing the conditions and possible scenarios. The ESS project involves an enormous scientific and technological potential for the Debrecen region.

It was a rich year of conferences organized or co-organized by our institute. The list is a part of the present volume and contains 11 items. I mention only three of them here, the RADAM 2008 Conference (Radiation Damage in Biomolecular Systems, 13th - 15th June 2008, Debrecen), the ICNMTA 2008 Conference (11th International Conference on Nuclear Microprobe Technology and Applications, 20-25 July 2008, Debrecen), and, last but not least, the double event on November 26-27, namely the Special Meeting of the Section of Physical Sciences of the Hungarian Academy of Sciences for celebrating Dénes Berényi, the founder of the Laboratory of Atomic Collision Physics in Debrecen at his 80th birthday, together with the School of Applications of Synchrotrons and Free-Electron Lasers.

We continued our outreach activities in 2008 as well: in collaboration with a local radio station FRISS we published a CD including about forty interviews with Atomki scientists presenting their research topics. This is a compilation of a regular Sunday Science Show aired by the radio. This year, we also started our activity in the European Researchers' Night movement, with a talk on physics and music, followed by a concert of Atomki researchers.

Further details of Atomki events, and the back issues of the Annual reports can be found on our homepage: [www.atomki.hu](http://www.atomki.hu)

Debrecen, 15 April 2008

Zs. Fülöp  
Director

# Organizational structure of ATOMKI

Director: Zs. Fülöp, D.Sc.  
Deputy directors: B. Sulik, D.Sc.  
J. Molnár, C.Eng.  
Finance director: Dr. M. Pálinkás

---

- Secretariat (Scientific Secretary: Z. Máté, C.Sc.)
  - Library (Librarian: Mrs. M. Nagy)
  - Accounting (Head: Mrs. G. Adriányné Fábián)
  - Basic Services and Maintenance (Head: Mr. I. Katona)
  - Mechanical Workshop (Head: Mr. I. Gál)
- 

## Scientific Sections

### Division of Nuclear Physics (Head: A. Krasznahorkay, D.Sc.)

- Section of Experimental Nuclear Physics (Head: J. Timár, C.Sc.)
  - Section of Electrostatic Accelerators (Head: I. Rajta, Ph.D.)
    - Nuclear Astrophysics Group
    - Laboratory of Ion Beam Applications
  - Section of Theoretical Physics (Head: A. Kruppa, D.Sc.)
- 

### Division of Atomic Physics (Head: L. Sarkadi, D.Sc.)

- Section of Atomic Collisions (Head: L. Gulyás, D.Sc.)
    - ECR Laboratory
  - Section of Electron Spectroscopy (Head: L. Kövér, Ph.D.)
    - Laboratory of Secondary Ion/Neutral Mass Spectrometry
- 

### Division of Applied Physics (Head: S. Mészáros, C.Sc.)

- Section of Environmental and Earth Sciences (Head: É. Svingor, Ph.D.)
    - Hertelendi Laboratory of Environmental Studies
    - Radon Group
    - K-Ar Laboratory
    - Radiation- and Environmental Protection Group
    - QMS Laboratory
  - DE TTK - ATOMKI Department of Environmental Physics (Head: S. Sudár, C.Sc.)
  - Cyclotron Section (Head: F. Ditrói, Ph.D.)
  - Section of Electronics (Head: J. Gál, C.Sc.)
-

## Data on ATOMKI

At present the Institute employs 193 persons. The affiliation of personnel to units of organization and the composition of personnel are given below.

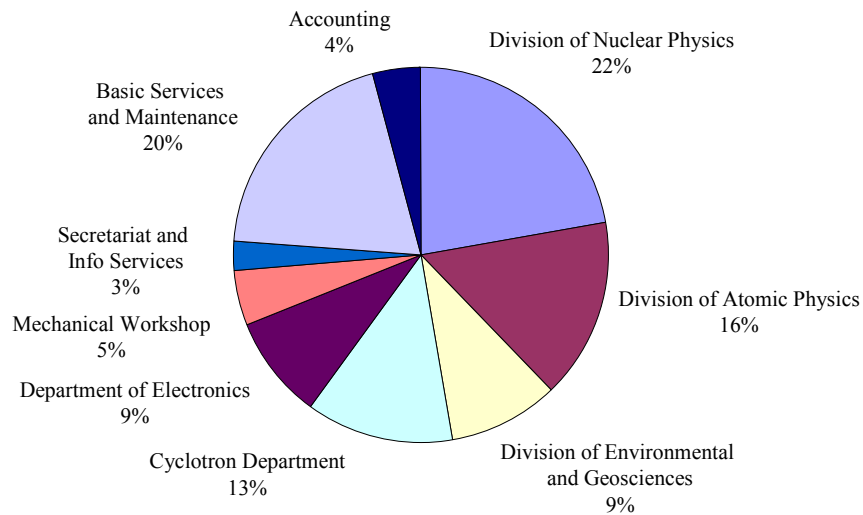


**Figure 1.** Affiliation of personnel to units of organization

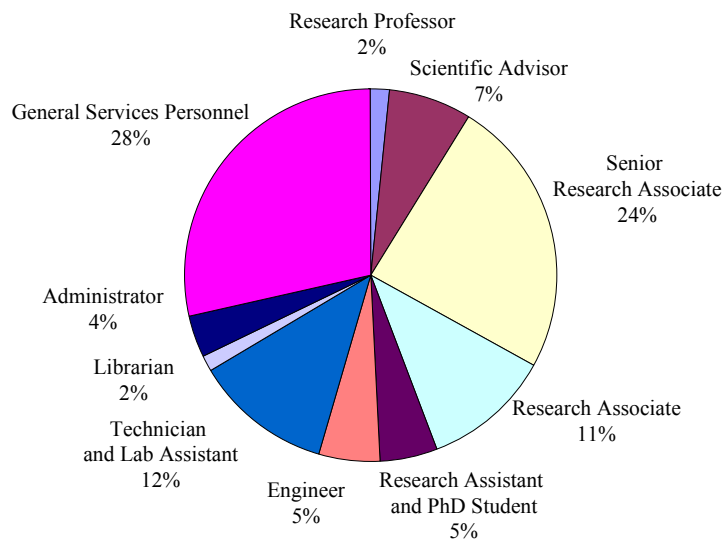


**Figure 2.** Composition of personnel

## **International connections**

Multilateral international programs: 15

Cooperations based on S&T (TéT) bilateral intergovernmental agreements: 14

Cooperations based on HAS bilateral agreements: 21

Cooperations based on specific collaboration agreements between institutes:

- in nuclear physics and applications with 22 countries in 38 topics
- in atomic physics and applications with 15 countries in 32 topics
- in detection and signal processing technique with 5 countries in 6 topics
- in ion beam analysis with 3 countries in 4 topics
- in environmental research and dating with 13 countries in 17 topics

Membership in international scientific committees: 25

## **Running research projects, grants**

European Research Council (ERC) Starting Grant: 1

Other EU (FP6 and FP7) projects: 5

European Organization for Nuclear Research (CERN) projects: 2

International Atomic Energy Agency (IAEA) projects: 3

Intercomparison programs and exercises: 5

(ESIR, VIRI, EURATOM, TRI-TOFFY, TRIC2008-IAEA)

Hungarian National Research Foundation (OTKA) projects: 21

National Office for Research and Technology (NKTH) projects: 17

Hungarian Science and Technology Foundation (TéT) projects: 14

## **Higher education activity**

Number of researchers teaching at universities: 34

Number of researchers teaching in doctoral (PhD) schools: 19

Gradual and postgradual teaching: 49 courses, 1021 hours

Number of undergraduate students participating in research work  
(organized by the Student's Science Association, TDK): 6

Number of students making diploma work: 15

Number of PhD students: 11

Supervision activity by Atomki researchers: 2126 hours

## Finance

The total budget of the Institute for the year 2008 was 1424 million Hungarian Forints. The composition of the budget and the share of personnel expenditure within the budget are shown below.

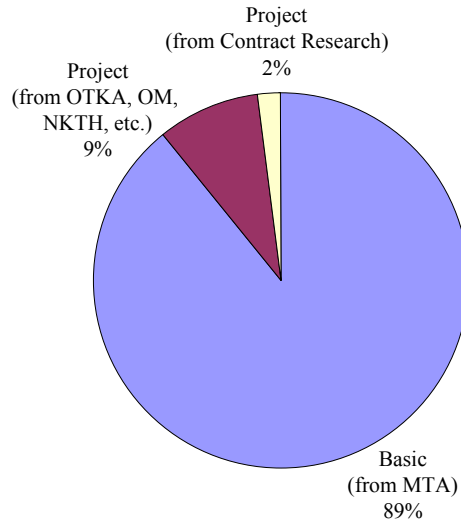


**Figure 3.** Composition of the budget of the Institute  
*MTA: Hungarian Academy of Sciences*  
*OTKA: Hungarian Scientific Research Fund*  
*OM: Ministry of Education*  
*NKTH: National Office for Research and Technology*

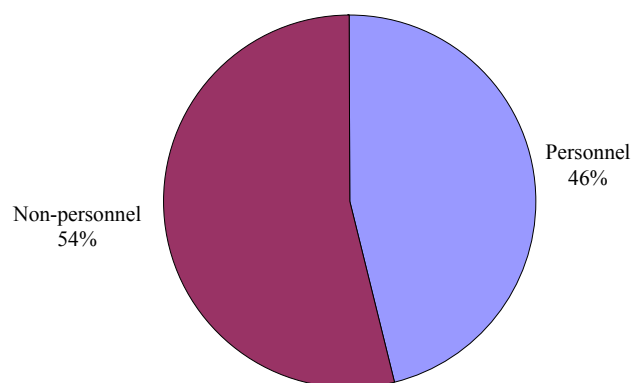


**Figure 4.** Breakdown of expenditure into personnel and non-personnel expenditures

# Table of contents

Preface . . . . .	i
Organizational structure of ATOMKI . . . . .	ii
Data on ATOMKI . . . . .	iii
International connections . . . . .	iv
Running research projects, grants. . . . .	iv
Higher education activity . . . . .	iv
Finance . . . . .	v
Table of contents . . . . .	vi

## Featured:

Laboratory of Ion Beam Applications at ATOMKI . . . . .	1
---	---

## 1. General Physics

1.1 On the $\mathcal{PT}$ -symmetric Rosen–Morse II potential . . . . .	15
1.2 Bound and scattering states of the $\mathcal{PT}$ -symmetric Coulomb potential problem . . . . .	16

## 2. Sub Atomic Physics

2.1 European Research Council supports an extensive study of the astrophysical p-process . . . . .	17
2.2 Coulomb suppression of the stellar enhancement factor . . . . .	18
2.3 Inelastic scattering studies of $^{16}\text{C}$ reexamined . . . . .	19
2.4 Observation of excited states in $^{17}\text{C}$ and $^{19}\text{C}$ . . . . .	20
2.5 In-beam $\gamma$ -ray spectroscopy of the neutron-rich $^{20,22}\text{N}$ . . . . .	21
2.6 Radioactive decay of $^{74}\text{As}$ embedded into different environments . . . . .	22
2.7 Total Absorption Spectroscopy study of the $^{152}\text{Yb}$ decay . . . . .	23
2.8 Search for Collinear Cluster Tripartition at low excitation energy of heavy nuclei . . . . .	24
2.9 Shell correction with finite-range smoothing . . . . .	25

## 3. Atomic and Molecular Physics

3.1 Interaction of intense ultrashort laser pulses with positronium . . . . .	26
3.2 Over-the-barrier ionization of $\text{H}_2\text{O}$ by intense ultrashort laser pulses . . . . .	27
3.3 Limitations of the strong field approximation in ionization of the hydrogen atom by ultrashort pulses . . . . .	28
3.4 Atomic ionization by a sudden momentum transfer . . . . .	29
3.5 Ionization of helium and argon by very slow antiproton impact . . . . .	30
3.6 On the double ionization of helium by very slow antiproton impact . . . . .	31
3.7 (e,2e) study of resonant Auger decay . . . . .	32
3.8 Selective enhancement of $1s2s2p\ ^4\text{P}_J$ metastable states populated by cascades in single-electron transfer collisions of $\text{F}^{7+}(1s^2/1s2s\ ^3\text{S})$ ions with He and $\text{H}_2$ targets . . . . .	33
3.9 Plasma diagnostics by X-ray crystal spectroscopy . . . . .	34
3.10 Study of the role of post-collision interaction and two-center effects in the formation of the two-electron cusp . . . . .	35
3.11 Electronic structure of nanocrystalline $\text{TiO}_2$ particles . . . . .	36

3.12	Comparative study of fragmentation of $H_2S$ and $H_2O$ molecules following slow ion-molecule collisions . . . . .	37
3.13	Ion guiding in alumina capillaries: MCP images of the transmitted ions . . . . .	39
<b>4. Condensed Matter</b>		
4.1	Magnetic particle hyperthermia: Néel relaxation in magnetic nanoparticles under circularly polarized field . . . . .	41
<b>5. Materials Science and Analysis</b>		
5.1	Transmission of 4.5 keV $Ar^{9+}$ ions through a single glass macrocapillary . . . . .	42
5.2	Production of a microbeam of slow highly charged ions with a single microscopic glass capillary . . . . .	43
5.3	Guiding of electrons through a single glass macrocapillary . . . . .	44
5.4	Investigation of electron spectra backscattered from polyethylene-terephthalate . . . . .	45
5.5	Energy dependence of ion guiding through nanocapillaries . . . . .	46
5.6	Simulation of streaking experiments at surfaces . . . . .	47
5.7	Application of SNMS in the investigation of doped perovskites . . . . .	48
5.8	Investigation of thermal stability of hydrogenated amorphous Si/Ge multilayers . . . . .	49
5.9	Investigations of failure mechanisms at Ta and TaO diffusion barriers by SNMS . . . . .	50
<b>6. Earth and Cosmic Sciences, Environmental Research</b>		
6.1	Improving argon, krypton and xenon measurements for environmental water samples . . . . .	51
6.2	Palaeoclimate reconstruction in the southern part of the Great Hungarian Plain based on noble gases and radiocarbon of groundwater samples . . . . .	52
6.3	Investigation of impact materials around Barringer Meteor Crater by SEM-EDX and micro-PIXE techniques . . . . .	53
6.4	Ion-beam analysis of a medieval glass bottle excavated in Győr . . . . .	54
6.5	Ion micro-beam analysis of single aerosol particles originating from Saharan dust episodes observed in Debrecen, Hungary . . . . .	56
6.6	Atmospheric aerosol particle analysis at the Debrecen Nuclear Microprobe . . . . .	57
<b>7. Biological and Medical Research</b>		
7.1	Desorption and catalytic study of vanadium modified MCM-41 silica by $^{11}C$ radiolabeled methanol . . . . .	58
7.2	X-ray Powder Diffraction and FTIR studies on Entacapone polymorphs . . . . .	59
7.3	Investigation of fish otoliths by combined ion beam analysis . . . . .	60
<b>8. Developments of Methods and Instruments</b>		
8.1	Status Report on Cyclotron Operation . . . . .	61
8.2	Activities at the Van de Graaff Accelerator Laboratory . . . . .	62
8.3	Activities in the Electron Cyclotron Resonance (ECR) Laboratory . . . . .	63

8.4	New results from the improved $^{14}\text{C}$ AMS graphite target line in ATOMKI . . . . .	64
8.5	Development of an atmospheric fossil fuel $\text{CO}_2$ monitoring station . . . . .	65
8.6	Testing automatic groundwater sampling unit by the help of isotope analytical and dissolved ion investigations . . . . .	66
8.7	PDMS patterning by proton beam . . . . .	67
8.8	First Experiments on a Microreactor Created by Proton Microbeam . . . . .	68
8.9	Si Micro-turbine by Proton Beam Writing and Porous Silicon Micromachining . . . . .	69
8.10	Analog and digital pulse shape discrimination of planar CdTe detector signals . . . . .	70
8.11	From the crystal structure to the light emission properties of GSO and LSO scintillators	71
8.12	A new generation of PET scanners for small animal studies . . . . .	72
8.13	A little sonochemistry again . . . . .	73
<b>9.</b>	<b>Conferences organized by HAS-ATOMKI</b>	
9.1	International conference on radiation damage in biomolecular systems . . . . .	74
9.2	International conference on elementary processes in atomic systems . . . . .	75
9.3	Organization of ICNMTA2008 . . . . .	76
9.4	Report on the 4th Conference on Environmental Science of the Carpathian Basin . . . . .	77
<b>10.</b>	<b>Appendix</b>	
10.1	Events . . . . .	78
10.2	Hebdomadal Seminars . . . . .	79
10.3	Awards . . . . .	81
10.4	List of Publications . . . . .	82
	Author index . . . . .	83

# Laboratory of Ion Beam Applications at ATOMKI

*I. Borbély-Kiss, R. Huszánk, Zs. Kertész, Á.Z. Kiss, E. Koltay, I. Rajta,  
A. Simon, Gy. Szabó, Z. Szikszai, S.Z. Szilasi, Z. Szoboszlai, I. Uzonyi*

## 1. Introduction

The Laboratory of Ion Beam Applications of ATOMKI is devoted to applications of atomic and nuclear physics in the fields of environmental research, biomedicine, geology, materials & surface science (including ion beam induced damage investigations and proton beam lithography) and cultural heritage research. We perform our work in the frame of various projects and collaborations: EU, IAEA, R&D, OTKA, etc. Our laboratory provides service for external (national and international) and internal users and contributes to higher education, as well.

The Laboratory is based on the home-made 5 MV Van de Graaff (VdG) electrostatic accelerator of the institute. The accelerator was put into operation in 1971 and in the beginning it supplied ion beams exclusively for nuclear physics.

A few years later with the measurements of K-shell ionization cross sections the door became open also for basic atomic physics. In parallel with this basic study, the application of proton induced X-ray emission (PIXE) for the elemental analysis of biological (hair, erythrocyte and blood plasma) samples and atmospheric aerosols also started. The first paper on PIXE, a methodological one, was published in 1978 [1]. The experience gained on these applications [2] and later on archaeology [3] led to the construction of complex PIXE chambers [4], which were sold, together with the corresponding know-how, to institutions in China, Portugal, Bangladesh, Jordan, North Korea, Singapore, Cuba and Mexico through the International Atomic Energy Agency (IAEA). For the evaluation of PIXE spectra the laboratory has been continuously developing its own computer programme package. The first version of this continuous development was published in 1988 [5]. In the meantime a second IBA analysis method, the proton induced gamma ray emission (PIGE), was introduced in the laboratory [6] and was applied simultaneously with PIXE. Application of deuteron induced gamma ray emission (DIGE) started more than a decade later [7,8].

A significant improvement of the IBA service was the installation of an Oxford Microbeams Ltd. type Scanning Nuclear Microprobe (SNM) facility in a minimal configuration with magnetic doublet lenses in 1994 [9]. The new facility widened the possibilities of new applications in geology [10], biology [11], archaeometry [12], materials science [13] and aerosol study [14], moreover, it made possible to introduce completely new fields like proton beam lithography [15] and Ion Beam Induced Charge studies [16].

The research infrastructure of the laboratory was upgraded in the framework of the EU co-funded Economic Competitiveness Operative Programme (GVOP-3.2.1.-2004-04-0402/3.0) in 2006, including oil-free vacuum system, vacuum coating system, nuclear electronics, X-ray detectors, optical microscope and a quadrupole magnet lens.

## 2. Beamlines

Three beamlines of the 5MeV VdG accelerator are dedicated to ion beam applications. On the *left*  $45^\circ$  *beamline* a macro-PIXE chamber is installed. It is predominantly used for elemental characterization of atmospheric aerosol samples, and more recently, irradiations of various polymers for radiation chemistry studies. Macro-PIGE, DIGE and NRA investigations are made on the *right*  $30^\circ$  *beamline*. The schematic layout of the laboratory is shown in Fig. 1.

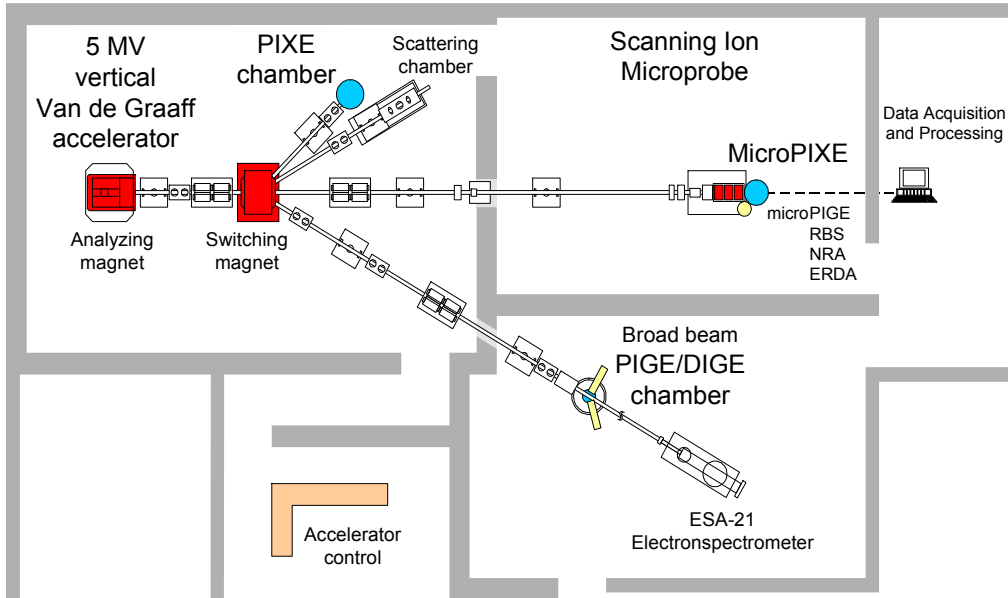


Figure 1. Schematic diagram of the Laboratory of Ion Beam Applications (IBA Lab)

On the  $0^\circ$  *beamline*, an Oxford type scanning nuclear microprobe is operated. The beam diameter is about 1-2  $\mu\text{m}$  at high beam current mode (100-1000 pA) and 700 nm at low beam current mode ( $<1$  pA beam intensity). The microprobe is equipped with a 5-axis goniometer (X-Y-Z translations and two rotations), optical microscope, cameras and several radiation and particle detectors. The available analytical techniques are PIXE, Rutherford backscattering spectrometry (RBS), nuclear reaction analysis (NRA), proton/deuteron induced  $\gamma$ -ray emission (PIGE/DIGE), elastic recoil detection analysis (ERDA) and scanning transmission ion microscopy (STIM). The detectable elements cover the whole H-U range. Besides the quantitative elemental composition and distributions, areal density and depth profile can also be determined on microscopic scale by using these analytical techniques. Proton Beam Writing (PBW) and ion beam induced charge (IBIC) studies are also carried out on the microprobe.

## 3. Development of ion beam methods and experimental setups

In the 15-year-old history of the Debrecen scanning nuclear microprobe facility significant developments were achieved in the field of analytical methods and data acquisition and data evaluation systems.

Application and development of IBA techniques belong to the main activities of the research group. The first significant achievement in this field was the elaboration of a fundamental parameter method and a *spectrum evaluation software* (PIXEKLM program package [17]) for standard-less (macro)PIXE analysis.

After the installation of the microprobe a *special micro-PIXE set-up* was mounted, which consists of a super ultra thin windowed (SUTW) and a Be windowed Si(Li) X-ray detector for the simultaneous detection of low energy X-rays from elements down to boron and high energy X-rays of the heavy elements [18]. For the first time, quantitative PIXE analysis became available for the light elements down to B [19]. Analytical applications motivated the further developments of the micro-PIXE technique towards the direction of true elemental mapping. The newly developed PIXEKLM-TPI program [20] allows:

- quantification of elements from B to U by K, L, and M lines;
- production of conventional intensity, concentration and STIM maps;
- simultaneous evaluation of major, minor and trace elements.



**Figure 2.** Oxford Microbeams Ltd. type Scanning Nuclear Microprobe facility

In *deuteron induced gamma ray spectrometry*, quantification is usually performed with standards or can be approximately achieved by tabulated absolute thick target yields with 15 and 25% accuracy. In order to increase analytical performance, we developed a new DIGE method which is based on the application of fundamental physical parameters such as cross-sections data for deuteron induced gamma ray emission, as well as on some standard reference materials. When this work was started, cross-sections data were not available in the literature. Therefore, we started a systematic investigation and determined them experimentally from thin target gamma ray yields for Li, Be, B, O and F in the 0.6–2 MeV energy range based on the  ${}^6\text{Li}(d,p\gamma){}^7\text{Li}$ ,  ${}^9\text{Be}(d,n\gamma){}^{10}\text{B}$ ,  ${}^{11}\text{B}(d,p\gamma){}^{12}\text{B}$ ,  ${}^{16}\text{O}(d,p\gamma){}^{17}\text{O}$  and  ${}^{19}\text{F}(d,p\gamma){}^{20}\text{F}$  nuclear reactions. Our results are published in NIM [21] as well as in the IAEA database.

An analytical technique with a special experimental setup was developed for the *analysis of boron* using the  ${}^{11}\text{B}(p,\alpha){}^8\text{Be}$  nuclear reaction with a proton bombardment of 675 keV [22]. The achievable limit of detection is unsurpassed ( $5 \mu\text{g/g}$ ). This technique is particularly useful in geological/geochemical studies.

*Micro-RBS and micro-ERDA analysis* can be performed simultaneously with micro-PIXE measurements on the nuclear microprobe. Three ORTEC-type surface barrier silicon detectors ( $50 \text{ mm}^2$  sensitive area and 18 keV system energy resolution) are used for micro-ERDA and micro-RBS experiments simultaneously. The ERDA detector is placed at a recoil angle of  $30^\circ$  (IBM geometry) mounted with a  $6 \mu\text{m}$  Mylar absorber and 1.1 mm wide vertical aperture. Two detectors collect the backscattered particles. One of them is placed at a scattering angle of  $165^\circ$  at Cornell geometry while the other one is set to  $135^\circ$  at IBM geometry. Data are usually collected in list-mode. Spectra are evaluated with the RBX [23] or WINDF [24] computer codes.

Characteristics of the technique:

- Quantitative for absolute areal density, stoichiometry
- Thin film thickness measurement without standards
- Provides multi-element depth concentration profiles
- Non-destructive analysis

- Matrix independent (unaffected by chemical bonding states)
- Wide range of element coverage: from B to U
- High precision (typically  $\pm 3\%$ ) and high sensitivity
- Depth range is from 10 nm to a few microns from the surface with a depth resolution of about 20-200 Å

A new application area of the Laboratory of Ion Beam Applications is *micromachining*. Proton Beam Micromachining, also known as P-beam Writing (PBW) [25], is a new direct-writing process that uses a focused beam of MeV protons to pattern various resist materials at micro and nanodimensions. (In our laboratory the micron scale is available, but there are a few state-of-the-art laboratories offering nanobeams.) The process, although similar in many ways to direct writing using electrons, offers some interesting and unique advantages. Protons, being more massive, have deeper penetration in materials while maintaining a straight path, enabling p-beam writing to fabricate three-dimensional, high aspect ratio structures with vertical, smooth sidewalls and low line-edge roughness. Calculations have also indicated that p-beam writing exhibits minimal proximity effects, since the secondary electrons induced in proton/electron collisions have low energy. A further advantage stems from the ability of protons to displace atoms while traversing material, thereby increasing localized damage especially at the end of range. P-beam writing produces resistive patterns at depth in Si, allowing patterning of selective regions with different optical properties as well as the removal of undamaged regions via electrochemical etching. In our laboratory, we have been doing micromachining since 2002.

An *X-ray Fluorescence measuring system* based on a medium power (Rh anode, 60 kV; 1 mA) X-ray tube is assembled. This is a quick and low-cost method for the preliminary and bulk investigation of materials.

## 4. Applications

### 4.1. Analytical Applications

#### 4.1.1. Aerosols

Systematic investigation of atmospheric aerosol [26] has been started in the Institute in 1991 to determine the total, PM10 and PM2.5 mass and their elemental composition and black carbon content in urban (Debrecen) site and a rural site nearby (Hortobágy-Nagyiván). Integral sampling has been made in measurements covering a time period of 10 years with a single stage Nuclepore sampler. Since 1993 atmospheric aerosol samples have been collected with a “Gent” stacked filter unit (SFU). Particle masses (PM) of the samples have been measured with a Sartorius microbalance. “Black Carbon” component (BC) collected on the fine stage samples has been measured by a Smokestain reflectometer. Proton induced X-ray emission analytical method (PIXE) has been applied for deducing absolute concentration data (in  $\text{ng}/\text{m}^3$ ) on elemental constituents (Al, Si, P, S, Cl, K, Ca, Ti, V, (Cr), Mn, Fe, Ni, Cu, Zn, (As), Br, Ba, Pb) of the samples.

During measuring campaigns *time resolved samples* were collected with Streaker air particulate sampler with 1 week sampling duration, and with a 7-stage Cascade Impactor allowing size separation [27]. Single aerosol particles on samples, collected by a Cascade Impactor, were analyzed by scanning nuclear microprobe [28].

*Seasonal variations*, correlations with the amount of precipitation and wind sector distributions were observed for separate elements. Absolute principal component analysis revealed four typical factors contributing to the aerosol burden (Fig. 3.) [29]. Trajectory sector analysis has been used for

studying the influence of long range transport from the heavily industrialized area in Central/Eastern Europe on one hand and from the Saharan area on the other [30].

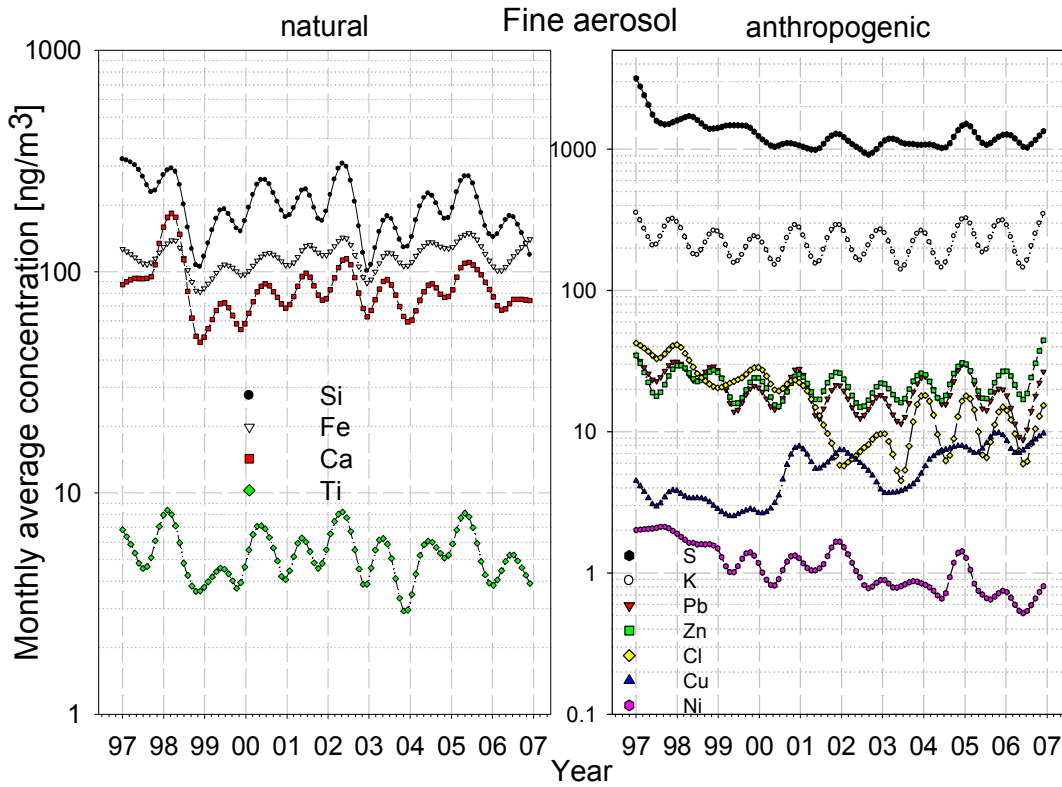


**Figure 3.** Seasonal variations and tendencies of the elemental concentrations in urban fine (PM<sub>2.5</sub>) aerosol samples

Enrichment of *desert soil* elements (mainly sulphure and chlorine) to be assigned to the accumulation of salts in the closed arid Tarim Basin has been observed in the Takla Makan desert. Elemental ratios Si/Fe and Ca/Fe were found to be used as regional tracers in following Takla Makan aerosols towards Chinese and Japan sampling stations in KOSA events [31]. Integral elemental constituents and individual aerosol particles collected during an eruption event of *Lonqimay volcano* in Chile have been subjected to detailed analysis [32].

Our data offer further basis to investigate the existence and nature of differences between air qualities in Western and Eastern Europe caused by structural and technological differences in the energy sector and industry of the regions [33].

In order to investigate the *health impact* of atmospheric aerosols, the obtained data is used to calculate lung deposition probabilities along the human respiratory tract with the help of a stochastic lung model [34]. The IBA laboratory also took part in the recent development of the model for asthma and emphysema [35].

The above described work was supported in part by the Hungarian National Foundation for Scientific Research (OTKA) and the National Research and Development Program (NRDP), as well as by the International Atomic Energy Agency (IAEA-CRP) [29,30].

### 4.1.2. Materials Science

The Oxford-microbeam facility makes it possible to collect the analytical data point by point with a focussed ion beam. Beside the full area, we can collect spectra belonging to a specific region or even a point. This way, we have the analytical information with a high lateral resolution [36], actually defined by the beam spot size. On the basis of the micro-RBS spectra, elemental maps are also generated in order to investigate the lateral elemental distribution. This method is very fruitful in studying the surface roughness [37] of thin samples. RBS is especially useful when not only the composition of the samples but also their depth profiles are to be determined in the first few  $\mu\text{m}$ . We can even demonstrate the elemental depth distribution in *tomographic images* (Fig. 4.) [38]. We have a wide experience in investigation of *thin films* [39], *multilayers* [40], *surface roughness* [41], and *diffusion profiles* [42] with an RBS microbeam.

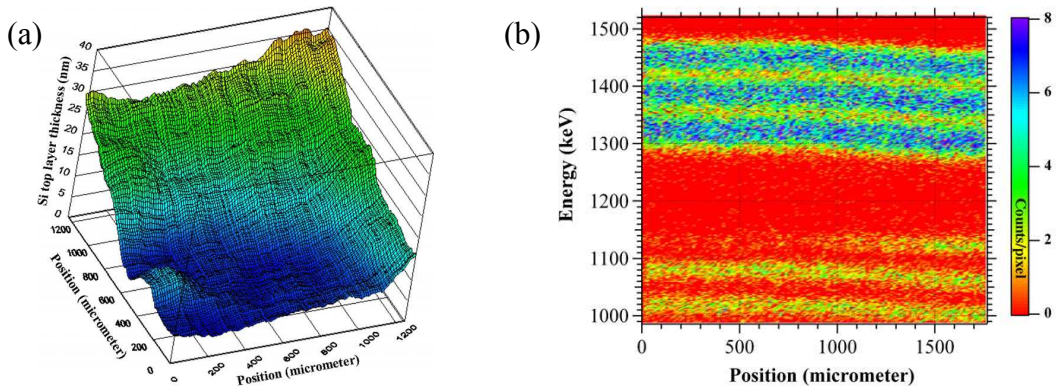


**Figure 4.** (a) Si micro-RBS elemental map of an ion-bombarded top layer of a Si/Cr multilayer sample. Full scan of  $1250 \times 1250 \mu\text{m}^2$ . Approximately a quarter of the crater is seen. The top Si layer thickness is about 5 nm in the bottom of the crater while it increases up to 37 nm in the virgin area. It is seen that the bottom of the crater is not flat. (b) Tomographic image along the diagonal. Energy of the backscattered particles is represented as a function of the position. Si: bottom three lines, Cr: top three lines. The separated Si and Cr signals belonging to the different layers and the missing Si counts, due to the Si removal, causing energy shift of the underlying layers are well seen.

### 4.1.3. Biology and biomedicine

In our laboratory, biomedical applications of the ion beam analytical techniques started in the early eighties with measuring trace elements in human blood samples. The time variation of elemental concentrations in *erythrocytes* and *blood plasma* during normal and pathological human pregnancies was investigated [43]. In further works prompt and prolonged *effects of radiotherapeutic irradiation* on iron concentration in human erythrocytes and blood plasma were tested [44].

The most significant stimulus for stepping further in the field of biological and biomedical applications was the EU5 NANODERM project between 2003 and 2007. The main goal of the project was to get quantitative information on the *penetration of ultra-fine* particles in the various strata of *skin*, on their penetration pathways as well as on their impact on human health. In order to meet the requirements of the biological and biomedical projects, we developed a new measurement setup and data evaluating system at the Debrecen scanning nuclear microprobe facility, providing an accurate, quantitative method for the analysis of thin biological tissues down to the cell level. In collaborations with our partners, we successfully applied the new bio-PIXE setup in several multidisciplinary studies related to human, animal and plant physiology, such as the above mentioned NANODERM project, in which we demonstrated that  $\text{TiO}_2$  nanoparticles did not penetrate intact skin [45]. Our results cover

a wide range of applications from the determination of trace elements in *aquatic plants* (Fig. 5.) [46] and *fish scales* to the investigation of calcium deposits in *human carotid arteries*, in relation to their thickness [47].

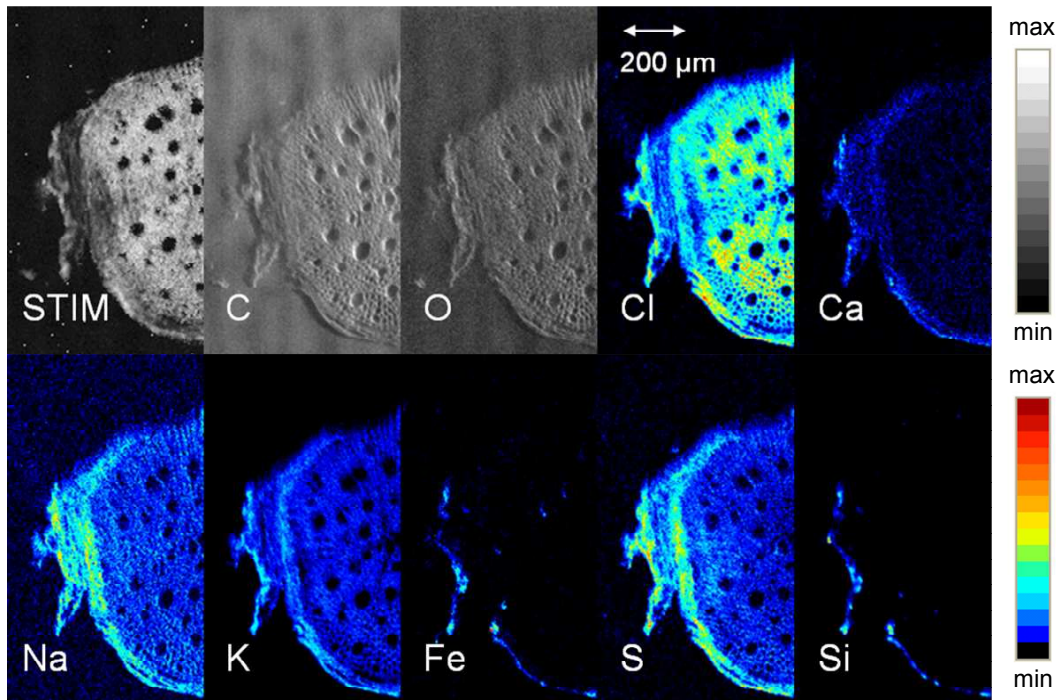


**Figure 5.** STIM energy loss map and elemental maps of a trifid blur marigold root section

#### 4.1.4. Geology

Part of our studies is focussed to the analysis of microscopic-sized ( $<1$  mm), usually rounded, magnetizable geological objects: so called *magnetic spherules* (Fig. 6.) [48]. Their origin has not been entirely determined, although it has been restricted to extraterrestrial (cosmic dust or meteoritic impact), igneous (volcanic or metamorphic), and industrial processes. Extraterrestrial spherules may provide clues to global geological correlations during the history of the Earth as well as they can be indicators of meteoritic impact.

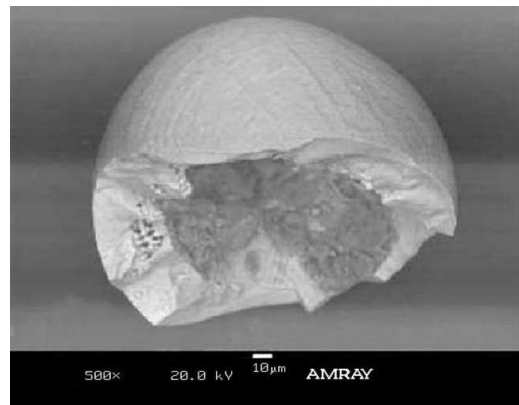


**Figure 6.** Magnetic spherule

An important period in the Earth's history was the transitional time between Permian and Triassic era. Then a global crisis had almost exterminated the life of the Paleozoic age and new living creatures appeared at the onset of the Triassic era. In a theory developed by a Hungarian team (MÁFI – ATOMKI – ELTE – Konkoly Observatory) it was supposed that this catastrophe had been originated by a nearby supernova explosion. A strong experimental evidence corroborating this hypotheses is that tiny ( $3\text{-}20$   $\mu\text{m}$ ) magnetic spherules were found in a lot of Upper Permian rocks of the Earth. They were identified by PIXE to be of cosmic origin and their presence can be explained by supernova explosion [49,50].

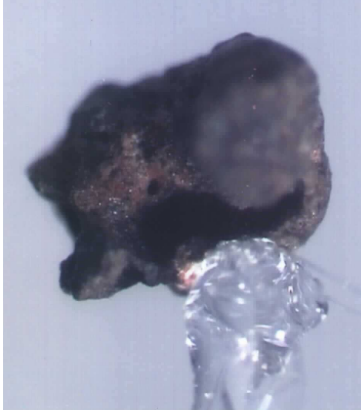


**Figure 7.** Analysed impact sample

Impact craters on the Earth created by incident asteroids, comets and meteorites are important sources of extraterrestrial materials. Thus they play a special role in the study of the composition of the primordial planetary matter and cosmic parent bodies. The most famous and well-preserved meteorite crater is the Barringer Meteor Crater in Arizona, USA. Supposedly, it was created by an iron meteorite. *Impact materials* collected at the crater have been studied extensively from a mineralogical point of view in ATOMKI – University of Debrecen collaboration.

It is particularly important to analyse their iron-rich inclusions (S-Fe-Ni-Cu-systems) attributable to the meteorite as well as the concentration of **Platinum Group Elements** (Ru, Rh, Pd, Os, Ir, Pt). In this atomic number region SRXRF offers superior detection limits (down to the sub-ppm level [51]), therefore SRXRF technique was also applied (Figs. 7,8.) complementary to PIXE [52].

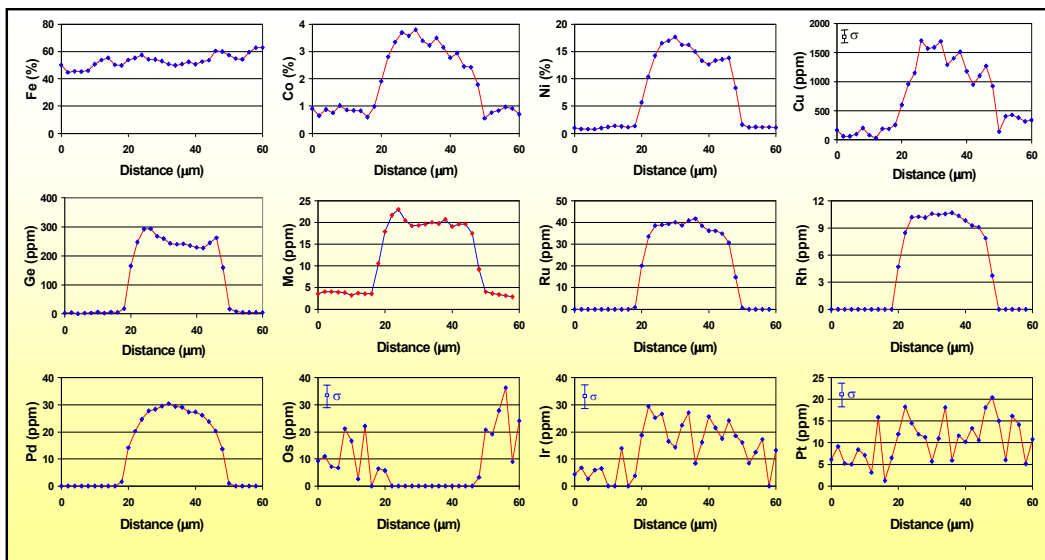


**Figure 8.** Concentration distribution of elements along a line in an impact material measured by  $\mu$ SRXRF method showing the segregation of Ni-rich phase containing PGEs

#### 4.1.5. Archaeometry

Ion beam analytical investigations are focussed on the determination of provenance, authenticity, production technology, and degradation due to environmental effects of art and archaeological objects. They also contribute to the elaboration of conservation technologies. Our research has been carried out in the framework of national and international projects such as: COST Actions G1 and G8, Hungarian Scientific Research Fund (OTKA) in co-operations with CNRS Centre Ernest Babelon (Orléans, France), Laboratoire de Recherche des Musées de France (Paris, France), Institutul de Fizică și Inginerie Nucleară (Bucharest, Romania), Centro Nacional de Aceleradores, Universidad de Sevilla (Seville, Spain), CSIC: Instituto de Historia, Departamento de Prehistoria (Madrid, Spain) and

primarily with the Hungarian National Museum and Budapest History Museum. There are published results in the field of analytical characterization of *radiolarite* samples from the Carpathian basin [53], prehistoric *incrusted potteries* [54], archaeological *bronze* metals [55], ancient *silver coins* (drachms) [56], classical *white lead pigments* [12], etc.

The IBA analysis of glassy materials is an important part of the activity of our laboratory in archaeometry. The aim of the analysis of *obsidians* originated from the Cenozoic volcanic Tokaj Mountains (NE Hungary-E Slovakia) [57] was to find sub-groups among the classified obsidian sources. The results completed the LITHOTECA database of the Hungarian National Museum. On the basis of elemental composition obtained by the analyses of *classical ring-stones and their imitations* [58] an unambiguous separation was made among groups of some artefacts related to their origin. Medieval glass products, came to light from archaeological excavations in the former royal palaces Buda and Visegrád (Fig. 9.) as well as close to the historical downtown of Győr, were the subjects of other studies [59-61]. Determination of major elemental composition of samples made it possible to unambiguously distinguish between local Hungarian products and imported Venetian ones. The trace element composition of cobalt blue Hungarian glasses exactly fitted into the chronological groups established in the earlier study.

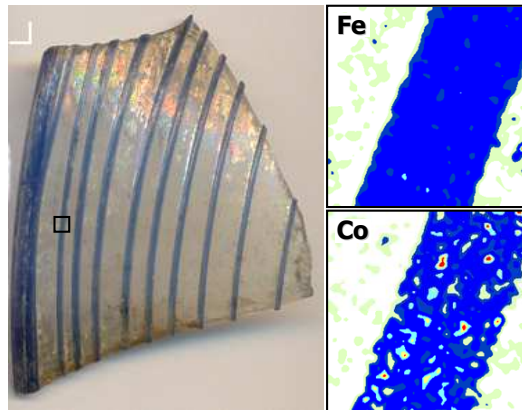


**Figure 9.** Venetian pottery piece from the 15th century (Visegrád Palace, Visegrád, Hungary)

## 4.2 Micromachining

### 4.2.1. Properties of resist materials

A large part of our activities is about investigation of new types of resist materials. Previously only PMMA and SU-8 have been used for proton beam writing (PBW). We first introduced *polyallyl diglycol carbonate* (PADC, also known as CR-39) as a potential candidate as resist material in PBW, as this polymer is widely used as a solid state nuclear track detector [62]. Furthermore, we have also shown in this paper the first demonstration of proton beam written microstructures *in Foturan<sup>TM</sup>* which is a photosensitive glass.

We have investigated a new type of negative resist material, developed in the Institute of Microelectronics in Greece, and shown that this material is suitable for production of 3D microstructures. The polymer mix is called *TADep*, and it consists of 78% (w/w) PHS with 12% degree of hydrogenation and 22% (w/w) EP and 1-(4-hydroxy-3-methylphenyl) tetrahydrothiophenium triflate (o-CS-triflate) 3% (w/w). In contrast to SU-8, this polymer is developable in aqueous base chemicals and thus not too harmful for the environment [63].

The third type of material that we investigated is *poly-(dimethylsiloxane)* (PDMS), a commonly used silicon-based organic polymer, optically clear, generally considered to be inert, non-toxic and

biocompatible. PDMS has been used as a resist material for direct write techniques only in very few cases [64]. PDMS is usually used as a replicating material. Our structures (e.g. optical gratings, Fresnel lenses, etc.) were irradiated directly into the polymer.

We have also explored the changes of the materials properties due to the irradiation. We measured the *refractive index change* in poly(methyl-methacrylate) (PMMA) as a function of the ions penetration depth [65] using ellipsometry method. This information is of crucial importance when one needs to produce optical waveguides in the polymer. Experiments on other physical and chemical properties are in progress.

#### 4.2.2. Devices produced by proton beam writing

A *3D Si micro-turbine* [66] characterized by high aspect ratio vertical walls was formed by the combination of PBW and subsequent selective porous Si (PS) etching. Characteristic feature of the proposed process is that the shape of the micro electromechanical (MEMS) components is defined by two implantation energies. A higher energy is applied for defining the housing of the device while the lower energy is used to write the moving components. *This work is the first demonstration of a silicon device containing a moving part made by proton beam writing.* The video can be seen here: <http://iba.atomki.hu/video/>

An *array of microcapillaries* has been produced by PBW (Fig. 10.). A PMMA (poly(methyl-metacrylate)) film of 50  $\mu\text{m}$  thickness was used, and circular holes of 10  $\mu\text{m}$  diameter were fabricated. These structures can be used in various fields in atomic physics (guiding of highly charged ions), and medical applications (filtering).

Due to the direct write way of PBW, the array of the capillaries allows a high ratio of open holes vs. substrate area. At the same time the holes have a circular shape, and unlike in the case of the conventional filters made by a broad beam of heavy ions, they are not overlapped.

A *microreactor* or microstructured reactor is a device in which chemical reactions take place in typical lateral dimensions below 1 mm. Microreactors are innovative and promising tools in technology nowadays because of their advantages compared to the conventional scale ones, including vast improvements in surface to volume ratio, energy efficiency, reaction speed and yield, increased control of reaction conditions, etc.

The most typical forms of microreactors are microchannels or microfluidic reactors [67]. These kinds of reactors are extremely important tools in technology today, because a large number of synthetic reactions have been carried out since the first successful synthesis of azo dyes. The microfluidic chip reactors require less space, reagents and energy and provide higher yields and improved reaction selectivity in short reaction time and nevertheless produce less wastes because of its short diffusion distance, large specific surface area and increased thermal transfer. Fig. 11. shows one of our microfluidic reactor designs.

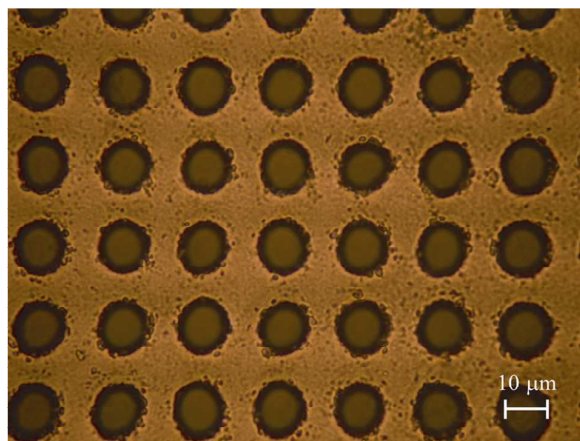


**Figure 10.** The polycapillary film applied in the microreactor and in biomedicine.

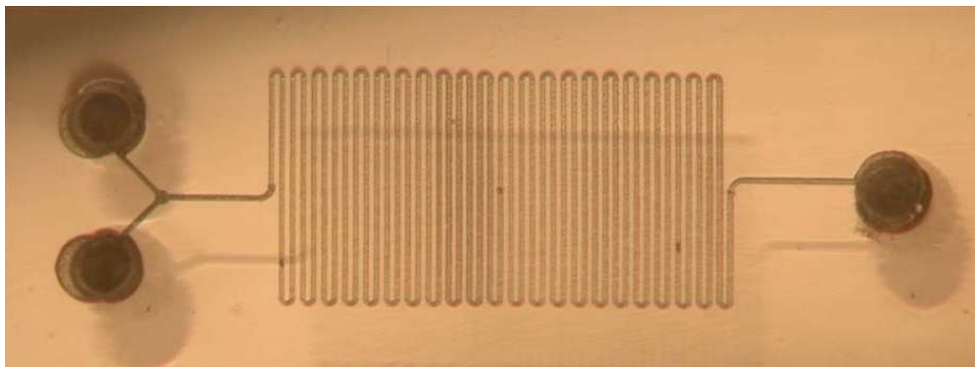


**Figure 11.** A microfluidic reactor created by 2 MeV ion beam. The channel diameter is 30  $\mu\text{m}$ , channel length is about 10 cm. Applicable in organic synthesis.

### 4.3. Spectral performance and radiation hardness of a Si pin photodiode

Advanced materials are being evaluated for use as novel radiation detectors and microelectronic devices. Use of a nuclear microprobe has allowed spatially resolved electrical properties of the detector material to be measured. Nuclear microprobe analysis is playing an increasingly prominent role in the analysis of detector materials and devices by ion beam induced charge (IBIC) collection technique [68].

We have been investigating systematically the influence of radiation damage on the detection properties of a Si PIN diode with high lateral resolution from the point of view of microbeam applications [69]. It is known that irradiation creates new energy levels in the forbidden energy gap of the detector material, which brings about changes in the leakage current, the capacitance, and charge collection efficiency (CCE). Recently an empirical model has been developed [70] to describe the radiation damage. Equations are derived for the variations of the normalized peak position and peak width. The derived empirical equations are physically correct, as far as they account for the superposition of the influence of charge carrier trapping by native and radiation-induced defects and for the effect of charge carrier velocity saturation with electric field strength, as well.

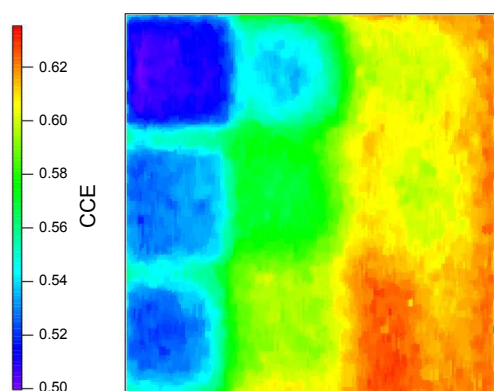


**Figure 12.** IBIC map at 0V bias. The full irradiated area ( $340 \times 340 \mu\text{m}^2$ ) is shown including the individually irradiated  $100 \times 100 \mu\text{m}^2$  squares by fluences from bottom to top and right to left: 0.01, 0.02, 0.05, 0.1, 0.2, 0.5, 1, 2 and  $5 \times 10^{11}$  ion/cm<sup>2</sup>, respectively.

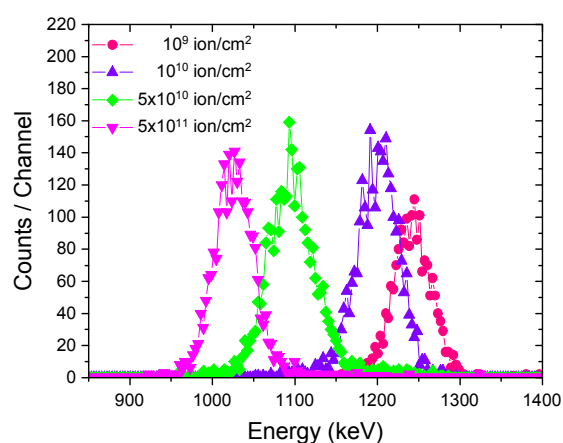
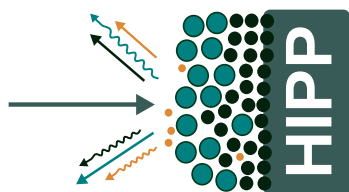


**Figure 13.** Pulse height amplitude spectra obtained from  $40 \times 40 \mu\text{m}^2$  central squares at various fluences of 2005 keV protons,  $U=0$  V.

## 5. Miscellaneous

### HIPP



HIPP (Hungarian Ion-beam Physics Platform) is an open consortium of two research institutes of the Hungarian Academy of Sciences (HAS), established for operating and developing the ion beam physics resources of the stakeholders as a unified distributed facility of common strategy and coordinated user access. Stakeholders of the consortium are the Institute of Nuclear Research (ATOMKI) of HAS, Debrecen, Northern Great Plain Region and the KFKI Research Institute for Particle Nuclear Physics (RMKI) of HAS, Budapest, Central Hungary Region. Both ATOMKI and RMKI are legal entities belonging to the network of research institutions of HAS. More information about the HIPP can be found at the website: <http://hipp.atomki.hu/>.

### ICNMTA

As an acknowledgement of our activities in the field, in 2006 the International Committee selected our group to host the 11th International Conference on Nuclear Microprobe Technology and Applications & 3rd International Workshop on Proton Beam Writing, ICNMTA2008. The IAEA was a co-organizer of this event. The conference took place in the new Kölcsey Convention Centre, Debrecen, Hungary. For more details about the conference see a separate short report in this volume [71].



## References

- [1] J. Végh, D. Berényi, E. Koltay, I. Borbély-Kiss, S.A.H. Seif El-Nasr, L. Sarkadi: *Concentration profile determination by PIXE analysis utilizing the variation of beam energy*, Nucl. Instr. Meth. B 153 (1978) 553
- [2] I. Borbély-Kiss, E. Koltay, Gy. Szabó, Á. Mészáros, S. László, S. Gödény: *Proton induced X-ray emission as a tool for analyzing biological and atmospheric samples*, Atomki Közlemények 22 (1980) 321
- [3] I. Borbély-Kiss, Zs. Fülöp, T. Gesztelyi, Á.Z. Kiss, E. Koltay, Gy. Szabó: *The PIXE-PIGE method for the classification of late Roman glass sealings*, Nucl. Instr. Meth. B 85 (1994) 836
- [4] I. Borbély-Kiss, E. Koltay, S. László, Gy. Szabó, L. Zolnai: *Experimental and theoretical calibration of a PIXE setup for K and L X-rays*, Nucl. Instr. Meth. B 12 (1985) 496
- [5] L. Zolnai, Gy. Szabó: *PIXASE: a computer package for evaluation of PIXE spectrum series. Part I: Spectrum evaluation*, Nucl. Instr. Meth. B 34 (1988) 118
- [6] Á.Z. Kiss, E. Koltay, B.M. Nyakó, E. Somorjai, A. Anttila, J. Raisanen: *Measurements of relative thick target yields for PIGE analysis on light elements in the proton energy interval 2.4–4.2 MeV*, J. Radioanal. Nucl. Chem. 89 (1985) 123
- [7] Á.Z. Kiss, I. Biron, T. Calligaro, J. Salomon: *Thick target yields of deuteron induced gamma-ray emission from light elements*, Nucl. Instr. Meth. B 85 (1994) 118
- [8] Z. Elekes, Gy. Szöör, Á.Z. Kiss, P. Rózsa, A. Simon, I. Uzonyi, J. Simulák: *Deuteron induced gamma-ray emission method applied at a nuclear microprobe for carbon and oxygen content measurements*, Nucl. Instr. Meth. B 190 (2002) 291
- [9] I. Rajta, I. Borbély-Kiss, Gy. Móri, L. Bartha, E. Koltay, Á.Z. Kiss: *The new Atomki scanning proton microprobe*, Nucl. Instr. Meth. B 109 (1996) 148
- [10] I. Rajta, I. Borbély-Kiss, Gy. Móri, L. Bartha, E. Koltay, Á.Z. Kiss, Gy. Szöör: *The Debrecen scanning proton microprobe facility and its applications to geological samples*, Nucl. Instr. Meth. B 118 (1996) 437
- [11] Zs. Kertész, Z. Szikszai, E. Gontier, P. Moretto, J.-E. Surleve-Bazeille, B. Kiss, I. Juhász, J. Hunyadi, Á.Z. Kiss: *Nuclear microprobe study of TiO<sub>2</sub>-penetration in the epidermis of human skin xenografts*, Nucl. Instr. Meth. B 231 (2005) 280
- [12] I. Rajta, M.A. Ontalba, E. Koltay, Á.Z. Kiss: *Study of white lead paint layers by the Debrecen nuclear microprobe*, Nucl. Instr. Meth. B 130 (1997) 315
- [13] A. Simon, F. Pászti, I. Uzonyi, A. Manuaba, Á.Z. Kiss: *Application of grazing exit angle in RBS microprobe measurements*, Nucl. Instr. Meth. B 136 (1998) 350
- [14] E. Koltay, I. Rajta, Zs. Kertész, I. Uzonyi, J.R. Morales, Á.Z. Kiss: *Cluster analysis of elemental constituents of individual atmospheric aerosol particles from the volcanic plume of Lonquimay eruption in 1989*, J. Radioanal. Nucl. Chem. 251 (2002) 25
- [15] I. Rajta, I. Gómez Morilla, M.H. Abraham, Á.Z. Kiss: *Proton beam micromachining on PMMA, Foturan and CR-39 materials*, Nucl. Instr. Meth. B 210 (2003) 260

- [16] A. Simon, G. Kalinka: *Investigation of charge collection in a silicon PIN photodiode*, Nucl. Instr. Meth. B 231 (2005) 507
- [17] Gy. Szabó and I. Borbély-Kiss: *PIXYKLM computer package for PIXE analyses*, Nucl. Instr. Meth. B 75 (1993) 123
- [18] I. Uzonyi, I. Rajta, L. Bartha, Á.Z. Kiss, A. Nagy: *Realization of the simultaneous micro-PIXE analysis of heavy and light elements at a nuclear microprobe*, Nucl. Instr. Meth. B 181 (2001) 193
- [19] I. Uzonyi, Gy. Szabó, I. Borbély-Kiss, Á.Z. Kiss: *Calibration of an UTW Si(Li) detector in the 0.28-22.1 keV energy range at a nuclear microprobe*, Nucl. Instr. Meth. B 210 (2003) 147
- [20] I. Uzonyi and Gy. Szabó: *PIXEKLM-TPI - a software package for quantitative elemental imaging with nuclear microprobe*, Nucl. Instr. Meth. B 231 (2005) 156
- [21] G.Á. Sziki, A. Simon, Z. Szikszai, Zs. Kertész, E. Dobos: *Gamma ray production cross-sections of deuteron induced nuclear reactions for light element analysis*, Nucl. Instr. Meth. B 251 (2006) 343
- [22] G.Á. Sziki, E. Dobos, Zs. Kertész, Z. Szikszai, I. Uzonyi, Á.Z. Kiss: *A PIN detector array for the determination of boron using nuclear reaction analysis at a nuclear microprobe*, Nucl. Instr. Meth. B 219 (2004) 420
- [23] E. Kótai: *Computer Methods for Analysis and Simulation of RBS and ERDA spectra*, Nucl. Instr. Meth. B 85 (1994) 588
- [24] N.P. Barradas, P.K. Marriott, C. Jeynes, R.P. Webb: *The RBS DataFurnace: Simulated annealing*, Nucl. Instr. Meth. B 136 (1998) 1157
- [25] F. Watt, M.B.H. Breese, A.A. Bettiol, J.A. van Kan: *Proton Beam Writing*, Materials Today 30 (2007) 20
- [26] <http://iba.atomki.hu/aeroen.html>
- [27] Zs. Kertész, E. Dobos, B. Fenyő, R. Kéki, I. Borbély-Kiss: *Time and size resolved elemental component study of urban aerosol in Debrecen, Hungary*, X-Ray Spectrometry 37 (2008) 107
- [28] Zs. Kertész, I. Borbély-Kiss, I. Rajta, I. Uzonyi, Á.Z. Kiss: *Analysis of single aerosol particles collected in urban and cave environment by proton microprobe*, Nucl. Instr. Meth. B 161 (2000) 808
- [29] I. Borbély-Kiss, E. Koltay, Gy. Szabó, L. Bozó, K. Tar: *Composition and sources of urban and rural atmospheric aerosol in Eastern Hungary*, J. Aerosol Sci. 30 (1999) 369
- [30] I. Borbély-Kiss, Á.Z. Kiss, E. Koltay, Gy. Szabó, L. Bozó: *Sahara dust episodes in Hungarian aerosol: elemental signatures and transport trajectories*, J. Aerosol Sci. 35 (2004) 1205
- [31] I. Makra, I. Borbély-Kiss, E. Koltay, Y. Chen: *Enrichment of desert soil elements in Takla Makan dust aerosol*, Nucl. Instr. Meth. B 189 (2002) 214
- [32] E. Koltay, I. Rajta, J.R. Morales, I. Borbély-Kiss, Á.Z. Kiss: *Characterization of individual aerosol particles from the eruption of Lonquimay volcano in Chile*, Nucl. Instr. Meth. B 150 (1999) 375
- [33] E. Dobos, I. Borbély-Kiss, Zs. Kertész, Gy. Szabó, E. Koltay: *Debrecen, Hungary on the fine fraction aerosol map of Europe*, J. Radioanal. Nucl. Chem. 279 (2009) 143
- [34] E. Dobos, I. Borbély-Kiss, Zs. Kertész, I. Salma: *Comparing the elemental concentration of aerosol from urban and rural areas with applying the calculation of stochastic Lung Model*, J. Aerosol Sci. 35 (2004) 139
- [35] E. Dobos, I. Borbély-Kiss, I. Balásházy, Zs. Kertész, W. Hofmann: *Development of the stochastic Lung Model for asthma and emphysema*, Proc. European Aerosol Conf. (2005) 267
- [36] A. Simon, T. Csákó, C. Jeynes, T. Szörényi: *High lateral resolution 2D mapping of B/C ratio in boron carbide films*, Nucl. Instr. Meth. B 249 (2006) 454
- [37] A. Simon, Z. Kántor: *Micro-RBS characterisation of the chemical composition and particulate deposition on pulsed laser deposited Si(1-x)Ge<sub>x</sub> thin films*, Nucl. Instr. Meth. B 190 (2002) 351
- [38] A. Simon, F. Pászti, I. Uzonyi, A. Manuaba, I. Rajta, Á.Z. Kiss: *Observation of surface topography using an RBS microbeam*, Nucl. Instr. Meth. B 136 (1998) 344
- [39] A. Simon, Z. Kántor: *New challenges in Rutherford backscattering spectrometric (RBS) analysis of nanostructured thin films*, Invited paper in Nanotechnology. Ed. by R. Vajtai, X. Aymerich and L.B. Kish, Proc. SPIE Vol. 5118 (2003) 179
- [40] A. Simon, A. Sulyok, M. Novák, G. Juhász, T. Lohner, M. Fried, A. Barna, R. Huszank, M. Menyhárd: *Investigation of an ion-milled Si/Cr multilayer using micro-RBS, ellipsometry and AES depth profiling techniques*, in press, Nucl. Instr. Meth. B (2009), doi:10.1016/j.nimb.2009.03.052
- [41] A. Simon, Z. Kántor, I. Rajta, T. Szörényi, Á.Z. Kiss: *Micro-RBS as a technique for the determination of the surface topography of Bi film prepared by pulsed laser deposition*, Nucl. Instr. Meth. B 181 (2001) 360
- [42] J. Slotte, A. Laakso, T. Ahlgren, E. Rauhala, R. Salonen, J. Räisänen, A. Simon, I. Uzonyi, Á.Z. Kiss, E. Somorjai: *Influence of surface properties on the diffusion profiles obtained by Rutherford backscattering spectrometry*, J. Appl. Phys. 87 (2000) 140
- [43] S. Gödény, I. Borbély-Kiss, E. Koltay, S. László, Gy. Szabó: *Determination of trace and bulk elements in plasma and erythrocytes of diabetic pregnant women by PIXE method*, Int. J. Gynaecol. Obstet. 24 (1986) 201
- [44] I. Borbély-Kiss, E. Koltay, Gy. Szabó, É. Pintye, E. Groska, A. Kiss: *The effect of radiotherapeutic irradiation on the elemental concentration of iron in human erythrocytes and blood plasma*, Nucl. Instr. Meth. 49 (1990) 254
- [45] B. Kiss, T. Bíró, G. Czifra, B.I. Tóth, Zs. Kertész, Z. Szikszai, Á.Z. Kiss, I. Juhász, Ch.C. Zouboulis, J. Hunyadi: *Investigation of micronized titanium dioxide penetration in human skin xenografts and its effect on cellular functions of human skin-derived cells*, Exp. Dermatology 17 (2008) 659
- [46] Z. Szikszai, Zs. Kertész, I. Kocsár, V. Oláh: *Quantitative elemental localisation in plants using ion beam microprobe analysis*, Acta Biologica Szegediensis 52 (2008) 81
- [47] M.T. Magyar, Z. Szikszai, Zs. Kertész, S. Molnár, I. Uzonyi, G.Á. Sziki, L. Csiba: *Calcium Distribution in the vessel wall and intima-media thickness of the human carotid artery*, Ultrasound in Medicine and Biology 33 (2007) 1171

- [48] Gy. Szöőr, Z. Elekes, P. Rózsa, I. Uzonyi, J. Simulák, Á.Z. Kiss: *Magnetic spherules: Cosmic dust or markers of a meteoritic impact?*. Nucl. Instr. Meth. B 181 (2001) 557
- [49] Cs.H. Detre, I. Tóth, Gy. Don, Á.Z. Kiss, I. Uzonyi, P. Bodó, Z. Schleder: *The Permian-Triassic supernova impact*. Meteoritics and Planetary Science 34 (1999) A125
- [50] Cs.H. Detre, I. Tóth, Gy. Don, Á.Z. Kiss, I. Uzonyi, P. Bodó, Zs. Schleder: *The paleozoic came to end by the biggest train of disasters known in the Earth's history*. Terrestrial and Cosmic Spherules. Proc. 1998 Annual Meeting TECOS. Ed.: Csaba H. Detre. Bp., Akadémiai Kiadó (2000) p. 45
- [51] I. Uzonyi, Gy. Szöőr, B. Vekemans, L. Vincze, P. Rózsa, Gy. Szabó, A. Somogyi, F. Adams, Á.Z. Kiss: *Application of combined micro-proton-induced X-ray emission and micro-synchrotron radiation X-ray fluorescence techniques for the characterization of impact materials around Barringer Meteor Crater*, Spectrochimica Acta Part B – Atomic Spectroscopy 59 (2004) 1717
- [52] I. Uzonyi, Gy. Szöőr, P. Rózsa, B. Vekemans, L. Vincze, F. Adams, M. Drakopoulos, A. Somogyi, Á.Z. Kiss: *Characterization of impact materials around Barringer Meteor Crater by micro-PIXE and micro-SRXRF techniques*, Nucl. Instr. Meth. B 219 (2004) 555
- [53] Z. Elekes, K.T. Bíró, I. Uzonyi, I. Rajta, Á.Z. Kiss: *Geochemical analysis of radiolarite samples from the Carpathian basin*, Nucl. Instr. Meth. B 170 (2000) 501
- [54] G.Á. Szíki, K.T. Bíró, I. Uzonyi, E. Dobos, Á.Z. Kiss: *Investigation of incrustated pottery found in the territory of Hungary by micro-PIXE method*, Nucl. Instr. Meth. B 210 (2003) 478
- [55] L. Reményi, A. Endrődi, E. Baradács, Á.Z. Kiss, I. Uzonyi, I. Montero, S. Rovira: *Possible links between Hungarian and Spanish Beaker metallurgy*, In: A. Denker et al.: COST Action G8: Non-destructive testing and analysis of museum objects. Fraunhofer IRB Verlag, 2006, ISBN-10: 3-8167-7178-5, P.O. Box 80 04 69, D-70504 Stuttgart, pp. 17-24.
- [56] I. Uzonyi, R. Bugoi, A. Sasianu, Á.Z. Kiss, B. Constantinescu, M. Torbágyi: *Characterization of Dyrhachium silver coins by micro-PIXE method*, Nucl. Instr. Meth. B 161 (2000) 748
- [57] Z. Elekes, I. Uzonyi, B. Gratuze, P. Rózsa, Á.Z. Kiss, Gy. Szöőr: *Contribution of PIGE technique to the study of obsidian glasses*, Nucl. Instr. Meth. B 161 (2000) 836
- [58] I. Borbély-Kiss, T. Gesztelyi, Z. Elekes, I. Rajta, E. Koltay, Á.Z. Kiss: *Investigation of classical ringstones and their imitations*, 5th International Conference on Non-Destructive Testing, Microanalytical Methods and Environmental Evaluation for Study and Conservation of Works of Art. ART'96. Budapest, Hungary, Proc. (1996) 131-143.
- [59] B. Gratuze, I. Uzonyi, Z. Elekes, Á.Z. Kiss, E. Mester: *Cobalt-blue glass pigment trade in Europe during medieval times*, In: G. Demortier and A. Adriaens: Ion beam study of art and archaeological objects. A contribution by members of the COST G1 Action. Office for Official Publications of the European Communities (2000). Luxembourg, pp. 50-53.
- [60] B. Gratuze, I. Uzonyi, Z. Elekes, Á.Z. Kiss, E. Mester: *A study of Hungarian medieval glass composition: Preliminary results*, Archaeometry 98, Proc. of the 31st Symposium, Budapest, Hungary, Ed.: E. Jerem and K.T. Bíró, Archaeopress, BAR International Series 1043, II (2002) 565-572.
- [61] I. Uzonyi, G. Tomka, Z. Szoboszlai, Zs. Kertész, A. Simon, Á.Z. Kiss: *Ion-beam analysis of a medieval glass bottle excavated in Győr*, see Paper 6.4 in this Annual Report
- [62] I. Rajta, I. Gómez Morilla, M.H. Abraham, Á.Z. Kiss: *Proton beam micromachining on PMMA, Futuran and CR-39 materials*, Nucl. Instr. Meth. B 210 (2003) 260
- [63] I. Rajta, E. Baradács, M. Chatzichristidi, E.S. Valamontes, I. Uzonyi, I. Raptis: *Proton beam micromachining on strippable aqueous base developable negative resist*, Nucl. Instr. Meth. B 231 (2005) 423
- [64] S.Z. Szilasi, R. Huszánk, C. Cserhádi, A. Csik, I. Rajta: *PDMS patterning by proton beam*, see Paper 8.7 in this Annual Report
- [65] I. Rajta, S.Z. Szilasi, J. Budai, Z. Tóth, P. Petrik, E. Baradács: *Refractive index depth profile in PMMA due to proton irradiation*, Nucl. Instr. Meth. B 260 (2007) 400
- [66] I. Rajta, S.Z. Szilasi, P. Fürjes, Z. Fekete, Cs. Dücső: *Si Micro-turbine by Proton Beam Writing and Porous Silicon Micromachining*, see Paper 8.9 in this Annual Report
- [67] R. Huszánk, S.Z. Szilasi, K. Vad, I. Rajta: *First Experiments on a Microreactor Created by Proton Microbeam*, see Paper 8.8 in this Annual Report
- [68] M.B.H. Breese, D.N. Jamieson, P.J.C. King: *Materials Analysis using a Nuclear Microprobe*, Wiley and Sons, New York, 1996.
- [69] A. Simon, G. Kalinka, M. Jakšić, Ž. Pastuović, M. Novák, Á.Z. Kiss: *Investigation of radiation damage in a Si PIN photodiode for particle detection*, Nucl. Instr. Meth. B 260 (2007) 304
- [70] G. Kalinka, M. Novák, A. Simon, Ž. Pastuović, M. Jakšić, Á.Z. Kiss: *Empirical approach to the description of spectral performance degradation of silicon photodiodes used as particle detectors*, in press, Nucl. Instr. Meth. B (2009), doi:10.1016/j.nimb.2009.03.053
- [71] I. Rajta, et al, *Organization of ICNMTA2008*, see Paper 9.3 in this Annual Report

## 1.1 On the $\mathcal{PT}$ -symmetric Rosen–Morse II potential

*G. Lévai, E. Magyari* <sup>a)</sup>

The investigation of non-hermitian quantum mechanical systems has gone through a renaissance in the past decade after the introduction of  $\mathcal{PT}$ -symmetric quantum mechanics. Quantum Hamiltonians exhibiting  $\mathcal{PT}$  symmetry, i.e. invariance with respect to simultaneous space ( $\mathcal{P}$ ) and time ( $\mathcal{T}$ ) reflection showed several features in common with hermitian ones, including real energy eigenvalues at least up to critical value of non-hermiticity, where the real energy eigenvalues merge pairwise and re-emerge as complex conjugate values. This is interpreted as the spontaneous breakdown of  $\mathcal{PT}$  symmetry, as the eigenfunctions cease to be the eigenfunctions of the  $\mathcal{PT}$  operator then. A conserved pseudo-norm can also be defined for  $\mathcal{PT}$ -symmetric systems, although it is not positive definite as in the hermitian case.

Considering non-relativistic potentials in one dimension  $\mathcal{PT}$  symmetry prescribes the condition  $V^*(-x) = V(x)$ , i.e. the real and the imaginary potential components have to be even and odd functions of the coordinate  $x$ , respectively. The Schrödinger equation has been solved for a large number of  $\mathcal{PT}$ -symmetric potentials (mainly the  $\mathcal{PT}$ -symmetric extensions of real potentials), and the exact results contributed significantly to the understanding of  $\mathcal{PT}$ -symmetric quantum mechanics.

We discussed the Rosen–Morse II potential

$$V(x) = -\frac{s(s+1)}{\cosh^2(x)} + 2\Lambda \tanh(x)$$

[1], the hyperbolic counterpart of the Rosen–Morse I potential [2]. In the real case ( $s(s+1)$  real,  $\Lambda = \lambda$ , real)  $V(x)$  represents an asymmetric potential well with  $V(x \rightarrow -\infty) \neq V(x \rightarrow \infty)$ , while in the  $\mathcal{PT}$ -symmetric case ( $s(s+1)$  real,  $\Lambda = i\lambda$ , imaginary) its real component vanishes asymptotically, while its imaginary component does not ( $V(x \rightarrow -\infty) = -2i\lambda = -V(x \rightarrow \infty)$ ). This latter feature of the Rosen–Morse II potential is unique among exactly solvable  $\mathcal{PT}$ -symmetric potentials studied to date.

In the  $\mathcal{PT}$ -symmetric case the bound-state eigenfunctions obeying  $\mathcal{PT}\psi_n(x) = \psi_n(x)$  are

$$\begin{aligned} \psi_n(x) &= c_n i^n (1 - \tanh(x))^{\frac{\alpha_n}{2}} (1 + \tanh(x))^{\frac{\beta_n}{2}} \\ &\times P_n^{(\alpha_n, \beta_n)}(\tanh(x)), \end{aligned}$$

while the corresponding energy eigenvalues are  $E_n = -(s-n)^2 + \lambda^2(s-n)^{-2}$ , where  $\alpha_n = s-n + i\lambda/(s-n)$  and  $\beta_n = s-n - i\lambda/(s-n)$ . The regularity of the wave functions requires  $s > n$ .

The normalization conditions and the asymptotically non-vanishing imaginary potential component lead to some unusual results concerning the bound states. One is that there will always be a bound state for  $n = 0$ , while another one is that positive-energy bound states can exist whenever the condition  $s > n > s - |\lambda|^{1/2}$  is met. In the extreme case of  $s < |\lambda|^{1/2}$  all the discrete energy eigenvalues will be positive.

We calculated the pseudo-norm  $I_{nn} = \langle \psi_n | \mathcal{P} | \psi_n \rangle$  for the bound states and found that similar to other  $\mathcal{PT}$ -symmetric potentials (although in contrast with the Scarf II potential) its sign alternates with  $n$  as

$$I_{nn} = \frac{(-1)^n c_n^2 2^{2s-2n} |\Gamma(s+1 + \frac{i\lambda}{s-n})|^2 (s-n)}{n! \Gamma(2s-n+1) [(s-n)^2 + \lambda^2/(s-n)^2]}.$$

We identified the scattering solutions too and calculated the reflection and transition coefficients. These were only known for the hermitian case before. We found that in the  $\mathcal{PT}$ -symmetric case these exhibit handedness, i.e. waves coming from the two directions lead to inequivalent results, although the transmission coefficients differ only in a phase factor. As a by-product, we also reproduced (and corrected) results on the real Rosen–Morse II potential.

a) Institut für Hochbautechnik, ETH Zürich

[1] G. Lévai, E. Magyari, J. Phys. A:Math. Theor. **42** (2009) 195302

[2] G. Lévai, Phys. Lett. A **372** (2008) 6484.

## 1.2 Bound and scattering states of the $\mathcal{PT}$ -symmetric Coulomb potential problem

*G. Lévai, M. Znojil<sup>a</sup>, P. Siegl<sup>a</sup>*

The complexification of potentials within the framework of  $\mathcal{PT}$ -symmetric quantum mechanics has led to a number of remarkable findings. These manifestly non-hermitian potentials that are invariant with respect to simultaneous space ( $\mathcal{P}$ ) and time ( $\mathcal{T}$ ) reflection shared several features with real (hermitian) potentials. These include partly or fully real energy spectrum and the conservation of the norm. There are, however, also differences, from which perhaps the most remarkable one is that  $\mathcal{PT}$ -symmetric potentials can be, and often even have to be defined on some trajectories of the complex  $x$  coordinate space. Avoiding the real  $x$  axis also means avoiding singularities occurring there (e.g. at  $x = 0$ ), so solutions not regular on the real  $x$  axis can become accepted, leading to a wider set of solutions in  $\mathcal{PT}$ -symmetric potentials. Often two sets of solutions can be identified with principal quantum number  $n = 0, 1, 2, \dots$ , discriminated by the quasi-parity quantum number  $q = \pm 1$ .

The  $\mathcal{PT}$ -symmetric version of a number of exactly solvable potentials can be defined in this spirit on a complex shifted  $x$  coordinate  $x - ic$  ( $c$  real), however, the Coulomb potential is an exception from this, as its bound-state wave functions cannot be regular at both  $x \rightarrow -\infty$  and  $x \rightarrow \infty$ . In our early paper [1] we got around this problem by obtaining the eigenstates of the  $\mathcal{PT}$ -symmetric Coulomb potentials through applying the well-known state by state harmonic oscillator–Coulomb mapping to the  $\mathcal{PT}$ -symmetric harmonic oscillator defined on the trajectory  $x - ic$ . The  $t$  trajectory obtained from the mapping was found to be a parabola in the first and fourth quadrant, circumventing the origin from the left. In order to make it  $\mathcal{PT}$ -symmetric, i.e. left-right symmetric in the coordinate space, it had to be tilted to the first and second quadrant by the multiplication  $it$ . In order to keep the  $kt$  quantity intact,  $k$  also had to be tilted in the opposite direction in the  $k$  wave number space as  $-ik$ . This resulted in the unusual finding that the energy spectrum was inverted.

Recently we revisited [2] the  $\mathcal{PT}$ -symmetric

Coulomb potential

$$\left[ -\frac{d^2}{dt^2} + \frac{L(L+1)}{t^2} + i\frac{Z}{t} \right] \Psi(t) = E \Psi(t).$$

in order to study both its bound-state and scattering solutions, the  $\mathcal{PT}$  symmetry of these and the possible spontaneous breakdown of  $\mathcal{PT}$  symmetry.

Assuming that  $2L$  is not an integer and that the  $t(x)$  trajectory is such that the solutions remain normalizable for  $x \rightarrow \pm\infty$ , the two independent solutions corresponding to  $q = +1$  and  $q = -1$  are

$$\begin{aligned} \Psi_q(x) &= C_q e^{-kt(x)} [t(x)]^{a(q,L)} \\ &\times {}_1F_1(a(q,L) + \frac{iZ}{2k}, 2a(q,L), 2kt(x)), \end{aligned}$$

where  $a(q,L) = \frac{1}{2} + q(L + \frac{1}{2})$ . In case of real values of  $L$  these solutions are eigenstates of the  $\mathcal{PT}$  operator with eigenvalue 1 provided that  $C_q^* = C_q e^{-i\pi a(q,L)}$ . The two sets of bound-state energy eigenvalues of [1] are recovered by choosing the first argument of the confluent hypergeometric functions to be a non-positive integer  $n$ . The spontaneous breakdown of  $\mathcal{PT}$  symmetry occurs if  $L$  is  $L = -\frac{1}{2} + i\lambda$ : in this case the energy eigenvalues turn into complex conjugate pairs and the solutions cease to be the eigenfunctions of the  $\mathcal{PT}$  operator, rather, it transforms them into each other.

The analysis of scattering solutions is under study. For this we considered a narrow U-shaped  $\mathcal{PT}$ -symmetric trajectory in the complex  $x$  plane circumventing the origin from below. The first results indicate that the consistency of this model requires not only a suitable  $\mathcal{PT}$ -asymmetrization of its “in” and “out” states but also a reversal of the sign of the asymptotic bare mass parameter [2].

<sup>a</sup> Nuclear Physics Institute of Academy of Sciences of the Czech Republic, Řež,

[1] M. Znojil, G. Lévai, Phys. Lett. A **271** (2000) 327.

[2] M. Znojil, P. Siegl, G. Lévai, Phys. Lett. A **373** (2009) 1921

## 2.1 European Research Council supports an extensive study of the astrophysical p-process

*Gy. Gyürky*

The astrophysical p-process, the production mechanism of the heavy proton rich isotopes (the so-called p-nuclei) is still one of the least understood processes of nucleosynthesis. The modeling of the process requires a huge network of thousands of reactions where the rates of the involved reactions represent one of the biggest uncertainty in the resulting abundances of p-nuclei. In lack of experimental data the required reaction rates are taken from statistical model calculations which proved to be inaccurate in the mass and energy range relevant for the p-process. The systematic experimental study of the relevant reactions is therefore crucial to test the calculated reaction rates, to select the best input parameters for the calculations and, consequently, to contribute to a better understanding of the astrophysical p-process.

The European Research Council (ERC) [1] has acknowledged this need for experimental data when they decided to support a project devoted to this subject. In 2007 the first call of the ERC Frontier Research Scheme (Starting Grants) has been launched within the FP7 Specific Programme 'IDEAS'. From the very high number of applications, the peer reviewers of the ERC Scientific Council has recommended for funding the proposal entitled 'Nuclear reaction studies relevant to the astrophysical p-process nucleosynthesis'. An amount of 750,000 Euro has been allocated to the project for a 5 year duration. The starting date of the project was 1st July, 2008 [2].

With the ERC support, an extensive experimental study of the p-process is being carried out. The experiments will be carried

out almost exclusively with the accelerators of the ATOMKI. The financial support allows to largely improve the available experimental technique. The purchase of two large volume HPGe detectors is in progress as a result of a public procurement. The upgrade of the nuclear electronics and data acquisition system used for p-process related experiments has also been started.

The particle beam selection and properties available in ATOMKI and the technical development provided by the ERC support will make it possible to extend substantially the experimental database relevant for the p-process. Proton as well as alpha induced reaction cross sections will be measured and compared with statistical model predictions. The completely unexplored higher mass region is hoped to be reached in the case of alpha capture reactions. The planned alpha elastic scattering experiments will contribute to the fine tuning of the statistical model calculations by probing one of its most important input parameters, the optical potential. With the planned experiments a significant improvement of the understanding of the p-process will be reached.

European Research Council  
Scientific Council



[1] <http://erc.europa.eu>

[2] ERC Starting Grant No. 203175

## 2.2 Coulomb suppression of the stellar enhancement factor

*G. G. Kiss, T. Rauscher<sup>a)</sup>, Gy. Gyürky, A. Simon, Zs. Fülöp, E. Somorjai*

Modern  $p$  process studies require large reaction networks, often including hundreds and thousands of nuclei and their respective reactions with light particles. Astrophysical reaction rates employed in reaction network calculations are determined either directly from cross sections or from the rate for the inverse reaction by applying detailed balance. The cross sections are known from experiment or predicted by theory. However, even when a reaction is experimentally accessible, often astrophysical rates cannot be directly measured. Excited states are thermally populated in an astrophysical plasma whereas only reactions on the ground state of the target can be investigated in the laboratory. A measure of the influence of the excited target states is given by the stellar enhancement factor  $f = r_{\text{stellar}}/r_{\text{g.s.}}$ , defined by the ratio of the stellar rate to the ground state rate.

The enhancement factor  $f_{\text{rev}}$  for the reverse reaction  $B(b,a)A$  (defined by having negative reaction  $Q$  value) is usually larger than the enhancement  $f_{\text{forw}}$  of the forward reaction  $A(a,b)B$  (being the one with positive  $Q$  value) because more excited states are energetically accessible in nucleus  $B$  than in nucleus  $A$ . Therefore, it was assumed so far that more astrophysically relevant transitions are neglected when experimentally studying a reaction with negative  $Q$  value.

However, there are cases for which  $f_{\text{rev}} < f_{\text{forw}}$  due to Coulomb suppression of a part of the energetically allowed transitions [1]. This effect will be most pronounced in reactions with a charged particle in one and a neutral particle in the other channel, e.g.  $(n,p)$ , but it can also appear when the entrance channel and exit channel have Coulomb barriers of different height, e.g.  $(p,\alpha)$ . Transitions from excited states to the same state in a compound nu-

cleus are proceeding at smaller relative energy and are stronger suppressed by the Coulomb barrier.

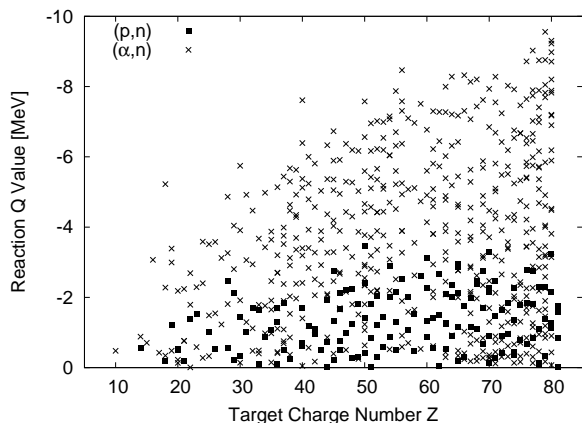


**Figure 1.** Reaction  $Q$  values for  $(p,n)$  and  $(\alpha,n)$  reactions with  $f_{\text{rev}} < f_{\text{forw}}$

Thus, a prerequisite is that  $|Q|$  is low compared to the Coulomb barrier. We find more than 1200 reactions exhibiting the suppression effect. Figure 1. shows the obtained range of  $Q$  values as a function of target charge  $Z$ . It can be clearly seen that larger  $|Q|$  is allowed with increasing Coulomb barrier. Although the strengths of the involved transitions also depend on spin and parity of the initial and final state, Coulomb repulsion dominates the suppression when the interaction energy is small.

The Coulomb suppression effect is not only theoretically interesting, but also important for experiments because it allows to directly determine an astrophysically relevant rate by measuring in the direction of suppressed enhancement factor.

a) Universität Basel, CH-4056 Basel, Switzerland

[1] G. G. Kiss *et al.*, Phys. Rev. Lett. **101**, 191101 (2008).

## 2.3 Inelastic scattering studies of $^{16}\text{C}$ reexamined

Z. Elekes, N. Aoi<sup>a)</sup>, Zs. Dombrádi, Zs. Fülöp, T. Motobayashi<sup>a)</sup>, H. Sakurai<sup>a)</sup>

$^{16}\text{C}$  nucleus has been in the forefront of nuclear structure studies in the past years because of several reasons. Its extended neutron distribution was suggested from a reaction cross section measurement [1]. In addition, an anomalously long lifetime of the first  $2^+$  excited state and a corresponding hindered E2 strength was measured by recoil shadow method in RIKEN [2]. Similar small  $B(E2)$  value and a strong dominance of neutron over proton excitations were concluded by analyzing the angular distribution of  $^{16}\text{C}$  nuclei inelastically scattered on a  $^{208}\text{Pb}$  target [3]. This picture seemed to be confirmed by a proton inelastic scattering measurement in inverse kinematics [4]. This year, the results of two new experiments aimed at redetermining the lifetime of the first  $2^+$  excited state have become available. RIKEN has come up with revised data [5] and Lawrence Berkeley National Laboratory has reported a value close to theirs [6]. These studies suggest a shorter lifetime and a corresponding larger  $B(E2; 0_{gs}^+ \rightarrow 2_1^+)$  between 10-20  $\text{e}^2\text{fm}^4$ .

Here, we present a reanalysis of the inelastic scattering experiments populating the  $2_1^+$  state using  $^{208}\text{Pb}$  [3] and hydrogen targets [4]. Since the Pb and H targets probe the neutron and proton distributions with different sensitivities, both mass and charge, and consequently, the neutron and proton deformation lengths ( $\delta_n$  and  $\delta_p$ ) can be extracted by comparing the integrated cross sections of the two processes in a simultaneous way.

As a first step, a pair of neutron and proton deformation lengths has been chosen. These are in the following correspondence with the matter and Coulomb deformation lengths for the two probes ( $\delta_M^{Pb}, \delta_M^{pp}, \delta_C^{Pb} = \delta_C^{pp} = \delta_p$ ):

$$(Z \cdot b_p^{Pb} + N \cdot b_n^{Pb}) \cdot \delta_M^{Pb} = N \cdot b_n^{Pb} \cdot \delta_n + Z \cdot b_p^{Pb} \cdot \delta_p \quad (1)$$

$$(Z \cdot b_p^{pp} + N \cdot b_n^{pp}) \cdot \delta_M^{pp} = N \cdot b_n^{pp} \cdot \delta_n + Z \cdot b_p^{pp} \cdot \delta_p \quad (2)$$

where  $b_n^{Pb}, b_p^{Pb}, b_n^{pp}$  and  $b_p^{pp}$  are the neutron and proton sensitivity parameters.

$\delta_{M,C}^{Pb}, \delta_{M,C}^{pp}$  are the input parameters in the coupled channel code ECIS97 which is used to retrieve calculated cross sections  $\sigma_{cal}^{Pb}$  and  $\sigma_{cal}^{pp}$ . The difference between the calculated and experimental cross sections has been quantified in a  $\chi^2$  value so we ended up with a set of data  $(\delta_n, \delta_p, \chi^2)$ . This procedure was repeated with varied initial  $(\delta_n, \delta_p)$  parameters and the results are visualized in a contour plot of  $\chi^2$  values. From this figure, the neutron and proton deformation lengths could easily be determined at  $\delta_n = 1.37 \pm 0.12$  (stat) fm,  $\delta_p = 0.90 \pm 0.13$  (stat) fm. The corresponding proton and neutron transition strengths are:

$$B(E2; 0_{gs}^+ \rightarrow 2_1^+)/e^2 = 15.2 \pm 4.4 \text{ (stat) fm}^4 \quad (3)$$

$$M_n^2 = 98 \pm 17 \text{ (stat) fm}^4. \quad (4)$$

The presently determined  $B(E2) = 15.2 \text{ e}^2\text{fm}^4$  value is close to the results coming from the two new lifetime measurements [5,6] of  $13.0 \pm 1.0$  (stat)  $\pm 3.5$  (syst)  $\text{e}^2\text{fm}^4$  and  $20.8 \pm 3.7 \text{ e}^2\text{fm}^4$  and they are consistent with each other taking into account the error bars. However, they are much smaller than  $82.3 \text{ e}^2\text{fm}^4$  which is expected using a global fit by Raman [7] based on the Grodzins rule [8]. On the other hand, our extracted neutron strength of  $98 \text{ fm}^4$  is about 6 times larger than the proton one, which shows the dominance of neutron over proton excitations in  $^{16}\text{C}$  nucleus.

a) The Institute of Physical and Chemical Research, 2-1 Hirosawa, Wako, Saitama 351-0198, Japan

- [1] T. Zheng *et al.*: Nucl. Phys. A **709** (2002) 103.
- [2] N. Imai *et al.*, Phys. Rev. Lett. **92** (2004) 062501.
- [3] Z. Elekes *et al.*, Phys. Lett. B **586** (2004) 34.
- [4] H. J. Ong *et al.*, Phys. Rev. C **73** (2006) 024610.
- [5] H. J. Ong *et al.*, Phys. Rev. C **78** (2008) 014308.
- [6] M. Wiedeking *et al.*, Phys. Rev. Lett. **100** (2008) 152501.
- [7] S. Raman *et al.*, Atom. Data Nucl. Data Tabl. **78** (2001) 1.
- [8] L. Grodzins: Phys. Lett. **2** (1962) 88.

## 2.4 Observation of excited states in $^{17}\text{C}$ and $^{19}\text{C}$

*M. Stanoiu<sup>a,b,c</sup>, D. Sohler, O. Sorlin<sup>b</sup>, F. Azaiez<sup>a</sup>, Zs. Dombrádi, B. A. Brown<sup>d</sup> M. Belleguic<sup>a</sup>, C. Borcea<sup>c</sup>, C. Bourgeois<sup>a</sup>, Z. Dlouhy<sup>e</sup>, Z. Elekes, Zs. Fülöp, S. Grévy<sup>b</sup>, D. Guillemaud-Mueller<sup>a</sup>, F. Ibrahim<sup>a</sup>, A. Kerek<sup>f</sup>, A. Krasznahorkay, M. Lewitowicz<sup>b</sup>, S. M. Lukyanov<sup>g</sup>, S. Mandal<sup>h</sup>, J. Mrazek<sup>e</sup>, F. Negoita<sup>c</sup>, Y. Penionskhevitch<sup>g</sup>, Zs. Podolyak<sup>i</sup>, P. Roussel-Chomaz<sup>b</sup>, M. G. Saint-Laurent<sup>b</sup>, H. Savajols<sup>b</sup>, G. Sletten<sup>j</sup>, J. Timár, C. Timis<sup>c</sup>, A. Yamamoto<sup>i</sup>*

Recently, a strong movement of the single particle states in neutron rich O and C isotopes has been revealed, which resulted in  $N=14,16$  subshell closures in the oxygen isotopes. As a consequence, a close lying doublet of neutron  $s_{1/2}$  and  $d_{5/2}$  states is expected along the whole C isotopic chain. In order to reveal this possibility, we studied the structure of the neutron-rich nuclei  $^{17,19}\text{C}$  using fragmentation reactions of radioactive beams. Based on particle- $\gamma$  and particle- $\gamma\gamma$  coincidence data, level schemes were constructed for the studied nuclei.

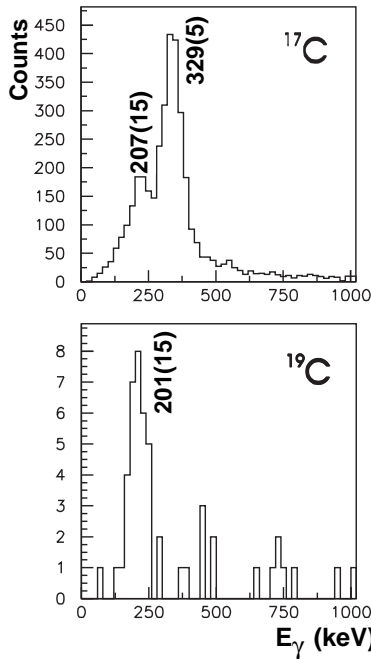


**Figure 1.** Gamma-ray spectra of  $^{17}\text{C}$  and  $^{19}\text{C}$ .

The  $\gamma$ -ray spectrum of the odd nucleus  $^{17}\text{C}$  exhibits two transitions (see figure 1). The relative intensity is the same in the  $\gamma$ -ray spectra of  $^{17}\text{C}$  obtained from the low and high  $\gamma$ -ray multiplicity events. This indicates that the two transitions correspond to the decay of two excited states at 207 and 329 keV directly to the

ground state. The  $^{17}\text{C}$  ground state has a  $3/2^+$  spin value. From the  $^{17}\text{C}(p,p')$  study a tentative spin  $1/2^+$  was assigned to the lower energy excited state and a spin  $5/2^+$  to the higher energy one. The proposed level scheme, shown in figure 2, is in a reasonable agreement with shell model calculations.

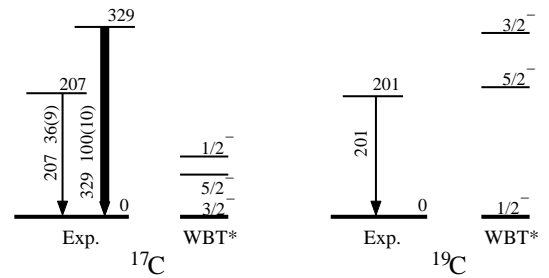


**Figure 2.** Proposed level schemes of  $^{17,19}\text{C}$  and their comparison with shell model calculations using the WBT\* interaction.

For  $^{19}\text{C}$  a  $1/2^+$  configuration have been proposed for the ground state. As the 201-keV  $\gamma$ -transition is observed in our work as a prompt radiation, it should connect states separated by small spin differences such as  $3/2^+ \rightarrow 1/2^+$ . Shell-model calculations predict the existence of three low-lying states with spins  $1/2^+$ ,  $3/2^+$ , and  $5/2^+$  within a few hundred keV (see figure 2). In the Riken (p,p') experiment the  $5/2^+$  has been found 72 keV above the  $3/2^+$  one. Thus, both in  $^{17}\text{C}$  and  $^{19}\text{C}$  the  $1/2^+$  and  $5/2^+$  states are a few hundred keV away.

- a) IN2P3-CNRS, Orsay, France
- b) GANIL, Caen, France
- c) IFIN-HH, Bucharest-Magulere, Romania
- d) NSCL, MSU, East Lansing, USA
- e) NPI, Rez, Czech Republic
- f) KTH, Stockholm, Sweden
- g) FLNR, JINR, Dubna, Russia
- h) LPC, Caen, France
- i) University of Surrey, Guildford, UK
- j) NBI, Copenhagen, Denmark

## 2.5 In-beam $\gamma$ -ray spectroscopy of the neutron-rich $^{20,22}\text{N}$

*D. Sohler, M. Stanoiu<sup>a,b</sup>, Zs. Dombrádi, F. Azaiez<sup>a</sup>, B. A. Brown<sup>c</sup>, M. G. Saint-Laurent<sup>b</sup>, O. Sorlin<sup>b</sup>, Y. Penionskhevitch<sup>d</sup>, N. L. Achouri<sup>e</sup>, J. C. Angélique<sup>e</sup>, M. Belleguic<sup>a</sup>, C. Borcea<sup>f</sup>, C. Bourgeois<sup>a</sup>, J. M. Daugas<sup>b</sup>, F. De Oliveira-Santos<sup>b</sup>, Z. Dlouhy<sup>g</sup>, C. Donzaud<sup>a</sup>, J. Duprat<sup>a</sup>, Z. Elekes, S. Grévy<sup>b</sup>, D. Guillemaud-Mueller<sup>a</sup>, F. Ibrahim<sup>a</sup>, S. Leenhardt<sup>a</sup>, M. Lewitowicz<sup>b</sup>, M. J. Lopez-Jimenez<sup>b</sup>, S. M. Lukyanov<sup>d</sup>, W. Mittig<sup>b</sup>, J. Mrazek<sup>g</sup>, F. Negoita<sup>f</sup>, Zs. Podolyak<sup>h</sup>, M. G. Porquet<sup>i</sup>, F. Pougheon<sup>a</sup>, P. Roussel-Chomaz<sup>b</sup>, H. Savajols<sup>b</sup>, G. Sletten<sup>j</sup>, Y. Sobolev<sup>d</sup>, C. Stodel<sup>b</sup>, J. Timár*

Recently, it has been shown that nuclei close to the neutron-drip line with 2–3 valence neutrons above the  $N=8$  shell closure have a weaker neutron-neutron effective interaction than expected. In order to see if there is a reduction also in the proton-neutron interaction, we studied the structure of  $^{20,22}\text{N}$  by in-beam  $\gamma$ -spectroscopic technique in fragmentation reaction of stable and radioactive beams. From particle- $\gamma$  and particle- $\gamma\gamma$  coincidence relations level schemes of the nuclei studied were constructed (figure 1 and 2) and compared with shell model calculations.

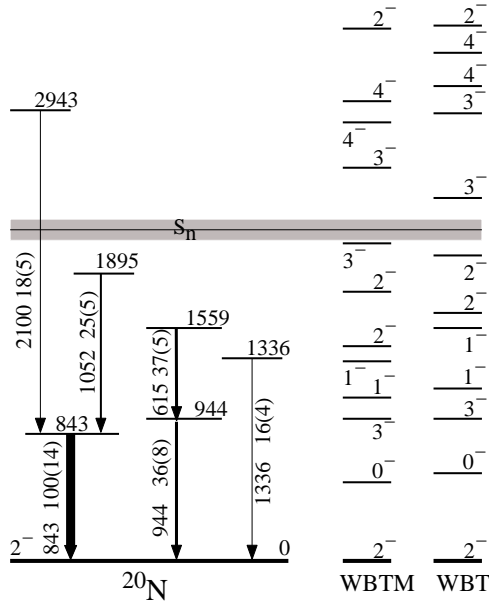


**Figure 1.** Proposed level scheme of  $^{20}\text{N}$  compared with shell model calculations based on the WBTM and WBT interactions.

For  $^{20}\text{N}$ , the ground state is calculated to be  $2^-$ . Even though, the calculated level density is much higher than the experimental one, the assignment of the 843 keV state to the  $3_1^-$  one, the 1895 keV state to the  $3_2^-$ , and the 2943 keV keV state to the  $4_1^-$  one seems to be reasonable.

The  $4^-$  state lying above the neutron separation energy cannot be created by coupling of the  $p_{1/2}$  proton hole to any of the low lying neutron configurations, thus it is based on a core excited state. The 1336 keV state may correspond either to a  $1^-$  or a  $2^-$  theoretical configuration. Due to the uncertainties in the spin assignment, it is hard to deduce any conclusion on the strength of the  $p$ - $n$  interaction.

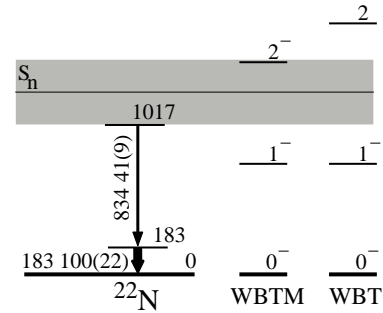


**Figure 2.** Proposed level scheme of  $^{22}\text{N}$  in comparison with shell model calculations based on the WBT and the WBTM interactions.

The  $\gamma$  cascade in  $^{22}\text{N}$  can be assigned to the decay of the  $2^-$  state through the  $1^-$  one to the ground state. The large difference between the calculated and the experimental splitting of the  $\pi p_{1/2} \nu s_{1/2}$  doublet shows a clear decrease of the proton-neutron interaction strength, which may arise from the spatially extended nature of the neutron  $s_{1/2}$  state.

- a) IN2P3-CNRS, Orsay, France
- b) GANIL, Caen, France
- c) NSCL, MSU, East Lansing, USA
- d) FLNR, JINR, Dubna, Russia
- e) LPC, Caen, France
- f) IFIN-HH, Bucharest-Magulere, Romania
- g) NPI, Rez, Czech Republic
- h) University of Surrey, Guildford, UK
- i) CSNSM, Orsay, France
- j) NBI, Copenhagen, Denmark

## 2.6 Radioactive decay of $^{74}\text{As}$ embedded into different environments

*J. Farkas, Gy. Gyürky, C. Yalçın<sup>a)</sup>, G. G. Kiss, Z. Elekes, Zs. Fülöp and E. Somorjai*

It is known for a long while that the half-life of radioactive nuclei is possibly subject to change due to many conditions [1, 2]. One of these conditions is the screening effect of the electrons surrounding the examined nuclei [3, 4]. Recent studies of low energy fusion reactions showed that the theoretical calculations cannot exactly reproduce the measured cross section values, especially when the target is not gaseous, but the target nuclei are embedded into metals [5, 6]. The competing theoretical explanations suggest that this phenomenon is in close relation with half-life changes due to electron screening effects, and prognosticate different influence of the host material and temperature on the half-life of embedded unstable nuclei [7, 8].

Our group investigated the decay of  $^{74}\text{As}$ , which isotope undergoes either a  $\beta^-$  or a  $\beta^+/\varepsilon$  decay. The intensity ratio of the  $E_\gamma = 634.8\text{ keV}$  ( $\beta^-$  decay) and the  $E_\gamma = 595.8\text{ keV}$  ( $\beta^+/\varepsilon$  decay)  $\gamma$ -radiation had been measured (Fig. 1) in order to detect any possible change of half-life when the  $^{74}\text{As}$  nuclei are embedded into Tantalum, Aluminium, Germanium and mylar [9, 10]. The sources have been produced by the  $^{74}\text{Ge}(p,n)^{74}\text{As}$  reaction using the cyclotron of ATOMKI. The activity of the samples were in the interval of about 200 Bq to 2 kBq. The  $\gamma$ -rays were detected by a shielded HPGe detector.

The result of the experiment is in agreement with a null dependence of the decay rate on the host material. The achieved statistical uncertainty allowed us to reject the Debye plasma model based calculations [7] as a possible explanation of our findings, but the modest change suggested by the dielectric function theory [8] can not be excluded. The suggestions of the two calculations on the low temperature

dependence of the half-life of embedded nuclei are very different, making measurements in the millikelvin temperature range highly desirable. The preliminary results of such an experiment has already been obtained [10].

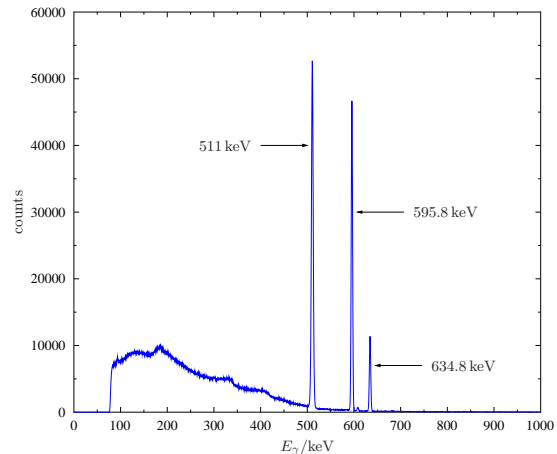


**Figure 1.** The spectrum of  $^{74}\text{As}$  embedded into natural Ge

- a) Kocaeli University, Department of Physics, TR-41380 Umuttepe, Kocaeli, Turkey
- [1] B. W. Sargent, Proc. Camb. Phil. Soc. **28**, 538 (1932)
  - [2] L. Durand, III, L. F. Landovitz and R. B. Marr, Phys. Rev. **130**, 1188 (1963)
  - [3] M. E. Rose, Phys. Rev. **49**, 727 (1936)
  - [4] L. Durand, III, Phys. Rev. **135**, B310 (1964)
  - [5] C. Rolfs and E. Somorjai, Nucl. Instr. Meth. B **99**, 297 (1995)
  - [6] F. Raiola *et al.*, Eur. Phys. J. A **13**, 377 (2002)
  - [7] K. U. Kettner *et al.*, J. Phys. G **32**, 489 (2006)
  - [8] K. Czerski *et al.*, Europhys. Lett. **68**(3), 363 (2004)
  - [9] Gy. Gyürky *et al.*, Eur. Phys. Lett. **83**, 42001 (2008)
  - [10] J. Farkas *et al.*, PoS(NIC X)209 (2008)

## 2.7 Total Absorption Spectroscopy study of the $^{152}\text{Yb}$ decay

*M. E. Estevez<sup>a)</sup>, A. Algora<sup>a)</sup>, B. Rubio<sup>a)</sup>, J. Bernabeu<sup>a)</sup>, E. Nacher<sup>a)</sup>, D. Cano<sup>b)</sup>, A. Gadea<sup>a)</sup>, J. L. Tain<sup>a)</sup>, L. Batist<sup>c)</sup>, K. Burkard<sup>c)</sup>, J. Döring<sup>c)</sup>, M. Gierlik<sup>c)</sup>, W. Hüller<sup>c)</sup>, R. Kirchner<sup>c)</sup>, I. Mukha<sup>c)</sup>, C. Plettner<sup>c)</sup>, E. Roeckl<sup>c)</sup>, J. J. Valiente<sup>d)</sup>*

The study of neutrino oscillation phenomena, which could open the possibility for Charge Conjugation-Parity violation in the lepton sector, is one of the most exciting problems in physics. In the appearance probability for neutrino oscillations, the CP-even terms and the CP-odd terms have different energy dependence, so the control of the neutrino beam energy has an added value. To study these topics, the construction of a monochromatic neutrino beam facility has been proposed recently [1]. As a source for this beam, accelerated nuclei that decay through electron capture (EC) in a storage ring with long straight sections could be used. In a recent annual report [2], a preliminary study of the candidate nucleus  $^{152}\text{Yb}$  was discussed. In this report we present the results of the Total Absorption Spectroscopy (TAS) analysis of these data.

In the analysis, a coincidence between the X ray of  $^{152}\text{Tm}$  (produced in the EC process) and the TAS spectrum is required. In the gated TAS spectrum the peaks are identified with levels fed in the decay, but it can also have contributions from contaminants and background, and it is modified by the detector response. The relation between the gated TAS spectrum and the feeding is:  $d_i = \sum_{j=1}^{j_{max}} R_{ij} f_j$ , where  $d_i$  is the number of counts in channel  $i$  of the measured spectrum,  $f_j$  is the feeding to level  $j$ , and  $R_{ij}$  is the probability that feeding to  $E_j$ , gives counts on channel  $i$  of the measured spectrum.  $R$  is called the "Response Function" of the detector, and depends on the decay scheme and on the detector. It was calculated by means of Montecarlo simulations [3]. The problem of finding the feedings is reduced to solve this equation, for which the "Expectation-Maximization Method" [4], [5] was used. It was shown [5] that this algorithm is a very effective way to solve the TAS inverse problem.

It is known that in some cases, the high resolution (HR) technique assigns incorrectly

more feeding to low lying energy levels (Pandemonium effect) [6]. With the present analysis we aim to study if the decay of  $^{152}\text{Yb}$  proceeds mainly to a single state at 482 keV excitation energy in  $^{152}\text{Tm}$  as measured using the HR technique. The data available in the Nuclear Data Sheets [7] gives an 87.2% of total beta feeding (EC +  $\beta^+$ ) to this level, with 29% of EC. From our analysis an 86.9% was obtained for the total and 29.4% for the EC decay, showing a good agreement with the known HR data. In Fig.1 the comparison of the analyzed spectrum and the reconstructed one after the analysis is presented.

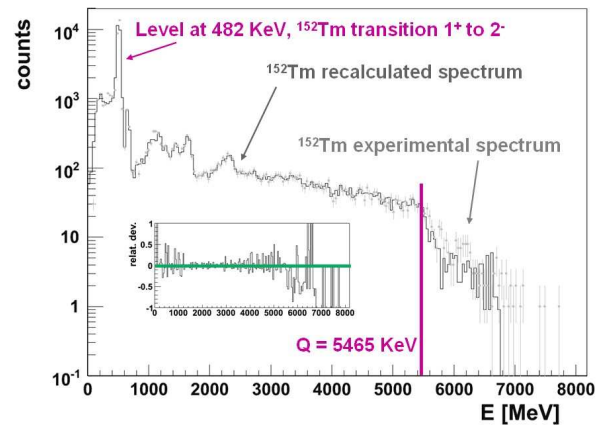


**Figure 1.** Grey dots: X rays gated TAS spectrum. Black line: recalculated spectrum after the analysis.

- a) IFIC, (CSIC-UV), Valencia, Spain,
- b) CIEMAT, Madrid, Spain,
- c) GSI, Darmstadt, Germany,
- d) INFN, Legnaro (Padova) Italy,

[1] J. Bernabeu *et al*, JHEP**12**(Dec.2005)014

[2] M. E. Estevez *et al*, Atomki Annual Report, **2.11** (2007)

[3] <http://geant4.web.cern.ch/geant4/>

[4] J. L. Tain *et al*, NIM A **571** (2007) 738

[5] D. Cano-Ott, Ph.D. thesis, UV, Spain (2000)

[6] J. C. Hardy *et al*, Phys. Lett. B **71** (1977) 307

[7] A. Artna-Cohen, Nuclear Data Sheets **79**, 1 (1996)

## 2.8 Search for Collinear Cluster Tripartition at low excitation energy of heavy nuclei

*D. V. Kamanin<sup>a)</sup>, A. Krasznahorkay, A. A. Aleksandrov<sup>a)</sup>, I. A. Aleksandrova<sup>a)</sup>, M. Csatlós, L. Csige, J. Gulyás, F. Naqvi<sup>b)</sup>, N. A. Kondratyev<sup>a)</sup>, E. A. Kuznyecova<sup>a)</sup>, Yu. V. Pyatkov<sup>a)</sup>, T. Tornyi, V. E. Zhuchko<sup>a)</sup>*

The “true ternary fission”, the case when the fragments have similar masses, started to be investigated soon after the discovery of fission. It became immediately clear that it was a very rare phenomenon. In low energy fission the most detailed studies were performed by Muga et al.[1,2], resulting in true ternary fission yields of about  $10^{-6}$  per binary for  $^{252}\text{Cf}$  spontan fission and for thermal neutron-induced fission of  $^{235}\text{U}$ ,  $^{239}\text{Pu}$  and  $^{241}\text{Pu}$ . Later it was shown [3] that scattering of the fragments have not been effectively eliminated in the work. The results were not confirmed as well by radiochemicalm[4,5] and mass-spectrometric studies [6]. Thus the question is opened so far.

During the last decade number of experiments was devoted to search for a new type of spontaneous ternary decay channel of  $^{252}\text{Cf}$ . It is called “collinear cluster tripartition” (CCT), because the decay fragments fly apart almost collinearly. In the early experiments at the FOBOS spectrometer at the FLNL of the JINR(Dubna, Russia) some unusual structures were observed in the mass-mass plot of fission fragments (FF) of  $^{248}\text{Cm}$  and  $^{252}\text{Cf}$  nuclei. These structures had the yield level of  $\sim 10^{-5}$  -  $10^{-6}$  with respect to conventional binary fission and were treated as an indication of CCT.

In collaboration with FLNR(JINR) we started to study this type of exotic decay mode in low excited nuclear systems in the Cyclotron Laboratory of ATOMKI, Debrecen. The fission was induced by low energy deuteron beam ( $E_d = 9.64$  MeV) on  $^{232}\text{Th}$  target.

In order to demonstrate the CCT in a direct way we were aiming at detecting the three fission fragments in coincidence. Using 3 x 3 Si detectors at both arms of a TOF-E spectrometer, two fragments going to similar direction with a relative angle of  $\geq 1^\circ$  could be separately detected. The MCP based position sen-

sitive start and stop detectors were similar to that is described in ref.[7].

Deatiled investigations of the features of the observed phenomom for evolving its physical model is believed to be a natural goal of the forthcoming experiments.

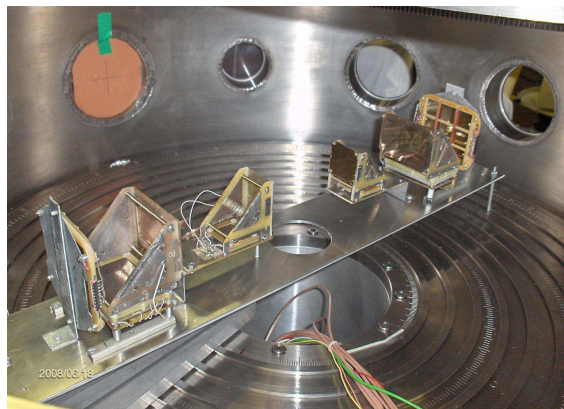


**Figure 1.** Overall view of the time-of-flight vs. energy spectrometer used for studying the  $^{232}\text{Th}(d,f)$  reaction.

### Acknowledgements

The work has been supported by the Hungarian OTKA Foundation No. K 72566 and the MTA-Dub/05 bilateral agreement.

- a) JINR Dubna, Russia
- b) Institute für Kernphysik, Universität zu Köln Köln, Germany
- [1] M. L. Muga *Phy. Rev. Lett.* **11** (1963) 129.
- [2] M. L. Muga *et al.*, *Phys. Rev.* **161** (1967) 1366.
- [3] E. P. Steinberg *et al.*, *Phys. Rev. C* **1** (1970) 2046.
- [4] J. Roy *Can J.Phys.* **39** (1961) 315.
- [5] R. W. Stoenner, M. Hillman *Phys. Rev.* **142** (1966) 716.
- [5] G. Kugler, W. B. Clarke Hillman *Phys. Rev. C* **3** (1971) 849.
- [7] E. M. Kozulin *et al.*, *Instruments and Experimental Techniques* **51** (2008) 44.

## 2.9 Shell correction with finite-range smoothing

*P. Salamon*<sup>a)</sup>, *A. T. Kruppa*, *T. Vertse*<sup>a)</sup>

In the microscopic-macroscopic model suggested by Strutinski [1] the shell correction  $\delta E_{shell} = \tilde{E} - E_{sp}$  is the difference of the smoothed total single particle energy  $\tilde{E}$  and the total single particle energy  $E_{sp}$ . The smoothed energy is calculated as

$$\tilde{E} = \int_{-\infty}^{\tilde{\lambda}} \epsilon \tilde{g}_p(\epsilon) d\epsilon, \quad (5)$$

where

$$\tilde{g}_p(E) = \frac{1}{\gamma} \int_{-\infty}^{+\infty} g_p(\epsilon') f_p\left(\frac{\epsilon' - E}{\gamma}\right) d\epsilon', \quad (6)$$

is the smoothed level density  $\tilde{g}(\epsilon)$  and  $\tilde{\lambda}$  is the smoothed Fermi-level. The smoothing function  $f_p(x) = w(x) h_p(x)$  is composed of a weight function  $w(x)$  and curvature correction polynomials  $h_p(x)$ . The  $h_p(x)$  polynomials are determined by the condition:

$$g_n(x) = \frac{1}{\gamma} \int_{-\infty}^{+\infty} g_n(x') f_p\left(\frac{x - x'}{\gamma}\right) dx'. \quad (7)$$

This later requires that smoothing should not change the original  $g_n(x)$  function if it is a polynomial with degree  $n \leq p + 1$ .

In most of the shell correction calculations so far a Gaussian  $w(x) = \frac{1}{\sqrt{\pi}} \exp(-x^2)$  weight function have been used. The Gaussian disappears only at infinity i.e. it has an infinite energy range. Far from the bottom of the stability valley the effect of the particle continuum should be included. It was observed [2] that in this case the plateau condition might not be fulfilled i.e.  $\delta E_{shell}$  depends on the smoothing width  $\gamma$  and the value of  $p$  used in Eq. (6). A typical example for the dependence is shown by the dashed line in Figure 1., where the dotted line represents the semi-classical value of the shell correction. The minimum value of the dashed curve deviates considerably from the semi-classical value.

We observed that a better agreement with the semi-classical value can be achieved by using a weight function with a finite range:

$$w(x) = \begin{cases} ke^{-\frac{1}{1-x^2}} & , \text{ if } |x| < 1 \\ 0 & , \text{ if } |x| \geq 1. \end{cases} \quad (8)$$

For this we calculated the  $h_p(x)$  polynomials for which the conditions in Eq. (7) are satisfied and computed  $\delta E_{shell}(\gamma)$  for several  $p$  values for a wide range of nuclei. We observed that by selecting the first minimum of the curves, the mean of the values for  $p \in \{4, 6, 8, 10, 12\}$  has a small variance and it is close to the semi-classical value [3]. A typical agreement is shown in Figure 1. Another advantage of the finite-range smoothing is that with this the method can be extended to lighter nuclei.

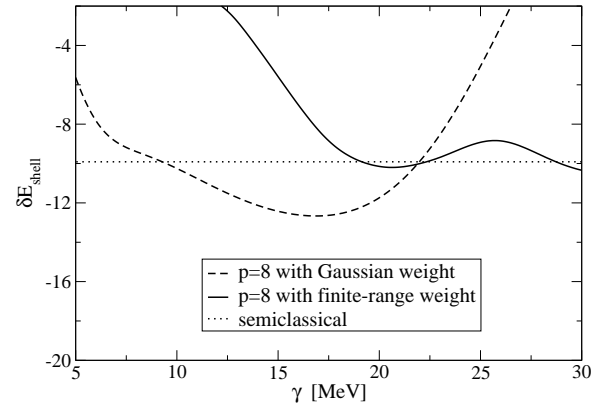


**Figure 1.** Shell corrections for neutrons in  $^{146}\text{Gd}$  nucleus calculated using Gaussian weight function (dashed line) and finite-range weight function (full line) in the smoothing function and the result of the semi-classical calculation (dotted line).

a) University of Debrecen, Faculty of Informatics,  
H-4010 Debrecen, P. O. Box 12, Hungary

- [1] V. M. Strutinski, Nucl. Phys. A **95** (1967) 420 .
- [2] T. Vertse, A. T. Kruppa, R. J. Liotta, W. Nazarewicz, N. Sandulescu, T. R. Werner, Phys. Rev. C **57** (1998) 3089.
- [3] P. Salamon, A. T. Kruppa, T. Vertse, in preparation.

### 3.1 Interaction of intense ultrashort laser pulses with positronium

*S. Borbély<sup>a)</sup>, K. Tókési, L. Nagy<sup>a)</sup>*

The recent development of the positron physics [1] made available the experimental investigation of the interaction between the positronium and short laser pulses [1]. The available studies are mainly focusing on the multiphoton [2] and above-threshold ionization (ATI) [2]. To the best of our knowledge, there is no theoretical study of the positronium ionization in the over-the-barrier (collisional) regime. The investigation of the ionization spectra in the collisional regime is a subject of interest, due to the fact that the underlying ionization mechanism is completely different from the multiphoton and ATI ionization mechanisms. In the present work, a classical trajectory Monte Carlo (CTMC), Volkov and momentum space strong field approximation (MSSFA) [3] models are applied to describe the ionization of the positronium [4] in the over-the-barrier regime. The positronium consists of a core with mass  $m_c$ , with charge  $Z_{eff}$  and of an active electron with mass  $m_e$ . This system is investigated by separating the motion of the center of mass (with mass  $M = m_e + m_c$ ) and the relative motion of the two particles reduced to the motion of a particle with the reduced mass  $\mu = \frac{m_e m_c}{M}$ . The linearly polarized laser pulse is represented by its electric component given by a sine-square enveloped plane wave [4]. In the framework of the Volkov model the ionization probability density for a hydrogen type system is given by

$$\frac{dP}{d\vec{k}} = (2\pi)^3 \left(\frac{q}{\pi}\right)^5 \frac{1}{\left(q^2 + (\vec{k} - \vec{A}(\tau))^2\right)^4},$$

where  $\vec{A}(\tau)$  is the momentum transferred to the active electron from the laser field and  $q = Z_{eff}\mu$ . It can be observed that the electrons are ejected with maximum probability with momentum  $\vec{k} = \vec{A}(\tau)$ , which is determined by the laser pulse. On the other hand the distribution of the electrons around this maximum is determined by the  $q$  parameter, which is defined by the parameters of the hydrogen type system.

For the characterization of the width of the distribution the full-width at half-maximum (FWHM) is used. In the Volkov model the FWHM can be written as  $d_{FWHM} \sim q = Z_{eff}\mu$ . For positronium ( $Z_{eff} = 1$ ,  $\mu = 0.5$ ) the FWHM is the half of the FWHM for hydrogen atom. The scaling laws established in the framework of the Volkov model are also valid for the CTMC and MSSFA results (see Table 1.). The same type of scaling of positron- and electron-impact ionization cross section was observed experimentally [5]. The good agreement between the scaling relations can be a pure coincidence, or it can hide a basic physical cause. To decide which statement is valid, further investigations are needed.

**Table 1.** The FWHM values of the ionization probability densities calculated for different pulse durations ( $\tau$ ).

	MSSFA		Volkov		CTMC	
	H/2	Ps	H/2	Ps	H/2	Ps
$\tau = 3$	0.58	0.63	0.50	0.50	0.51	0.51
$\tau = 5$	0.61	0.66	0.50	0.50	0.51	0.50
$\tau = 10$	0.61	0.69	0.50	0.50	0.54	0.51

#### Acknowledgements

This work was supported by the Romanian academy of Sciences (grant no. 35/2007), the Romanian National Plan for Research (PNII) under contract No. ID 539, the Hungarian National Office for Research and Technology, the grant "Bolyai" from the Hungarian Academy of Sciences, and the Hungarian research Found OTKA (K72172).

a) Babeş-Bolyai University, Faculty of Physics, 400084 Cluj-Napoca, str. Kogălniceanu nr. 1, Romania

- [1] P. Baling *et al.*, NIMB **221**, (2004) 200.
- [2] L. B. Madsen, L. Lambropoulos, Phys. Rev. A **59**, (1999) 4574.
- [3] S. Borbély, K. Tókési, L. Nagy, Phys. Rev. A **77**, (2008) 033412.
- [4] S. Borbély, K. Tókési, L. Nagy, NIMB (2008), doi:10.1016/j.nimb.2008.10.041
- [5] M. Szluinska, P. Van Reeth, G. Laricchia, J. Phys. B **35** (2002) 4059.

### 3.2 Over-the-barrier ionization of H<sub>2</sub>O by intense ultrashort laser pulses

S. Borbély<sup>a)</sup>, K. Tókési, L. Nagy<sup>a)</sup>, D. G. Arbó<sup>b)</sup>

In the last years advanced laser facilities have achieved intensities of the order of  $10^{15}$  W/cm<sup>2</sup> and pulse lengths of the order of 10 fs [1]. With the possibility of fine manipulation of these ultrashort pulses they became a very useful tool in various medical research and application [2-3]. Most of the processes induced by the ultrashort laser pulses in biological tissues can be explained based on the investigation of the interaction between the water molecules and the laser field. In the present work we studied the ionization of the H<sub>2</sub>O molecule by intense half-cycle laser pulses in the over-the barrier regime applying the hydrogenic approximation [4] using classical (CTMC) and quantum mechanical (Volkov) models [5]. In our investigations the single active electron approximation is used, and only the electrons from the two highest occupied molecular orbitals (HOMO), 1B1 and 3A1, were taken into account. In the hydrogenic approximation the active electron is moving in a one center effective Coulomb potential generated by the core with effective charge of  $Z_{eff}$ . The linearly polarized laser pulse is represented by its electric component given by a sine-square enveloped plane wave [5]. Ionization probability densities were calculated using laser pulses with duration of 3 a.u., 5 a.u. and 10 a.u. at laser field intensity  $E_0 = 1$  a.u. The carrier wave frequency is 0.05 a.u. These pulse parameters lead to the value of 0.05 for the Keldysh parameter, which is a characteristic value for the over-the-barrier ionization regime. At first sight both models predict the same probability densities. In each case the electrons are ejected with maximum probability with momentum value  $\vec{A}(\tau)$ , which is the momentum gain from the external laser field. However, important differences can be observed in the maxima of the ionization probabilities. For the CTMC the maxima of the predicted probability densities are shifted toward smaller momenta (see Figure 1). This shift is caused by the Coulomb attraction of the core, which was not taken into account in the Volkov model during and after the ionization.

Beside this shift the probability densities obtained using CTMC and Volkov models are in good agreement at high momentum transfer. In both models the 3A1 probability densities are wider than the 1B1 probability densities, and in the case of the CTMC results the 3A1 probabilities have their maxima at lower energies according to the higher ionization potential. The obtained probability densities have a cylindrical symmetry around the polarization vector. This would not be true, if a correct description of the molecule would be applied. Based on these arguments (strong approximation for the initial state and neglecting the multicenter character of the Coulomb potential) we note that the obtained angular resolved probability densities are not precise within the hydrogenic approximation.

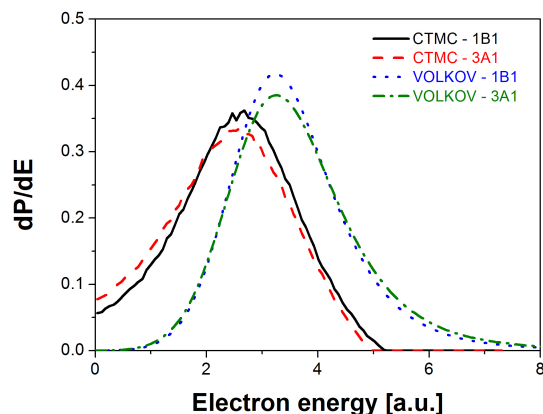


**Figure 1.** Ionization probability density for  $\tau = 5$  a.u. pulse duration.

- a) Babeş-Bolyai University, Faculty of Physics, 400084 Cluj-Napoca, str. Kogălniceanu nr. 1, Romania
- b) IAFE, Institute for Astronomy and Space Physics, Buenos Aires, CC 67, Suc. 28(1428), Argentina
- [1] B. Schenkel *et al.*, Opt. Lett. **28** (2003) 1987.
- [2] T. Juhász *et al.*, IEEE J. Sel. Top. Quant. **5** (1999) 902.
- [3] S. H. Chung *et al.*, BMC Neuroscience **7**, **30** (2006).
- [4] S. Borbély, K. Tókési, L. Nagy, D. G. Arbó, AIP Conference Proceedings 1080, 2008, 145.
- [5] S. Borbély, K. Tókési, L. Nagy, Phys. Rev. A **77**, (2008) 033412.

### 3.3 Limitations of the strong field approximation in ionization of the hydrogen atom by ultrashort pulses

*D. G. Arbó<sup>a)</sup>, K. Tórkési, J. E. Miraglia<sup>a,b)</sup>*

We presented a theoretical study of the ionization of hydrogen atoms as a result of the interaction with an ultrashort external electric field. Doubly-differential momentum distributions and angular momentum distributions of ejected electrons calculated in the framework of the Coulomb-Volkov and strong field approximations, as well as classical calculations are compared with the exact solution of the time dependent Schrödinger equation.

We have shown that the Coulomb-Volkov approximation (CVA) describes the quantum atomic ionization probabilities exactly when the external field is described by a sudden momentum transfer [1]. The velocity distribution of emitted electrons right after ionization by a sudden momentum transfer is given through the strong field approximation (SFA) within both the CVA and CTMC methods. In this case, the classical and quantum time dependent evolutions of an atom subject to a sudden momentum transfer are identical. The difference between the classical and quantum final momentum distributions resides in the time evolution of the escaping electron under the subsequent action of the Coulomb field. Furthermore, classical mechanics is incapable of reproducing the quantum angular momentum distribution due to the improper initial radial distribution used in the CTMC calculations, i.e., the microcanonical ensemble. We find that in the limit of high momentum transfer, based on the SFA, there is a direct relation between the cylindrical radial distribution  $dP/d\rho$  and the final angular momentum distri-

bution  $dP/dL$ . This leads to a close analytical expression for the partial wave populations  $(dP/dL)^{\text{SFA-Q}}$  given by

$$\frac{dP^{\text{SFA-Q}}}{dL} = \frac{4Z^3 L^2}{(\Delta p)^3} K_1(2ZL/\Delta p). \quad (9)$$

which, together with the prescription  $L = l + 1/2$ , reproduces quite accurately the quantum (CVA) results. Considering the inverse problem, knowing the final angular momentum distribution can lead to the inference of the initial probability distribution, and consequently, the atomic potential. The SFA prediction for the most probable partial population results to be very accurate except in the dipole regime, when  $l_0 = 1$ .

The authors acknowledge fruitful discussions with M. S. Gravielle. This work was performed with financial support of CONICET, UBACyT, and ANPCyT PICT 772 of Argentina, the Hungarian-Argentine collaboration PA05-EIII/007, the Bolyai grant from the Hungarian Academy of Sciences, the Hungarian National Office for Research and Technology and the Hungarian Scientific Research Found OTKA (K72172). One of us (KT) was also partially supported by the European COST Action CM0702.

a) Institute for Astronomy and Space Physics, IAFE, CC 67, Suc. 28 (1428) Buenos Aires, Argentina

b) Department of Physics, FCEN, University of Buenos Aires, Argentina

[1] D. G. Arbó, K. Tórkési, J. E. Miraglia, *Eur. Phys. J. D.* in press.

### 3.4 Atomic ionization by a sudden momentum transfer

*D. G. Arbó<sup>a)</sup>, K. Tórkési, J. E. Miraglia<sup>a,b)</sup>*

The Coulomb-Volkov approximation (CVA) has been widely used to describe the ionization of atoms by short laser pulses in the last decade. The CVA is a time-dependent distorted-wave theory that allows us to include the effect of the remaining core into the final state at the same approximation level as the external field. In this way, the collision dynamics due to the effects of the core potential on the detached electron can be directly probed. Several studies have been performed so far to determine the accuracy of the CVA.

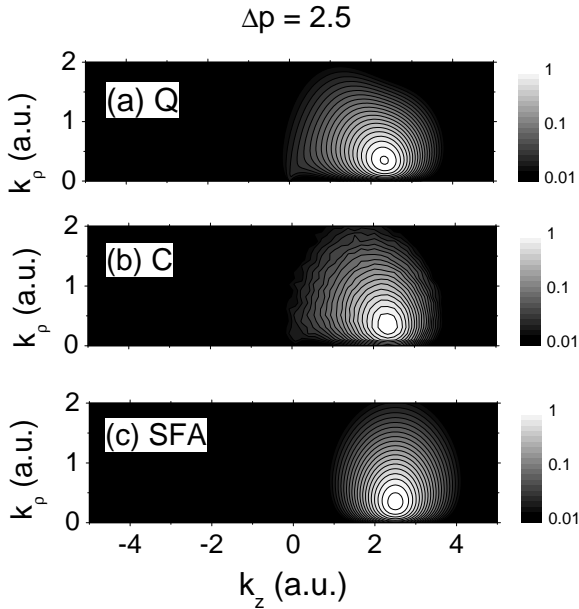


**Figure 1.** Doubly-differential electron momentum distributions (logarithmic scale) in cylindrical coordinates  $(k_z, k_\rho)$ . (a) quantum, (b) classical, and (c) SFA. The momentum transfer is  $\Delta p = 2.5$ .

On the other hand, in the last two decades there was a great revival of the classical tra-

jectory Monte Carlo (CTMC) calculations applied to atomic collisions involving three or more particles. These approximations gain importance in those cases when higher order perturbations should be applied or many particles take part in the processes. The CTMC method has been quite successful also in dealing with the ionization process in laser-atom collisions, when, instead of the charged particles, electromagnetic fields are used for excitation of the target.

In the present work we study the efficiency of the strong field approximation (SFA), which is a variant of the CVA [1]. The electron emission spectra of a hydrogen atom excited by ultra-short pulses are calculated within the framework of CVA and a classical trajectory Monte Carlo (CTMC) method (see Fig. 1.). We analytically prove that in the limit of zero pulse duration and finite momentum transfer, CVA reproduces the exact quantum mechanical electron yields.

The authors acknowledge fruitful discussions with M. S. Gravielle. This work was performed with financial support of CONICET, UBACyT, and ANPCyT PICT 772 of Argentina, the Hungarian-Argentine collaboration PA05-EIII/007, the Bolyai grant from the Hungarian Academy of Sciences, the Hungarian National Office for Research and Technology and the Hungarian Scientific Research Found OTKA (K72172). One of us (KT) was also partially supported by the European COST Action CM0702.

a) Institute for Astronomy and Space Physics, IAFE, CC 67, Suc. 28 (1428) Buenos Aires, Argentina

b) Department of Physics, FCEN, University of Buenos Aires, Argentina

[1] D. G. Arbó, K. Tórkési, J. E. Miraglia, Nucl. Instr. Meth. B in press.

### 3.5 Ionization of helium and argon by very slow antiproton impact

*H. Knudsen<sup>a)</sup>, H.-P. E. Kristiansen<sup>a)</sup>, H. D. Thomsen<sup>a)</sup>, U. I. Uggerhoj<sup>a)</sup>, T. Ichioka<sup>a)</sup>, S. P. Moller<sup>b)</sup>, C. A. Hunniford<sup>c)</sup>, R. W. McCullough<sup>c)</sup>, M. Charlton<sup>d)</sup>, N. Kuroda<sup>e)</sup>, Y. Nagata<sup>e)</sup>, H. A. Torii<sup>e)</sup>, Y. Yamazaki<sup>e,f)</sup>, H. Imao<sup>f)</sup>, H. H. Andersen<sup>g)</sup>, K. Tókési*

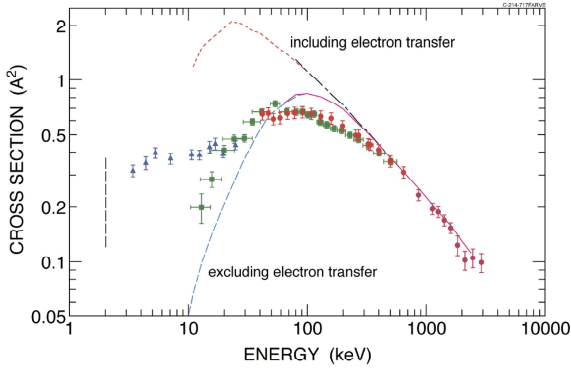


**Figure 1.** Single ionization of He by antiproton impact. The present data (triangle, [1]) are compared with the antiproton data by (circle) Andersen et. al. [2] and (square) Hvelplund et. al. [3]. Also shown are proton data by the Belfast group [4,5] as curves. The vertical line indicates the limit for total ion and projectile collection of our apparatus.

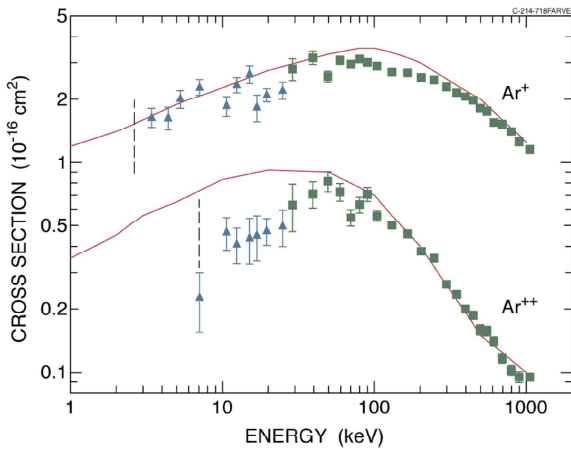


**Figure 2.** Present data (triangle) and the results of (square) Paludan et. al. [6] are compared with the calculations of Kirchner et. al. [7] which are shown as curves. The vertical lines indicate the lower limit for total collection of our apparatus.

The total cross sections for single ionization of helium (Fig. 1.) and single and double ionization of argon by antiproton impact (Fig. 2.) have been measured in the kinetic energy range from 3 to 25 keV using a new technique for the creation of intense slow antiproton beams. The

new data provide benchmark results for the development of advanced descriptions of atomic collisions and we show that they can be used to judge, for the first time, the validity of the many recent theories.

We would like to thank our collaborators in the CERN ASACUSA collaboration and the staff at the CERN AD for much help and support. Also thanks are due Poul Aggerholm for his tireless practical help. This work was supported by the Danish Natural Science Research Council, the UK Engineering and Physical Sciences Research Council and the Hungarian Scientific Research Fund OTKA (K72172). We also acknowledge the Grant-in-Aid for Specially Promoted Research (no. 19002004) of MEXT (Monbukagakaku-Sho).

- a) Department of Physics and Astronomy, University of Aarhus, Denmark
- b) Institute for Storage Ring Facilities, University of Aarhus, Denmark
- c) Department of Physics, Queens University Belfast, UK
- d) Department of Physics, University of Swansea, UK
- e) Institute of Physics, Komaba, University of Tokyo, Japan
- f) Atomic Physics Laboratory, RIKEN, Saitama, Japan
- g) Niels Bohr Institute, University of Copenhagen, Denmark

- [1] H. Knudsen *et al.*, Phys. Rev. Lett. **101** (2008) 043201.
- [2] L. H. Andersen *et al.*, Phys. Rev. A **41** (1990) 6536.
- [3] P. Hvelplund *et al.*, J. Phys. B **27** (1994) 925.
- [4] M. B. Shah and H. B. Gilbody J. Phys. B **18** (1985) 899.
- [5] M. B. Shah, P. McCallion and H. B. Gilbody J. Phys. B **22** (1989) 3037.
- [6] K. Paludan, *et al.*, J. Phys. B **30** (1997) 3951.
- [7] T. Kirchner, M. Horbath and H. J. Lüdde Phys. Rev. A **66** (2002) 052719.

### 3.6 On the double ionization of helium by very slow antiproton impact

*H. Knudsen<sup>a)</sup>, H.-P. E. Kristiansen<sup>a)</sup>, H. D. Thomsen<sup>a)</sup>, U. I. Uggerhoj<sup>a)</sup>, T. Ichioka<sup>a)</sup>, S. P. Moller<sup>b)</sup>, C. A. Hunniford<sup>c)</sup>, R. W. McCullough<sup>c)</sup>, M. Charlton<sup>d)</sup>, N. Kuroda<sup>e)</sup>, Y. Nagata<sup>e)</sup>, H. A. Torii<sup>e)</sup>, Y. Yamazaki<sup>e,f)</sup>, H. Imao<sup>f)</sup>, H.H. Andersen<sup>g)</sup>, K. Tókési*

In this work we present experimental data for the double ionization cross section of helium for 3–25 keV antiproton impact and we also compare these data with the various calculations as well as with previously published experimental data. Our present results can be used to discern between many advanced theoretical calculations. Earlier measurements of the ratio  $R$  between the double and single ionization cross sections for antiproton impact on helium show a persistent increase for the projectile energy decreasing from 10 MeV to 10 keV. The present data show that below 10 keV this increase stops and we give an upper limit to  $R$ . For double ionization of helium by slow antiproton impact, the mutual disagreement between various published theoretical calculations is even worse - amounting to as much as a factor of 20 at 1 keV.

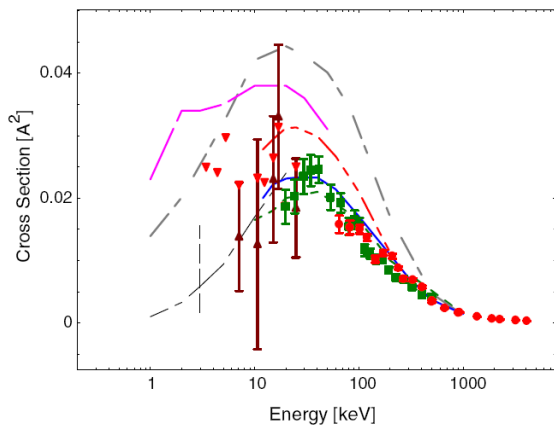


**Figure 1.** The cross section for double ionization of helium by antiproton impact. The vertical dashed line indicates the lowest impact energy for which our apparatus accepts more than 90% of the ions and the scattered antiprotons. Triangle: present experiment [1], circle: experiment [2], square: experiment [3], Theories: Blue solid line [4], dot-dot-dashed line [4], dashed line [5], thin dash-dotted line [6], thick dash-dotted line [7], pink solid line [8].

#### Acknowledgement

We would like to thank our collaborators in the CERN ASACUSA collaboration and the staff at the CERN AD for much help and support. Also thanks are due Poul Aggerholm for his tireless practical help. This work was supported by the Danish Natural Science Research Council, the UK Engineering and Physical Sciences Research Council and the Hungarian Scientific Research Fund OTKA (K72172). We also acknowledge the Grant-in-Aid for Specially Promoted Research (no. 19002004) of MEXT (Monbukagakaku-Sho).

- a) Department of Physics and Astronomy, University of Aarhus, Denmark
- b) Institute for Storage Ring Facilities, University of Aarhus, Denmark
- c) Department of Physics, Queens University Belfast, UK
- d) Department of Physics, University of Swansea, UK
- e) Institute of Physics, Komaba, University of Tokyo, Japan
- f) Atomic Physics Laboratory, RIKEN, Saitama, Japan
- g) Niels Bohr Institute, University of Copenhagen, Denmark

- [1] H. Knudsen *et al.*, Nucl. Instr. and Meth. B, in press (2009).
- [2] L. H. Andersen *et al.*, Phys. Rev. A **41** (1990) 6536.
- [3] P. Hvelplund *et al.*, J. Phys. B **27** (1994) 925.
- [4] J. F. Reading, T. Bronk, A. L. Ford, L.A. Wehrmann, K. A. Hall, J. Phys. B **30** (1997) L159.
- [5] M. Foster, J. Colgan, M. S. Pindzola, Phys. Rev. Lett. **100** (2008) 033201.
- [6] G. Bent, P.S. Kristić, D. R. Schultz, J. Chem. Phys. **108** (1998) 1459.
- [7] M. Keim, A. Aschenbach, H. J. Lüdde, T. Kirschner, Phys. Rev. A **67** (2003)
- [8] T. Kirschner, M. Horbatsch, E. Wagner, H. J. Lüdde, J. Phys. B **35** (2002) 925.

### 3.7 (e,2e) study of resonant Auger decay

*M. Žitnik<sup>a)</sup>, M. Kavčič<sup>a)</sup>, K. Bučar<sup>a)</sup>, B. Paripás<sup>b)</sup>, B. Palásthy<sup>b)</sup>, K. Tőkési*

We have measured for the first time a series of resonant Auger spectra emitted after the electron impact excitation of the  $[2p]$  hole in argon [1]. The electron spectra were measured at 10 different primary energies at an electron energy between 442.6 eV and 461.7 eV by the (e,2e) technique (see Fig. 1.).

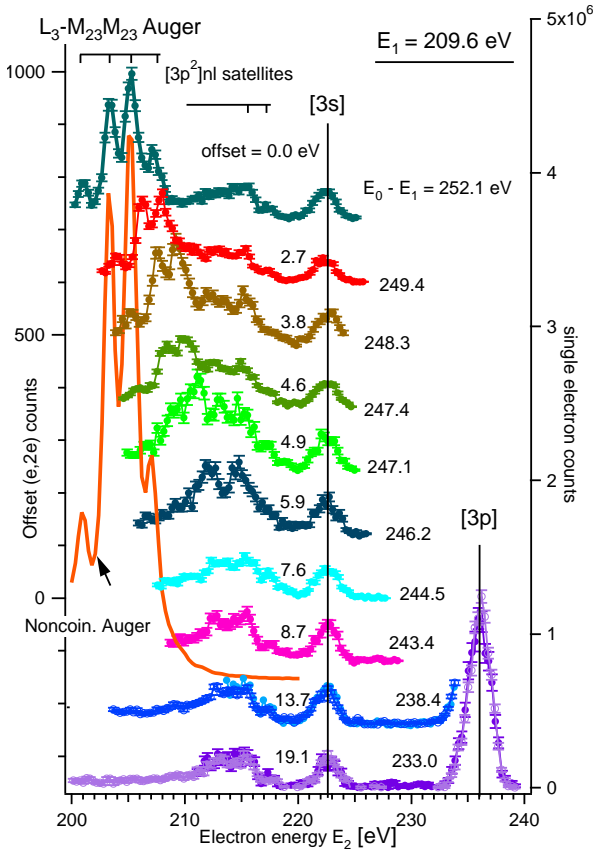


**Figure 1.** Coincidence spectra measured at 10 different values of  $E_0$  primary energies. The energy loss  $E_0 - E_1$  falls into the region of argon L threshold. There is an offset in energy  $E_2$  to align the peaks pertaining to  $[3s]$  final state (a constant ionic state - CIS spectrum). The energy of single pass detector was fixed to  $E_1=209.6$  eV. For comparison the non-coincidence Auger L-MM of double pass detector is given (full line curve).

During the measurement of spectra the en-

ergy of the second electron was kept fixed at 209.6 eV which is one of the strongest resonant Auger transitions from the  $[2p_{3/2}]3d$  state. The peaks, produced by the direct outer-shell ionization ( $[3p]$  and  $[3p^2]nl$  satellites), dominate in each spectra, under 244 eV energy loss (bottom two spectra) it is the only component. The remaining part of the other spectra is caused by inner-shell processes: normal Auger (upper two spectra) and resonant Auger (six spectra in the middle) processes. The resonant Auger spectra are explained on the basis of the photon impact data (e. g.  $[2p_{3/2}]3d$  state at 247.1 eV and  $[2p_{3/2}]4s$  state at 244.5 eV energy loss). However, more precise modelling would require the inclusion of monopole excitation of  $[2p_{3/2}]4p$  at 246.2 eV energy loss. The Auger energies and transition rates connecting the intermediate  $[2p]np$  and final  $[3p^2]np$  states could be calculated, in a manner similar to [2] and the expected nondipole component of the Resonant Auger spectra could be generated and included it into the modelling of the measured coincidence spectra.

#### Acknowledgment

This work was supported by the Tét Grant No. SLO-15/05 (BI/HU-06-07-015), the grant “Bolyai” from the Hungarian Academy of Sciences, the Hungarian National Office for Research and Technology and the Hungarian Scientific Research Found OTKA (K72172).

- a) J. Stefan Institute, Jamova 39, P.O.B. 3000, SI 1000, Ljubljana, Slovenia, EU
- b) Department of Physics, University of Miskolc, 3515 Miskolc-Egyetemváros, EU
- [1] M. Žitnik, M. Kavčič, K. Bučar, B. Paripás, B. Palásthy, K. Tőkési, Nucl. Instr. Meth. B in press.
- [2] J. A. de Gouw, J. van Eck, A. C. Peters, J. van der Weg and H. G. M. Heideman, J. Phys. B **28** (1995) 2127.

### 3.8 Selective enhancement of $1s2s2p\ ^4P_J$ metastable states populated by cascades in single-electron transfer collisions of $F^{7+}(1s^2/1s2s\ ^3S)$ ions with He and $H_2$ targets

T. J. M. Zouros<sup>a,b</sup>), B. Sulik, L. Gulyás, K. Tókési

A mechanism for the selective population of  $1s2s2p\ ^4P_J$  states by electron capture in energetic collisions of  $F^{7+}(1s2s\ ^3S)$  ions with  $H_2$  and He is elucidated [1].

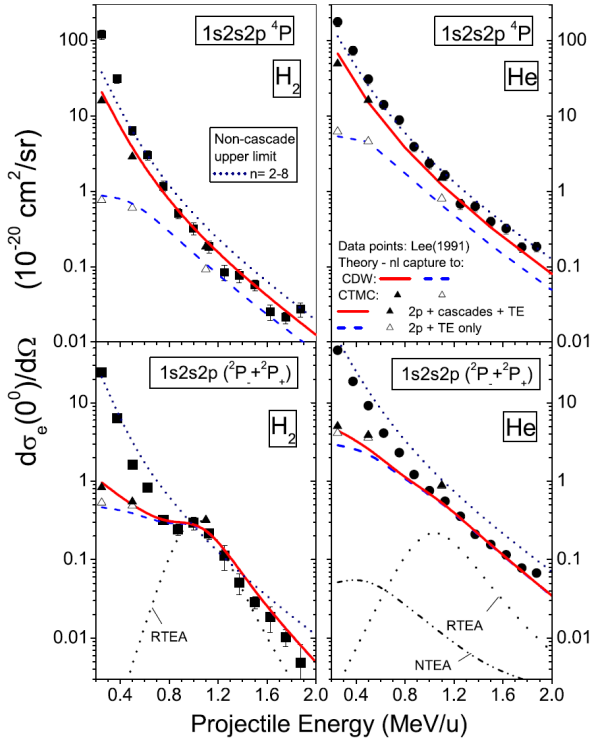


**Figure 1.** Data points: Absolute  $0^\circ$  Auger emission single differential cross sections for the  $1s2s2p\ ^4P$  (top) and the sum of  $1s2s2p\ ^2P_\pm$  (bottom) levels for  $H_2$  (left) and He (right) from [2]. Theory: Lines (continuum distorted wave) and triangles (classical trajectory Monte Carlo). Red continuous lines and filled triangles include feeding by cascades from  $(1s2s\ ^3S)nl$  with  $n=3-5$ , while dashed blue lines and open triangles do not ( $n=2$  only). Transfer excitation, TE (resonant transfer excitation, RTE and nonresonant transfer excitation, NTE) Auger contributions to the  $^2P_\pm$  from the  $1s^2$  are also shown. There is no TE contribution to the  $^4P$ . An upper limit estimate to capture into the sum of  $n=2-8$  levels is also given (densely dotted line).

Capture calculations indicate  $(1s2s\ ^3S)nl\ ^{2,4}L$  doublet and quartet levels to be strongly populated for  $n=2-5$ . Following capture the dou-

blets Auger decay strongly to the  $1s^2$  ground state allowing for negligible feeding of other lower-lying doublets by radiative transitions. The quartets, however, find this decay channel blocked by spin conservation and instead radiatively cascade through lower lying quartets, eventually strongly populating the lowest-lying  $1s2s2p\ ^4P_J$  levels in agreement with older experimental results for collision energies above  $0.7\text{ MeV/u}$ .

We gave a detailed analysis demonstrating the existence of a selective cascade-feeding mechanism resulting in the preferential population of low-lying long-lived metastable levels. For the particular collision system reported here, at collision energies above  $0.7\text{ MeV/u}$ , this mechanism is found to be largely responsible for the recently reported nonstatistical enhancement of the  $1s2s2p\ ^4P$  states [3]. Below  $0.7\text{ MeV/u}$ , our understanding of both  $^2P_\pm$  and  $^4P$  production seems incomplete and further investigation is clearly necessary to understand the large discrepancies between theory and experiment. These results also underscore the significance of cascades, especially when metastable states are involved.

This work was supported by Greek–Hungarian S&T Grant No. GR–11/03, the grant Bolyai from the Hungarian Academy of Sciences, and OTKA Grants No. T046905 and No. IN64319.

- a) Department of Physics, University of Crete, P.O. Box 2208, 71003 Heraklion, Crete, Greece
- b) Institute of Electronic Structure and Laser, FORTH, P.O. Box 1385, GR-71110 Heraklion, Crete, Greece

- [1] T. J. M. Zouros, B. Sulik, L. Gulyás, K. Tókési, *Phys. Rev. A* **77** (2008) 050701(R).
- [2] D. H. Lee *et al.*, *Phys. Rev. A* **44** (1991) 1636; *Nucl. Instrum. Methods Phys. Res. B* **56/57**, (1991) 99.
- [3] J. A. Tanis *et al.*, *Phys. Rev. Lett.* **92** (2004) 133201; **96**, (2006) 019901(E).

### 3.9 Plasma diagnostics by X-ray crystal spectroscopy

R. Rácz, E. Takács<sup>a)</sup>, S. Biri

Years ago the ECRIS group set oneself an aim to understand the features and behaviour of plasmas better. For the sake of the cause plasma diagnostics measurements have been realised. One of these is the X-ray spectroscopy.

Two methods of plasma diagnostics have been used since 2002: imaging of ECR plasmas with pinhole X-ray camera and X-ray crystal spectroscopy. Methods are based on the fact that the plasma emits radiations in X-ray electromagnetic spectrum.

The first way (pinhole X-ray camera) has good spatial resolution. Ar, Xe and Fe plasmas were generated and analysed. For example these measurements manifested that the well-known "triangle" or "star" shape at the plasma electrode has surprising structure at low magnetic field. Furthermore this behaviour is independent on the ionization degree of the plasma and depends only on the magnetic field strength at the extraction side [1].

The second way (X-ray crystal spectroscopy) has good energy resolution. This method is based on the Bragg diffraction. We used a Johann-type variable-radius curved crystal spectrometer. Curved crystal spectrometers are generally used when the efficiency of the instrument is important. With extended diffuse X-ray source, such a plasma, the source was placed on the Rowland circle. The Johann geometry focuses all rays from a point source on the Rowland circle.

Because of the minimum spatial resolution of position sensitive detector and because of the fixed crystal-to-detector distance we had to use a variable curved radius spectrometer to provide satisfactory resolution at wide Bragg interval.

K-alpha lines intensity of different charge state Ar ions of the ATOMKI-ECRIS plasma were compared with extracted beam spectra. We have used a CCD camera (direct detection of X-ray) as position-sensitive detector.

Ar plasmas were generated by injecting different microwave power into the ECR plasma. First we increased the microwave power from 25W to 150W and we measured K-alpha line intensities. Increasing of microwave power resulted in higher Ar K-alpha line intensity.

Then highly charged Ar plasma was generated at 900W microwave power. We measured K-alpha lines intensities of different charge state Ar ions. At the same time extracted beam current spectra were recorded. We have compared the two measured values and the most important result is the strong correlation between the X-ray spectra and the extracted beam spectra (fig. 1.) [2].

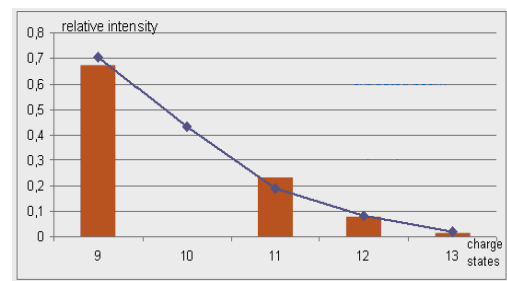


**Figure 1.** Comparison of characteristic X-ray (columns) and extracted beam (line) spectra

a) Institute of Experimental Physics, University of Debrecen

[1] S. Biri, A. Valek, T. Suta, L. T. Hudson, B. Radics, J. Imrek, B. Juhász and J. Pálkás, *Review of Scientific Instruments* **75** (2004) 1420-1422.

[2] Rácz R., *X-ray crystal spectroscopy of highly charged ion plasma*. Diploma work University of Debrecen, 2008.

### 3.10 Study of the role of post-collision interaction and two-center effects in the formation of the two-electron cusp

*L. Sarkadi and A. Orbán*

In a recent experiment [1] we found evidence for the existence of the two-electron cusp in atomic collisions, i.e., the enhanced simultaneous emission of two electrons in forward direction with velocities equal to that of the projectile. In the experiment the energies of the two electrons resulting from the mutual target and projectile ionization in 100 keV  $\text{He}^0 + \text{He}$  collisions were measured. The strong correlation observed between the energies of the electrons was explained by an angular correlation of  $180^\circ$  in the projectile-centered reference system. For the interpretation of the experimental results we carried out a Monte Carlo simulation based on the Wannier theory [2] for the two-electron break-up process at threshold.

We found only a qualitative agreement between the results of the Monte Carlo simulation and the experimental data. We attributed the deviations from the predictions of the Wannier theory to the occurrence of a post-collision interaction (PCI) between the electrons and the receding ionized target. To account for this effect, in the present work we included PCI in the Monte Carlo simulation by a simple model calculation [3].

In our model we assumed that PCI can be treated independently for the two ejected electrons. As a result of this approximation, the Coulomb three-body problem could be reduced to the analytically solvable two-body problem of the electron - target system. The model has one free parameter: The internuclear distance at which the evolution of the collision system into the Wannier-type correlated two-electron final state terminates.

Although the inclusion of PCI resulted in a significant improvement in the description of the shape of the two-electron cusp, the energy of the peak shifted to lower energies, in strong disagreement with the observation. This finding indicates the presence of a two-center effect in the process: The time evolution of the correlated two-electron state is affected not only by the electric field of the target but also that

of the projectile. For the inclusion of the effect in the simulation, we developed a simple correction procedure on the basis of physical considerations. The good performance of the latter model in the description of the experimental data (see Figure 1) supports the picture that two-center effect might have a notable importance in the formation of the two-electron cusp.

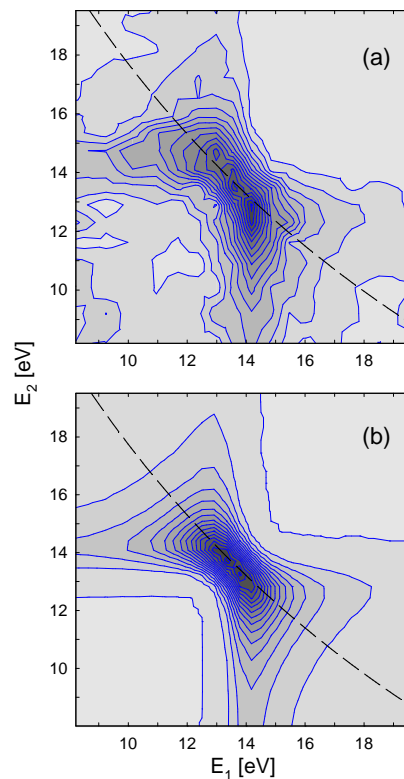


**Figure 1.** Contour plots of the fourfold differential cross section (FDCS) for the two-electron ejection as a function of the electron energies. Part (a): Measured FDCS. Part (b): FDCS obtained by the present Monte Carlo simulation with inclusion of the two-center effect. The dashed line shows the case of infinitely sharp  $180^\circ$  angular correlation between the electrons.

- [1] L. Sarkadi and A. Orbán, *Phys. Rev. Lett.* **100** (2008) 133201.
- [2] G. H. Wannier, *Phys. Rev.* **90** (1953) 817.
- [3] L. Sarkadi and A. Orbán, *Nucl. Instr. Meth. B*, in press.

### 3.11 Electronic structure of nanocrystalline TiO<sub>2</sub> particles

Zs. Jánosfalvi, I. Cserny, L. Kövér

There are three different phases of natural crystalline form of TiO<sub>2</sub>; rutile, anatase and brookite. Recent studies have pointed out that at nano sizes these phases have different environmental effects [1]. Nano-anatase particles proved to be most cytotoxic to human cells in culture. Comparing the toxicity of nano-anatase particles to that of nano-rutile particles, it was found that the nano-anatase is more than hundred times toxic [1].

Although earlier studies are available [2] concerning the electronic structure of the bulk TiO<sub>2</sub> of different crystalline forms, much less is known for nano-crystalline TiO<sub>2</sub> particles. In Ref [2] for all the three crystalline form of bulk TiO<sub>2</sub> the electronic structure and the respective optical properties were calculated. Comparing the total and partial density of states (DOS) and the optical properties for all crystalline phases of TiO<sub>2</sub> only minor differences can be seen.

The calculated optical properties[3] of anatase single crystals obtained by the FP-LAPW method [4] agree well with the recent experimental data. For small nano-clusters first principle calculations were made; and in addition, for smaller and larger nano-clusters the self-consistent tight binding model was used. After full geometry optimization surface relaxation and a small overall contraction of the nano-particles were found [5].

Our preliminary results show that the discrete variational  $X_\alpha$  molecular orbital calculations [6] for clusters of different sizes are suitable for investigating the electronic structures of anatase and rutile TiO<sub>2</sub> nano-particles. Due to surface effects, in the case of clusters the band gap is narrower and for anatase the DOS at lowest unoccupied electronic states is higher, promoting higher photocatalytic activity (Fig.1.). Further theoretical and experimental (using photoelectron and electron energy loss spectroscopy) studies on the size dependence of the electronic structure of TiO<sub>2</sub> nanocrystals are in progress.

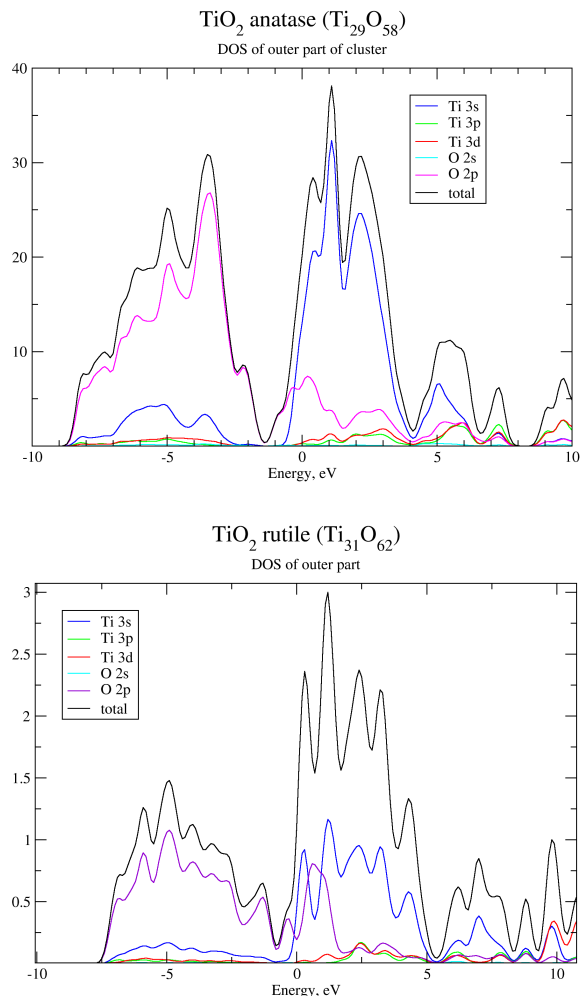


**Figure 1.** Comparison of densities of electronic states for very small nanoparticles ( 1.2 nm). Contributions from outer groups of atoms are separated to indicate surface effects.

- [1] Sayes, Ch.M., *et al.*, *Toxicological Sciences* **92** (2006) 174.
- [2] Mo, Shang-Di and Ching, W.Y. *Phys. Rev., B* **51** (1995) 13023.
- [3] Asahi, R., *et al.*, *Phys. Rev., B* **61** (2000) 7459.
- [4] P. Blaha *et al.*, WIEN2K (2002) Technische Universität Wien, <http://www.wien2k.at/>
- [5] Barnard, A. S., *et al.*, *Phys. Rev., B* **73** (2006) 205405.
- [6] Adachi, H., *et al.*, *J. Phys. Soc. Jpn.*, **45** (1978) 875.

### 3.12 Comparative study of fragmentation of $H_2S$ and $H_2O$ molecules following slow ion-molecule collisions

Z. Juhász, B. Sulik, F. Frémont<sup>a)</sup>, A. Hajaji<sup>a)</sup>, J.-Y. Chesnel<sup>a)</sup>

Fragmentation of water molecules by highly charged ions is of relevance in radiation damage of biological tissues, and was recently studied by different groups [1, 2]. Anisotropic fragment emission was observed, and molecular orientation sensitivity of electron transfer processes was considered as a possible origin.

Our previous studies have shown asymmetric fragment emission with forward enhancement [3, 4]. This was difficult to explain by post collision effects of the projectile or direct nucleus-nucleus interaction so it was considered as a strong indication of molecular orientation effects. Therefore we proposed to do similar experiments with the  $H_2S$  molecule, which has a similar structure, expecting similar anisotropic behavior.

Previously we also found that there is large difference in the efficiency of different fragmentation channels in fragmentation by H like projectiles ( $N^{6+}$ ,  $O^{7+}$ ) in case of methane target. This was an unexpected finding. We also investigated this effect on water and  $H_2S$ .

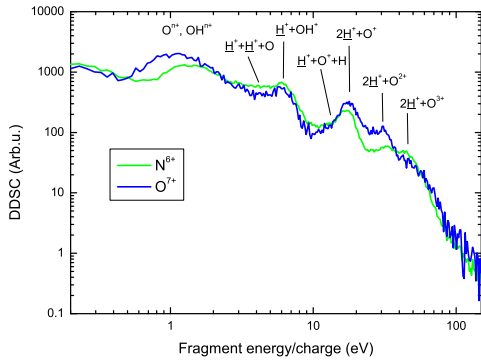


**Figure 1.** Energy spectra of light (proton) and heavy fragments in collision systems of 60 keV  $N^{6+} + H_2O$  and 70 keV  $O^{7+} + H_2O$  at 90° observation angle.

We performed our experiments at the ARIBE facility in GANIL, Caen, France within the framework of the ITS-LEIF collaboration.

Double differential cross sections with respect to energy and solid angle have been measured for molecule fragments. Fragmentation of  $H_2O$  and  $H_2S$  molecules were investigated by 60 keV  $N^{6+}$  and 70 keV  $O^{7+}$  impact.

It was found that despite their similarity,  $H_2O$  and  $H_2S$  exhibit significantly different fragmentation patterns. We did not find anisotropies with forward enhancement for any of the fragmentation channels in the case of  $H_2S$  target that would indicate molecular orientation effects. Other types of anisotropies were found indicating the presence of post collision and nucleus-nucleus effects.

Comparing the results for different projectiles it is obvious that the efficiency of different fragmentation channels is highly dependent on the projectile. This is true both for  $H_2O$  and  $H_2S$  targets and is shown in Fig. 1 and 2. It seems that some of the fragmentation channels corresponding to certain multiple ionization of the target are enhanced in the case of  $O^{7+}$  projectile, while the others are reduced.

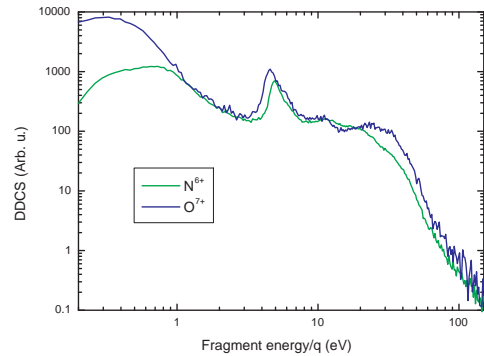


**Figure 2.** Energy spectra of light (proton) and heavy fragments in collision systems of 60 keV  $N^{6+} + H_2S$  and 70 keV  $O^{7+} + H_2S$  at 90° observation angle.

Clear theoretical explanations has not been developed so far, but the most likely explanation is that deep inner shell capture processes

are possible with the  $O^{7+}$  projectile, which may be followed by Auger processes leading to extra ionization of the targets.

### *Acknowledgements*

This experiment has been performed at the distributed LEIF-Infrastructure at ARIBE, GANIL, France, supported by Transnational Access granted by the European Project HPRI-CT-2005-026015. The work was supported by the French-Hungarian S&T Grant No. F-30/06 and the Hungarian National Science Foundation OTKA (Grant No's: T046905, K73703 and PD050000).

a) Centre de Recherche sur les Ions, les Matériaux et la Photonique (CIMAP) Unité Mixte CEA-CNRS-EnsiCaen-Université de Caen Basse-Normandie UMR 6252, 6 Boulevard Maréchal Juin, F-14050 CAEN cedex 04, FRANCE

- [1] P. Sobocinski, Z. D. Pešič, R. Hellhammer, D. Klein, B. Sulik, J.-Y. Chesnel and N. Stolterfoht, *J. Phys. B* **39** (2006) 927.
- [2] F. Alvarado, R. Hoekstra and T. Schlathölder, *J. Phys. B: At. Mol. Opt. Phys.* **38** (2005) 4085-4094.
- [3] Z. Juhász, B. Sulik, F. Frémont, A. Hajaji, J.-Y. Chesnel, *Nucl. Instr. and Meth. in Phys. Res. B* **267** (2006) 326.
- [4] Z. Juhász, J.-Y. Chesnel, F. Frémont, A. Hajaji, B. Sulik, *Proceedings of the 5th International Conference RADAM 2008*, AIP Conference Proceedings 1080 (2008)118-121.

### 3.13 Ion guiding in alumina capillaries: MCP images of the transmitted ions

Z. Juhász, B. Sulik, Gy. Vikor, S. Biri, I. Iván, K. Tókési,  
S. Mátéfi-Tempfli<sup>a)</sup>, M. Mátéfi-Tempfli<sup>a)</sup>, E. Takács<sup>b)</sup>, J. Pálinkás<sup>b)</sup>

Guiding properties of insulating nanocapillaries have recently attracted a considerable attention. From the discovery that slow highly charged ions are efficiently transmitted and directed by insulating nanocapillaries without altering the initial charge state [1], different groups investigated this remarkable phenomenon for different capillary materials including our group [2,3]. Guiding effect has been found for all the investigated insulating materials. The technique in the majority of these experiments was single ion detection by electrostatic spectrometers, with which data are collected only from a small solid angle at an instant. Experiments with position sensitive detectors are scarce [4].

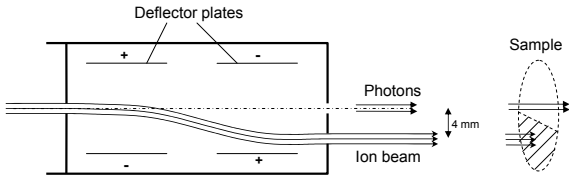


**Figure 1.** Schematic view of the ion beam deflector for separating the incoming ion and photon beams, and the half-foil sample, which was used for testing it.

Recently, we installed a micro channel plate (MCP) detector in order to study two-dimensional angular distributions in capillary-guiding experiments [3]. The experiments were carried out at the Institute of Nuclear Research (ATOMKI), Debrecen. Ions were provided by a 14.5 GHz electron cyclotron resonance (ECR) ion source. In the early stage of the experiments it was noticed that significant amount of ultra-violet photons, for which the detector is sensitive, are in the ion beam. The ions could be separated from the photons with an electrostatic deflection system as in Fig. 1 it can be seen.

We studied the transmission of  $Ne^{6+}$  ions through  $Al_2O_3$  capillaries by the MCP detector, in order to extend our one-dimensional data, which were collected earlier. The capillaries were prepared at Université Catholique de Louvain using the self-ordering phenomena during a two-step anodization process[2]. The target samples were nearly circularly shaped membranes of nanochanneled  $Al_2O_3$  with a diameter of about 8 mm. The thickness of the samples was about 15  $\mu m$  and the capillaries were ordered in a honeycomb structure. The average inner capillary diameters of the two samples used in the present experiments were about 140 and 260 nm.

In Fig. 2a, a MCP image is shown. Here the sample foil filled only half of a circular opening on the sample holder (see the right side of Fig. 1). The UV photons passed the sample holder above the sample foil, and hit the MCP detector directly. The 3 keV  $Ne^{6+}$  ion beam, which was shifted by 4 mm downwards by the deflector system, hit the untilted target sample of 140 nm diameter capillaries. The lowest broad spot is due to ions transmitted through the sample. It has a width of about  $4^\circ$  at half maximum. Similar angular distributions were measured earlier with the electrostatic spectrometer. The upper, sharp and intense spot is due to the photons, which directly hit the detector. In Fig. 2b the same scattering pattern is shown, but with a horizontal electric field applied in front of the detector in order to separate different charge states. As a result, the spots due to ions are deflected toward right. The magnitude of the deflection depends on their charge state. The small, bright spot due to the photons remains in the same position. The most important fact is that only one charge state is visible for the ions transmitted through the foil.

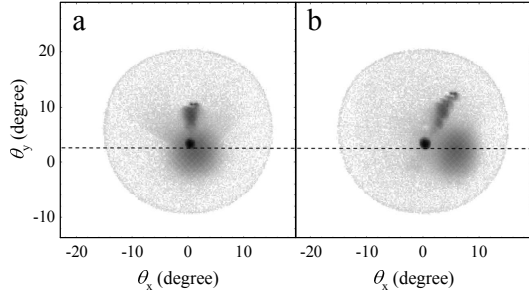


**Figure 2.** MCP images of the two-dimensional angular distribution of 3 keV  $Ne^{6+}$  ions transmitted through the 140 nm sample foil (for the arrangement, see Fig. 1) at  $0^\circ$  tilt angle. Panel (a): without a deflection field, Panel (b): with a horizontal electrostatic deflection field in order to separate different charge states (see text). The upper edge of the capillary foil is indicated with the dashed line.

In Fig. 3a, MCP images are shown for 6 keV  $Ne^{6+}$  ions transmitted through the 260 nm capillary samples at  $5^\circ$  tilt angles. The photon beam was blocked in this case. There is a clear indication of the capillary guiding since the maxima of the transmission nearly coincide with the tilt angle. The nice circular shape of the spot indicates that the angular distribution is azimuthally symmetric. In Fig. 3b, the same image with charge state separation is presented (positive ions are deflected to the right direction). As it shows, significant amount of non-deflected particles are present beside the  $Ne^{6+}$  ions. Again, this emission is most likely due to photons, because there is no emission of ions with lower charge states are observed.

It is well known that when a multiply charged ion gets close to a solid surface, electron capture processes occur. The captured electrons populate highly excited Rydberg states on the projectile, and subsequently decay to lower lying states by Auger process or radiative de-excitation leading to UV or X-ray emission [5]. The identification of the non-deflected particles as photons is affirmed by the fact that such emission is observable only for tilted samples, i.e. when a significant fraction of the incoming ions are impinging on the capillary walls.

In conclusion, two-dimensional angular distributions of ions guided through  $Al_2O_3$  nanocapillaries have been measured by a MCP detector.

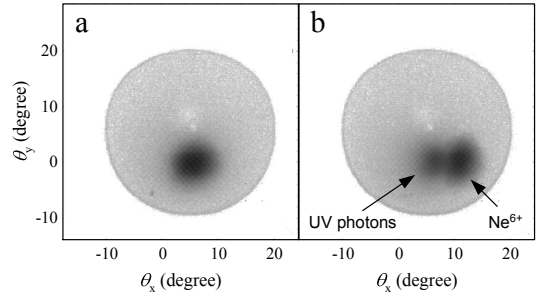


**Figure 3.** MCP images of the two-dimensional angular distribution of 6 keV  $Ne^{6+}$  ions transmitted through the 260 nm sample foil at  $5^\circ$  tilt angle. Panel (a): without a deflection field, Panel (b): with a horizontal electrostatic deflection field.

The results compare well to earlier one-dimensional data of electrostatic spectrometers showing similar angular broadening and guiding effect up to few degree. Significant amount of UV photons originating from the capillaries were observed for the first time. This phenomenon as result of ion - surface interactions may trigger further studies.

#### Acknowledgements

This work was supported by the Hungarian National Science Foundation OTKA (Grant No's: T046905, T046454, T042729, K73703 and PD050000), and in part by the Interuniversity Attraction Pole Program (P6/42) – Belgian State – Belgian Science Policy. The work was also supported by the grant “Bolyai” from the Hungarian Academy of Sciences, and the Hungarian National Office for Research and Technology.

- a) Unité de Physico-Chimie et de Physique des Matériaux, Université Catholique de Louvain, Place Croix du Sud, 1, 1348-Louvain-la-Neuve, Belgium
  - b) Dep. of Exp. Physics, University of Debrecen, Egyetem tér 1, H-4032 Debrecen, Hungary
- [1] N. Stolterfoht *et al.* Phys. Rev. Lett. **88** (2002) 133201-1.
  - [2] S. Mátéfi-Tempfli *et al.* Nanotechnology **17**, 3915 (2006)
  - [3] K. Tókési *et al.* Phys. Rev. A **64**, 042902 (2001).
  - [4] Y. Kanai, *et al.* Nucl. Instrum. Methods B **258** (2007) 155.
  - [5] Hannspeter Winter, Friedrich Aumayr, J. Phys. B **32** (1999) R39.

## 4.1 Magnetic particle hyperthermia: Néel relaxation in magnetic nanoparticles under circularly polarized field

*P. F. de Châtel<sup>a)</sup>, I. Nándori, J. Hakl, S. Mészáros, K. Vad*

The mechanism of magnetization reversal in single-domain ferromagnetic particles is of interest in many applications, in most of which losses must be minimized. In cancer therapy by hyperthermia the opposite requirement prevails: the specific loss power should be maximized.

Of the mechanisms of dissipation, on the first stage we studied the effect of Néel relaxation on magnetic nanoparticles unable to move or rotate and compared the losses in linearly and circularly polarized field [1]. The results were obtained through exact analytical solutions of the Landau–Lifshitz equation as derived from the Gilbert equation. We used the calculated time-dependent magnetizations to find the energy loss per cycle.

In figure (a) the resulting energy loss per cycle is depicted as a function of frequency and the dimensionless damping parameter  $\alpha$ . Regarding the merits of linear or circular polarization of the magnetic field, we find opposite preferences for frequencies below and above the Larmor frequency. At lower frequencies, which is relevant to hyperthermia, the energy absorbed by the magnet from linearly polarised

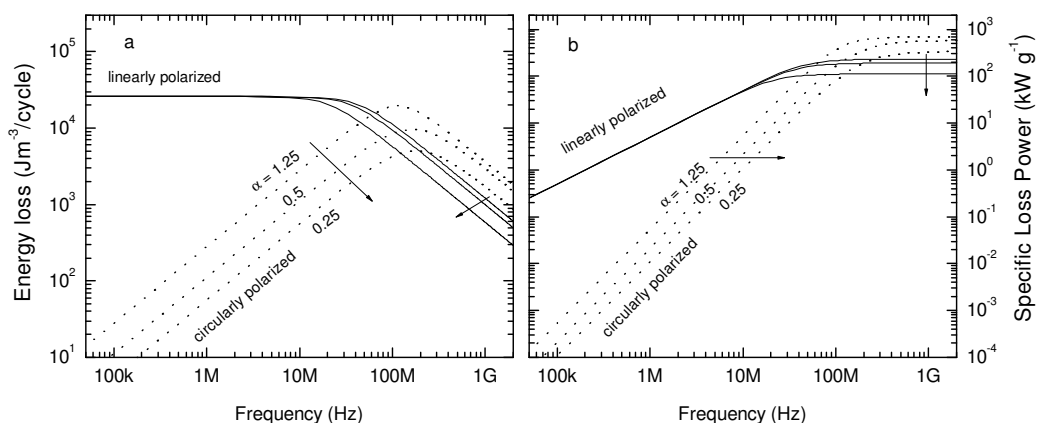
field exceeds the absorption from rotating field by orders of magnitude. In the case of high frequencies, which is not lacking technological relevance since the recent interest in materials with high microwave absorption, the relaxation is slow compared to the rate of change of the magnetic field and the loss per cycle becomes frequency dependent.

Figure (b) shows the specific absorption power in W/g for a single-domain particle of magnetite. At frequencies relevant to hyperthermia ( $\sim 10^5$  Hz) with linearly polarized field, respectable losses of kW/g order can be achieved, while the power absorbed from circularly polarized field is two to three orders of magnitude lower.

The authors acknowledge support from the Hungarian National Office for Research and Technology NKFP-5/006/2005, Contract OM-00077/2005.

a) Institute of Metal Research, Chinese Academy of Sciences, Shenyang 110016, P.R. China

[1] P. F. de Châtel, I. Nándori, J. Hakl, S. Mészáros, K. Vad, arXiv: 0810.1455, *J. Phys.: Condens. Matter* **21** (2009) in press.



**Figure 1.** Energy loss per cycle (a) and specific loss power (b) for linearly and circularly polarised fields for magnetite as a function of driving field frequency for different  $\alpha$  damping parameters. Arrows point towards the direction of decreasing  $\alpha$ . Driving field amplitude  $H = 10^4$  A/m.

## 5.1 Transmission of 4.5 keV Ar<sup>9+</sup> ions through a single glass macrocapillary

R. J. Berczky , G. Kowarik <sup>a)</sup>, F. Aumayr <sup>a)</sup>, K. Tókési

Investigations of the interactions of highly charged ions (HCI) with internal surfaces recently became available due to the advances in the fabrication of nano-, micro-, and macrocapillaries. In contrast to the case of metallic capillaries [1], the experiments with insulating ones showed not only directional guiding of the ions, but also the remarkable fact that the ions keep their initial charge state as a consequence of a self-organized charge-up inside the capillary. Following the pioneering work of Stolterfoht *et al.* [2] several groups studied the ion guiding through insulating foils with randomly distributed capillaries or ordered arrays of regular nanocapillaries. It follows from the type of the used samples, collective effects due to the presence of neighboring capillaries must be taken into account for an accurate simulation of the ion trajectories [3]. These collective effects make a full theoretical description of the interaction between charged particles and insulator capillary walls rather difficult.

In order to obtain an easier situation for comparison with simulation, we investigated the transmission of Ar<sup>9+</sup> ions through a single, cylindrical-shaped glass capillary of macroscopic dimensions, thus avoiding these collective effects [4]. For our investigations we used a single macroscopic glass capillary with a total length of 11.4 mm, the inner diameter was 170  $\mu\text{m}$ , which corresponds to an aspect ratio of about 67. The capillary was produced in the ATOMKI, Debrecen. The measurements were carried out using HCI beams produced by the 14.5 GHz Electron Cyclotron Resonance Ion Source in Vienna. In this work we investigated the transmission of 4.5 keV Ar<sup>9+</sup> ions through the capillary as a function of the tilting angle of the capillary,  $\phi$  (Fig. 1.) as well as the angular distributions of the transmitted ions. Fig. 1. shows the transmission of ions through the capillary as a function of tilt angle, covering a range of roughly  $\pm 3^\circ$ .

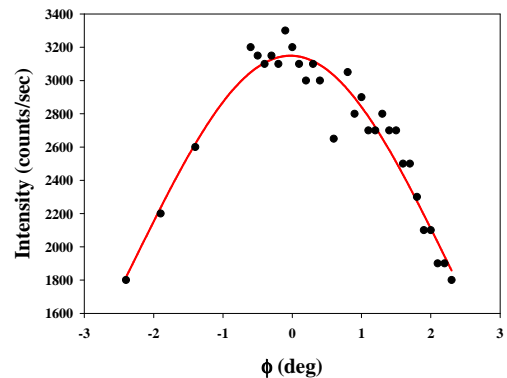


**Figure 1.** Transmission of 4.5 keV Ar<sup>9+</sup> projectiles passing through a single glass macrocapillary depending on the tilt angle  $\phi$ . The solid line is a Gaussian fit of the measured data.

The results strongly support that the guiding effect known from nano-capillaries is also valid up to macroscopic dimensions of the order of mm, so an electric guiding field can also build-up inside a macro-scale single capillary, and thereby slow highly charged ions can be transmitted through the macrocapillary, keeping their initial charge state in a similar manner as for the case of nanocapillaries for tilt angles up to roughly  $5^\circ$ . The charging-up of the insulating wall material could be observed in time-dependent transmission measurements.

### Acknowledgements

This work was supported by the “Stiftung Aktion Österreich-Ungarn” grant no. 67öu3, the grant “Bolyai” from the Hungarian Academy of Sciences, the TeT Grant no. AT-7/2007, the Hungarian National Office for Research and Technology, as well as Austrian FWP (P17499), and the Hungarian Scientific Research Found OTKA (K72172). We also thank to Mr. Ferenc Turi for the technical support.

a) Institut für Allgemeine Physik, Technische Universität Wien, Austria

[1] K. Tókési *et al.*, Phys. Rev. A **64**, 1199 (2001).

[2] N. Stolterfoht *et al.*, Phys. Rev. Lett. **88**, 133201 (2002).

[3] K. Schiessl *et al.*, Phys. Rev. A. **72**, 062902 (2005).

[4] R. J. Berczky *et al.*, in press, NIMB (2008).

## 5.2 Production of a microbeam of slow highly charged ions with a single microscopic glass capillary

G. Kowarik<sup>a)</sup>, R. J. Berezky, F. Aumayr<sup>a)</sup>, K. Tókési

In our work we investigated the angular distribution of 4.5 keV Ar<sup>9+</sup> projectiles passing through a single glass microcapillary for various tilt angles against the beam axis [1]. The presented data strongly support that the guiding effect known from nano-capillaries is also valid up to microscopic dimensions of the order of 0.1 mm. We took the advantage of this special property of microscopic glass capillaries and present an alternative way to produce a microbeam of slow highly charged ions by using a glass capillary [2]. Due to the guiding effect, one can position the beam and adjust the direction of it mechanically, without the necessity of electric or magnetic deflection and focusing systems. This opens the possibility of producing cheap alternatives to complex electron-optical tools with their electronic equipment, like e.g. external power-supplies, still having reasonable brilliance.

The measurements were carried out using 4.5 keV Ar<sup>9+</sup> ions, produced by the 14.5 GHz Electron Cyclotron Resonance Ion Source in Vienna. The cylindrical-shaped glass capillary with diameter of 0.17 mm and a length of 11 mm was prepared in the ATOMKI, Debrecen. Figure 1. shows the transmitted angular distributions of the ions for various tilt angles. These angular distributions are calculated from the spatial ones at the PSD by a proportionality constant. The intensity profile is indicated in figure 1. by a Gaussian fit-curve around the beam axis with a FWHM of approximately  $\pm 3.3^\circ$ . The angular distributions of the transmitted ions have similar width than the incident beam. Considerable stable transmission of guided ions could be observed for tilt angles of up to roughly  $5^\circ$ , after a charge-up period showing a smooth increase of ion transmission as well as deflection angle as a function of time (dose) until saturation is reached.

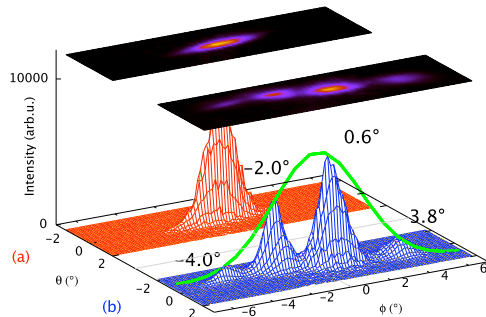


**Figure 1.** Angular distributions of the direct beam, collimated by a 0.5 mm aperture (a) in comparison with the guided distributions (b) for four different tilt angles as indicated. The z-axis shows the number of ion impacts per unit area. The solid curve is the result of a Gaussian fit of the maxima of the distributions.  $\phi$  denotes the lateral deflection angle in the horizontal plane, the elevation angle is  $\theta$ .

The observations indicate, that the initial charge-state of the ions is kept during the guiding through the glass capillary, which is an important feature concerning possible applications. Eventually, the usage of such microcapillaries could be an interesting alternative ion-optical tool for various applications, especially where the size, the costs or the accessibility are a critical factor.

### Acknowledgements

This work was supported by the “Stiftung Aktion Österreich-Ungarn” grant no. 67öu3, the grant “Bolyai” from the Hungarian Academy of Sciences, the TeT Grant no. AT-7/2007, the Hungarian National Office for Research and Technology, as well as Austrian FWP (P17499), and the Hungarian Scientific Research Found OTKA (K72172). We also thank to Mr. Ferenc Turi for the technical support.

a) Institut für Allgemeine Physik, Technische Universität Wien, Austria

[1] R. J. Berezky *et al.*, in press, NIMB (2008).

[2] G. Kowarik *et al.*, accepted in NIMB.

### 5.3 Guiding of electrons through a single glass macrocapillary

*B. S. Dassanayake*<sup>a)</sup>, *R. J. Berezky*, *S. Das*<sup>a)</sup>, *K. Tőkési*, *J. A. Tanis*<sup>a)</sup>

Guiding of charged particles through various types of insulating nanocapillaries has attracted considerable attention in recent years. This phenomenon is of interest because of potential applications in the field of nanotechnology and also from the fundamental understanding view point. The first measurements were performed using metallic microcapillaries, showing good agreement between theoretical predictions and experimental results [1]. The main interest later focused on the investigation of the interaction between highly charged ions (HCI) and insulating nanocapillaries. In contrast to the case of metallic capillaries, the slow HCI can be transmitted through the nanocapillaries keeping their initial charge state as a consequence of a self organizing charge-up process inside the capillary. Recently, guiding of slow HCIs through a single glass macrocapillary has been reported [2]. It was shown that guiding effect is valid up to macroscopic dimensions.

In our present work we investigated the transmission of 500 eV electrons through a single glass macrocapillary. We were interested to see whether the “guiding effect” would also be observable in the case of macroscopic dimensions when the injected projectiles are electrons. This kind of measurement is important to have a better and more general idea about the fundamental phenomena.

Here we report our preliminary results for the transmission of 500 eV electrons through a single glass macro-capillary of length 14.4 mm and diameter 0.18 mm which corresponds to an aspect ratio of about 80. The sample was prepared at ATOMKI. The measurements were performed in the accelerator laboratory at Western Michigan University in Kalamazoo.

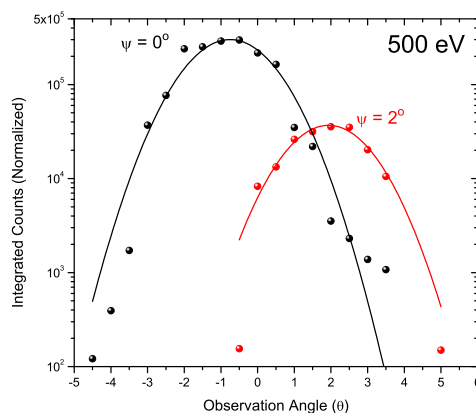


**Figure 1.** Angular distributions of 500 eV electrons transmitted through the single glass macrocapillary at tilt angles of  $0^\circ$  and  $2^\circ$ .

Figure 1. shows the angular distributions of 500 eV electrons transmitted through the glass capillary for tilt angles ( $\psi$ ) of  $0^\circ$  and  $2^\circ$ . From the figure it is evident that electrons are guided through the capillary. Measurements are in progress for other capillary tilt angles and for other electron energies in the range 300 - 1000 eV. The energy loss of the transmitted electrons also was investigated.

#### Acknowledgements

This work was supported by an award from Research Corporation. One of us (K. T.) was partially supported by the grant Bolyai from the Hungarian Academy of Sciences and the Hungarian National Office for Research and Technology. We also thank Mr. Ferenc Turi for technical support.

a) Department of Physics, Western Michigan University, Kalamazoo, USA

[1] K. Tőkési *et al.*, Phys. Rev. A **64**, 1199 (2001).

[2] R. J. Berezky *et al.*, in press, NIMB (2008).

## 5.4 Investigation of electron spectra backscattered from polyethylene-terephthalate

*R. J. Berezsky, K. Schiessl<sup>a)</sup>, M. Novák, C. Lemell<sup>a)</sup>, D. Varga, J. Burgdörfer<sup>a)</sup> and K. Tókési*

Recently, guiding of medium energy electrons (a few hundred eV) through insulating polyethylene-terephthalate (PET) capillaries was observed. The poorly characterized spatial structure and, even more challenging, local charge-up of the material pose consideration of difficulties for a microscopic treatment of electron transport through PET. In order to identify the processes giving rise to guiding [1] we investigate scattering from a flat PET surface both experimentally and theoretically.

Reflection electron energy loss (REEL) and elastic peak electron spectra (EPES) were taken using a high-energy, high-resolution, home built ESA-31 electron spectrometer. Primary electron energies range from 200 eV to 1000 eV. The cleanliness of sample surfaces was monitored analyzing X-ray photoelectron spectra. Photoelectrons were excited using the  $K(\alpha)1$ -line of Al (1486,67 eV).

To interpret our experimental data, classical-transport simulations were performed to obtain electron-energy loss spectra, angular distributions, and the secondary-electron (SEE) yield for PET. Apart from elastic and inelastic scattering processes along the trajectory within the target material we also include the effect of charge-up of the surface based on the SEE yield of previously scattered trajectories which leads to a partial suppression of electron emission in later stages of the simulation. The inelastic mean free path (IMFP) of electrons in PET was determined from EPES spectra using

Cu and Ni standards. Experimentally obtained IMFPs were compared with theoretical predictions derived from optical data. As Figure 1 shows good agreement between measured and simulated energy loss spectra is found.

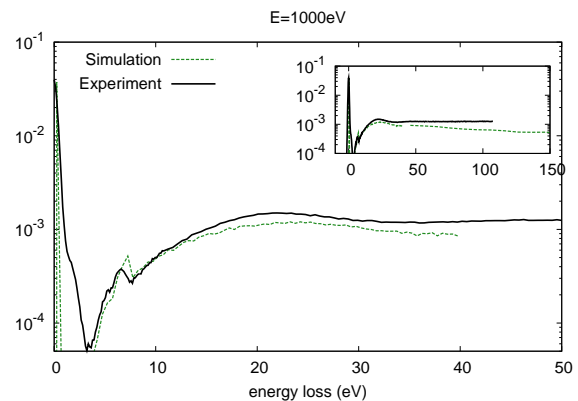


**Figure 1.** Comparison of the measured data and simulated PET loss spectra recorded at 1000 eV.

### *Acknowledgements*

One of us (K. T.) was partially supported by the grant Bolyai from the Hungarian Academy of Sciences and the Hungarian National Office for Research and Technology. We also thank Dr. József Tóth for technical support.

a) Institute for Theoretical Physics, Vienna University of Technology, Wiedner Hauptstrasse 8-10, A-1040 Vienna, Austria

[1] K. Schiessl, W. Palfinger, K. Tókési, H. Nowotny, C. Lemell, and J. Burgdörfer, *Phys. Rev. A* **72**, 062902 (2005).

## 5.5 Energy dependence of ion guiding through nanocapillaries

*K. Schiessl<sup>a)</sup>, C. Lemell<sup>a)</sup>, K. Tókési, J. Burgdörfer<sup>a)</sup>*

In this work, we model the transmission of  $\text{Ne}^{7+}$  ions with varying kinetic energies ranging from 2 to 9 keV through Polyethyleneterephthalate (PET) nanocapillaries with a diameter of 200 nm (see Fig. 1) [1].

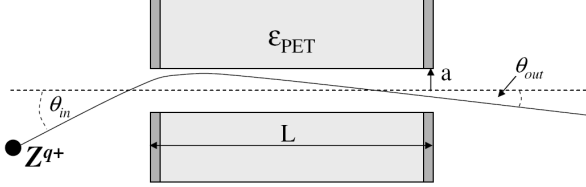


**Figure 1.** Schematic view of ion guiding through insulating capillaries. Parameters used in our simulation are projectile charge state  $\text{Ne}^{7+}$ , capillary radius  $a = 100$  nm, length  $L = 10$   $\mu\text{m}$ , entrance angle  $\theta_{in}$ , and dielectric constant  $\epsilon_{PET} = 3.3$ .

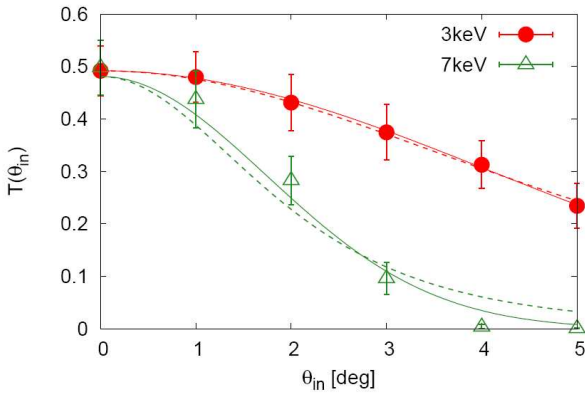


**Figure 2.** Transmission function  $T(\theta_{in})$  as obtained for a capillary as described in Fig. 1 for two different energies. Circle:  $E=3$  keV, triangle:  $E=7$  keV. Solid lines: Gaussian fits to the simulation [2] with  $\theta_g=5.84^\circ \pm 0.05^\circ$  (3 keV), and  $\theta_g=2.47^\circ \pm 0.11^\circ$  (7 keV). The dashed line offers an alternative fit to the data given by  $T(\theta_{in}) = T(\theta_0) / [1 + (\theta_{in}/\theta_l)^2]^2$  with  $\theta_l=7.71^\circ \pm 0.1^\circ$  (3 keV) and  $\theta_l=2.97^\circ \pm 0.27^\circ$  (7 keV).

We have simulated the ion transmission through insulating nanocapillaries using a

mean-field classical-transport theory (see Fig. 2.). Ion trajectories are propagated in the combined fields of charges deposited on the capillary wall, their polarization charges, the projectile image charge, and the macroscopic field from neighboring capillaries. The simulation avoids any freely adjustable parameters in order to be predictive and to provide qualitative insights into underlying mechanisms. We have varied projectile energy and angle of incidence and have tested different models of dielectric shielding. Best agreement with experimental data is found for dielectrically screened surfaces charges. Response and transport employs linear response only. Reasonable agreement with data could be found employing only macroscopic material parameters of PET like dielectric constant, surface and bulk conductivity.

### Acknowledgements

This work was supported by the Austrian Fonds zur Förderung der wissenschaftlichen Forschung under grant no. FWF-SFB016 ADLIS and the TeT Grant No. AT-7/2007. One of us (K.T.) was partially supported by the grant Bolyai from the Hungarian Academy of Sciences and the Hungarian National Office for Research and Technology. K.S. also acknowledges support by the IMPRS-APS program of the MPQ (Germany).

a) Institute for Theoretical Physics, Vienna University of Technology, Wiedner Hauptstrasse 8-10, A-1040 Vienna, Austria, EU

[1] K. Schiessl, C. Lemell, K. Tókési, J. Burgdörfer, Journal of Physics: Conference Series, in press.

[2] Hellhammer R, Bundesmann J, Fink D and Stolterfoht N 2007 Nucl. Instr. and Meth. B **258** 159.

## 5.6 Simulation of streaking experiments at surfaces

C. Lemell<sup>a)</sup>, B. Solleder<sup>a)</sup>, K. Tókési and J. Burgdörfer<sup>a)</sup>

Recently, first streaking experiments at a tungsten surface [1,2] were performed. An extreme ultraviolet (XUV) laser pulse was directed on a tungsten surface together with a collinear ultrashort near infrared (NIR) probe pulse. Surprisingly large run-time differences of  $110 \pm 70$  as for different regions of the electron spectrum were observed.

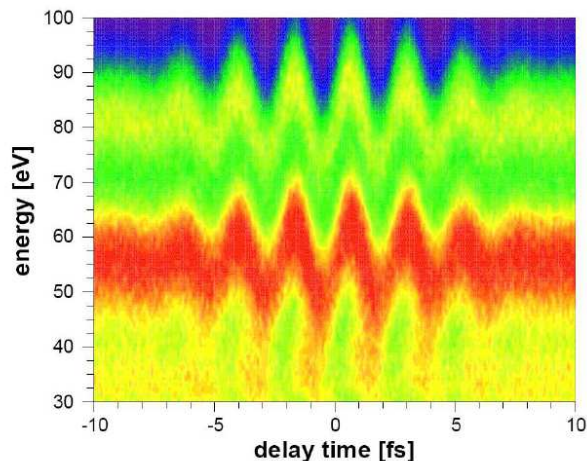


**Figure 1.** Streaking image for electrons detected in XUV-NIR laser-pulse surface interactions.

In this work we present our theoretical investigation of the recent experiment by Cavalieri *et al.* [1]. In our simulation of this experiment we model first the electron excitation by the XUV laser pulse. We determine the energy distribution and emission depths of excited electrons from material and laser-pulse properties. These electrons are then propagated in the target material by a classical transport simulation. Along their trajectory, electrons undergo elastic and inelastic collisions with the target material [3]. Furthermore, trajectories are detected due to the probe laser field penetrating into the metal. Electrons escaping the target are subject to the laser field

in vacuum and may eventually reach the detector mounted perpendicular to the surface.

Fig. 1 shows the streaking image for the energy range from 30-100 eV. Momentum transfer due to the interaction with the probe laser field leads to the observed energy shift of the lines at 56 and 82 eV. We found that influence of the streaking field on the trajectory does not change the observed run-time difference. We also found qualitative agreement with experiment [4], quantitative differences remain so far unexplained.

### Acknowledgements

This work was supported by the Austrian Fonds zur Förderung der wissenschaftlichen Forschung under grant no. FWF-SFB016 ADLIS and the Tét Grant No. AT-7/2007. One of us (K.T.) was partially supported by the grant Bolyai from the Hungarian Academy of Sciences and the Hungarian National Office for Research and Technology.

- a) Institute for Theoretical Physics, Vienna University of Technology, Wiedner Hauptstrasse 8-10, A 1040 Vienna, Austria
- [1] A. L. Cavalieri, N. Müller, Th. Uphues, V. S. Yakovlev, A. Baltuska, B. Horvath, B. Schmidt, L. Blümel, R. Holzwarth, S. Hendel, M. Drescher, U. Kleineberg, P. M. Echenique, R. Kienberger, F. Krausz, U. Heinzmann, *Nature*, **449** (2007) 1029.
- [2] R. Kienberger, E. Goulielmakis, M. Uiberacker, A. Baltuska, V. Yakovlev, F. Bammer, A. Scrinzi, Th. Westerwalbesloh, U. Kleineberg, U. Heinzmann, M. Drescher, F. Krausz, *Nature*, **427** (2004) 817.
- [3] B. Solleder, C. Lemell, K. Tókési, N. Hatcher, J. Burgdörfer, *Phys. Rev. B* **76** (2007) 075115.
- [4] C. Lemell, B. Solleder, K. Tókési, and J. Burgdörfer, *Publ. Astron. Obs. Belgrade* **84** (2008) 241.

## 5.7 Application of SNMS in the investigation of doped perovskites

*K. Vad, J. Hakl, A. Csik, S. Mészáros, M. Kis-Varga, G. A. Langer<sup>a)</sup>, Á. Pallinger<sup>b)</sup>, M. Bódog<sup>c)</sup>*

Doped perovskites have become a highlight of modern solid state physics due to the discovery of high-temperature superconductivity (HTS) and colossal magnetoresistance (CMR). Some types of perovskites (cuprates) show superconductivity, others (manganates, cobaltates) show CMR. The common feature of these two families of compounds is that their electromagnetic properties – the superconducting and other phase transition temperatures, the temperature and magnetic field dependence of the resistivity, etc. – depend sensitively on the doping level and oxygen content of the sample. Both the superconducting transition temperature of  $\text{Bi}_2\text{Sr}_2\text{Ca}(\text{Pr})\text{Cu}_2\text{O}_{8+\delta}$  compounds and the magnetic and electronic transport properties of  $\text{La}(\text{Sr})\text{Co}(\text{Fe})\text{O}_3$  perovskites change dramatically with the doping level. Apart from doping, oxygen deficiency is influenced by the details of preparation processes such as calcination and sintering. Simultaneous determination of constituents is of crucial importance from sample characterization point of view. The determination of doping levels with the required accuracy calls for a precise composition analysis. We demonstrated that Secondary Neutral Mass Spectrometry (SNMS) is an adequate technique for the analysis of perovskites, and that SNMS can be employed for the chemical analysis of very tiny samples in both metallic and insulating phases. To determine the oxygen content, which is the crucial characteristic of perovskites, the escaped oxide molecules have to be taken into account. Quantitative analysis of perovskite oxides can be performed by SNMS which is a suitable technique to measure the chemical composition of almost any sample because the flux of atoms sputtered from the sample is representative of the stoichiometry of the top-most layers. The composition and oxygen content of  $\text{Bi}_2\text{Sr}_2\text{Ca}_{0.86}\text{Pr}_{0.14}\text{Cu}_2\text{O}_{8.4}$  and  $\text{La}_{1-x}\text{Sr}_x\text{Co}_{0.975}\text{Fe}_{0.025}\text{O}_{3-\delta}$ , where

$0 \leq x \leq 0.5$ , were determined by SNMS. The results show that the method is equally applicable for insulating and conducting compounds. The observed electromagnetic properties reflect well the compositions obtained experimentally. From the mass spectra measured by SNMS the correct elemental concentrations were determined as shown in Fig. 1. It is clear from the measurements that the oxygen content depends on the doping level of Sr. This result was checked by Electron Dispersive X-Ray (EDX) analysis, which also supported the Sr dependence of oxygen content.

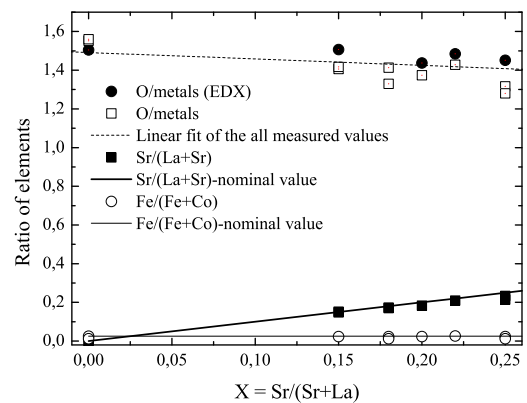


**Figure 1.** The SNMS analysis of  $\text{La}_{1-x}\text{Sr}_x\text{Co}_{0.975}\text{Fe}_{0.025}\text{O}_{3-\delta}$  samples. The oxygen content of the samples also was checked by Electron Dispersive X-ray analysis (EDX) as it is shown.

### Acknowledgement

This work was supported by OTKA K-62866.

- a) Dept. of Solid State Physics, Uni. Debrecen, P.O. Box 2, H-4010 Debrecen, Hungary
- b) Research Institute for Solid State Physics and Optics of the Hungarian Academy of Sciences, H-1525, Budapest, P.O. Box 49, Hungary
- c) Pannon University, H-8201, Veszprém, P.O. Box 158, Hungary

## 5.8 Investigation of thermal stability of hydrogenated amorphous Si/Ge multilayers

*A. Csik, M. Serényi<sup>a)</sup>, Z. Erdélyi<sup>b)</sup>, A. Nemcsics<sup>a)</sup>, G. A. Langer<sup>b)</sup>, D. L. Beke<sup>b)</sup>, C. Frigeri<sup>c)</sup>, A. Simon*

Hydrogenated amorphous silicon germanium alloys ( $a\text{-Si}_{1-x}\text{Ge}_x\text{:H}$ ) are used in multi-junction solar cells in order to increase the efficiency of the cells. One of the advantages of this material is the possibility to vary its band gap with the germanium concentration and thus the exploitation of the solar spectrum is optimized. In order to improve the stability of solar cells, a multijunction structure is useful because each photovoltaic layer can be thinner than that of single-junction solar cells. In case of Si/Ge amorphous multilayers the improvement of electronic properties is also accomplished by enriching them with hydrogen to passivate the dangling bonds of Si and Ge.

It is known that multilayers, as artificial compositionally modulated materials, are not equilibrium structures. In particular, they have high interfacial density gradients and sufficient atomic mobility even at moderate temperatures, hence changes in the composition profiles are expected to occur. Thus, not only the light induced structural changes, but investigation of the thermal stability and understanding of the factors controlling structural changes of these multilayers would be useful. Exploration of these mechanisms is very important for the interpretation of operation and for the prediction of lifetime before integrating these structures into microelectronics devices. In this work we present preliminary results on diffusion intermixing in amorphous Ge/Si multilayers prepared with different hydrogen content.

After heat treatments of the samples, it was observed that the hydrogenated Si/Ge multilayers underwent significant structural changes. The originally flat surfaces of the samples, prepared with 6ml/min hydrogen flow-rate, were visibly roughened at both applied annealing temperatures (673 and 723 K); gas bubbles were formed and the craters were created. However the samples prepared with lower  $\text{H}_2$  concentration (with 1,5 ml/min flow-

rate of  $\text{H}_2$ ) showed a similar effect only at 723 K. During annealing at 673 K the surface of these samples remained smooth (no craters) and only moderate bubble formation has occurred. This indicated that the structure of samples with low hydrogen concentration was more stable at 673 K, but at higher temperature (723 K) they can also degrade similarly as samples with higher hydrogen content.

The gas bubbles at 723 K are formed due to the enhanced precipitation of the supersaturated hydrogen and the intensive growth of these can eventually locally blow up the multilayered film. On the other hand, the small angle X-ray measurements show that despite the formation of craters, the multilayer structure is preserved. This offers an opportunity to perform a diffusion experiment, indicating classical intermixing between amorphous Ge and Si, still containing some hydrogen. Thus after each annealing the small angle X-ray spectrum has been recorded and the logarithm of the normalized intensity of the first order Bragg-peak has been plotted as the function of the annealing time. The slope of the curves can show that diffusion take place between the Si and Ge layers and the non-linearity of the time dependence of  $\ln I/I_0$  indicating that the diffusion coefficient strongly depends on the composition and/or significant stresses of diffusion origin have been formed during the heat treatments.

From these results we suggest that the still remaining hydrogen can inactivate the dangling bonds of Si and Ge and the diffusion intermixing slows down until the hydrogen remains in the layers.

*a)* MTA-MFA Institute, Konkoly-Thege ut 29-33, Budapest H-1121, Hungary

*b)* Dept. of Solid State Physics, Uni. of Debrecen, P.O. Box 2, H-4010 Debrecen, Hungary

*c)* CNR-IMEM Institute, Parco Area delle Scienze, 37/A, 43010 Parma, Italy

## 5.9 Investigations of failure mechanisms at Ta and TaO diffusion barriers by SNMS

*A. Lakatos<sup>a)</sup>, A. Csik, G. A. Langer<sup>a)</sup>, G. Erdélyi<sup>a)</sup>, G. L. Katona<sup>a)</sup>, L. Daróczy<sup>a)</sup>, K. Vad, J. Tóth, D. L. Beke<sup>b)</sup>*

Copper is widely used interconnect material as a replacement of aluminum in semiconductor devices because of its high electrical conductivity and electromigration resistance. The most important life-time limiting process in devices is diffusion between semiconductor and interconnects layers. It was an early observation that Cu can easily migrate to silicon, forming silicides with even at temperatures as low as 473 K. In order to prevent mixing and silicide formation, reliable diffusion barriers are needed. As for barrier materials for copper metallization, Ta and its alloys are expected to be the best candidates due to their high melting points, lack of reactivity with Cu, as well as relatively good adhesion to SiO<sub>2</sub>.

In this work we report on the thermal stability and barrier performance of Ta, TaO<sub>x</sub> and TaO<sub>x</sub>Ta films. Our research is focused on the very early stage of the degradation of these systems. Structural and compositional changes in the thin films were investigated by an X-Ray Diffractometer (XRD, equipped with a Siemens-made Cu-anode x-ray tube), an X-ray Photoelectron Spectroscopy (XPS) and a Transmission Electron Microscope (TEM). Secondary Neutral Mass Spectrometry (SNMS) was applied to map the depth profiles.

Our investigations, based on depth profile analysis, show, that early degradation of Ta barrier takes place by the diffusion of Ta through the Cu layer and simultaneously the diffusion of Si into the Ta layer. Around 773 K, Ta-silicide formation was observed. Furthermore, deterioration of the barrier layer is strongly affected by the coarsening of the Ta film.

The failure mechanism in the TaO<sub>x</sub> barrier seems to be a crystallization controlled process (823 K). At higher temperature (873 K) the decomposition of the TaO<sub>x</sub> film also influences the degradation.

The combined TaO<sub>x</sub>-Ta barrier proved to be much more effective than the Ta or TaO<sub>x</sub> single film. The observed outstanding performance of the combined film can be explained by the continuous oxidation of Ta film in TaO<sub>x</sub>-Ta bilayer. The reaction product of the oxidation process, the freshly formed TaO<sub>x</sub> film between the as-deposited TaO<sub>x</sub> and Ta is probably amorphous (metastable TaO). This oxide layer in amorphous state is less permeable to Si and Cu than the layer in crystalline form, therefore it successfully prevents the degradation of samples up to 1023 K.

*a)* Dept. of Solid State Physics, Uni. of Debrecen, P.O. Box 2, H-4010 Debrecen, Hungary

## 6.1 Improving argon, krypton and xenon measurements for environmental water samples

*L. Palcsu, Z. Major, L. Papp*

The analysis of dissolved noble gas concentrations in groundwater has proven to be a reliable method to determine quantitative palaeotemperatures and water ages. The aim of instrumental and methodological improvements in the noble gas laboratory is to achieve a reliable accuracy of mass spectrometric noble gas measurements for environmental water samples. Helium and neon can be measured with an acceptable precision since 2007 [1]. We have started developing a new measurement for the heavier noble gases dissolved in water samples.

While in case of helium and neon measurements for environmental water samples, where all noble gas isotopes including the rarest  $^3\text{He}$  are expected to be measured, almost all gas is admitted into the mass spectrometer, the heavier noble gas fraction has to be reduced by a factor of about 4000 so that its abundance is not too high for the mass spectrometer. To reduce the argon, krypton, xenon fraction, a splitting volume of 2 litres was built that was equipped with a gas pipette. During a sample preparation, after removal of water vapour, all gas including chemically active gases such as nitrogen, oxygen, etc. (except helium and neon) are adsorbed in a cold trap held at 25 K. Afterwards, helium and neon are trapped in a charcoal trap of 8 K. The gas, that is already trap by heating it up to 150 K, and admitted into a puffer volume, the so-called splitting volume. The volume of this splitting vessel is about 2 litres. For further analysis, only  $0.5 \text{ cm}^3$  of gas is taken from the splitting volume. This tiny split is then purified by getters, and then admitted into the mass spectrometer. The three heavy noble gas elements are measured simultaneously. They do not affect the sensitivities of each other.

Measurements are calibrated with air aliquots. Moreover, fast calibration procedure has been initiated as it had been done for he-

lium and neon. The accuracy for calibration measurements were obtained to be less than 1 % for argon and less than 2 % for krypton and xenon (Fig. 1). Air equilibrated water (AEW) samples have been prepared under well know circumstances to check the precision of the whole measurement process. The results of three different standard water samples are in good agreement with the expected values. To demonstrate the overall precision, here the values of the heavy noble gas measurements are shown for an AEW sample prepared at  $18.7 \text{ }^\circ\text{C}$  and  $0.991 \text{ atm}$ . The measured and expected values are  $3.175 \cdot 10^{-4}$  and  $3.171 \cdot 10^{-4} \text{ ccSTP/g}$  for argon,  $7.123 \cdot 10^{-8}$  and  $7.131 \cdot 10^{-8} \text{ ccSTP/g}$  for krypton,  $9.814 \cdot 10^{-9}$  and  $9.809 \cdot 10^{-9} \text{ ccSTP/g}$  for xenon. These measurement precisions, including He and Ne, allow us to determine noble gas temperatures with a precision of about  $0.5 \text{ }^\circ\text{C}$ .

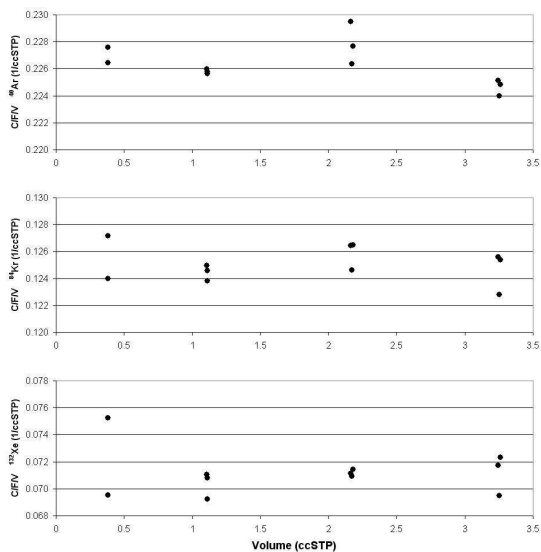


**Figure 1.** Linearity plots of argon, krypton and xenon measurements: C/F/V's are fast calibration corrected linearity values, where C is the mass spectrometric signal of the calibration sample, F is the signal of the fast calibration, and V is the volume of the calibration sample.

- [1] L. Palcsu and Z. Major: Improving helium and neon measurements for environmental water samples. Annual Report (2007)

## 6.2 Palaeoclimate reconstruction in the southern part of the Great Hungarian Plain based on noble gases and radiocarbon of groundwater samples

*L. Palcsu, I. Varsányi<sup>a)</sup>, M. Molnár*

In case of confined or semi-confined aquifers that are not affected by extreme heat effects and gas formation, noble gas concentration dissolved in the groundwater do not change along the flow path even for thousands of years from the recharge because they take part neither in chemical nor biological processes. Previous studies on palaeoclimate have shown that noble gases dissolved in groundwater can provide reliable temperatures at which the precipitation infiltrated under the surface. The solubility dependency of noble gases enables the determination of the recharge temperature, the so-called noble gas temperature (NGT), which being complemented with groundwater dating is a very powerful tool for palaeoclimate reconstruction. Around the world, numerous studies on palaeoclimate reconstruction using NGT's have found 4 – 6 °C temperature rising between the Last Glacial Maximum (LGM) and the Holocene. Only two study areas are known so far where larger temperature differences between late Pleistocene and early Holocene have been obtained based on noble gas concentrations in groundwater. Using NGT's, Aeschbach-Hertig et al. [1] revealed 9 °C warming for that period in Maryland, USA. In the northern part of the Great Hungarian Plain, Stute and Deák [2] found at least 8.6 °C temperature increase that could be even more, when we take into account that during the LGM permafrost was present at that area.

One of the aims of our investigation was to confirm this unusual temperature shift after the LGM. Additionally, we wanted to find an area where continuous infiltrations occurred during the last 40 kyr, thus a confined aquifer could have been a suitable record for palaeoclimate researches. Palaeobotanical and quartermalacological studies have shown that the southern part of the Great Hungarian Plain was never continuously frozen, not even during the LGM.

18 groundwater samples have been analysed for radiocarbon and noble gases as well as water chemistry and stable isotopes. Inverse calculations were performed to find those parameters, namely temperature, excess air amount, and fractionation of the excess air, with which the closed-system model [3] described the measured values best. The goodness of the fit was checked by a chi-square test. We obtained very good NGT's with low temperature unaccuracy, that were plotted against  $^{14}\text{C}$  values (Fig. 1). Two data groups can be distinguished: the first one contains NGT's from 10 to 13 °C with a mean of  $12.39 \pm 0.81$  °C. These samples might represent the Holocene. The other group involves the cold NGT's that seems to derive from the late Pleistocene, namely the LGM. These samples compose an average of  $3.26 \pm 0.38$  °C. As a result, we obtained a difference of  $9.13 \pm 0.89$  °C between the Holocene and late Pleistocene. Our study has confirmed that the temperature increase was much higher in the Carpathian Basin than in most of the other parts of the world at that time.

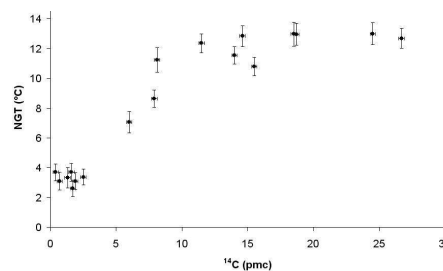


**Figure 1.** NGT's in function of radiocarbon of the groundwater samples

- a) Univ. of Szeged, Dept. of Geochemistry, Szeged, Egyetem str. 2-6, Hungary
- [1] W. Aeschbach-Hertig, M. Stute, J. F. Clark, R. F. Reuter and Peter Schlosser, *Geochim. Cosmochim. Acta*, Vol. **66**, Issue 5 (2002) 797-817
- [2] M. Stute and J. Deák, *Radiocarbon*, Vol. **31**, No. 3, (1989) 902-919
- [3] W. Aeschbach-Hertig, F. Peeters, U. Beyerle, and R. Kipfer, *Wat. Res. Research*, Vol. **35**, No. 9, (1999) 2779-2792

### 6.3 Investigation of impact materials around Barringer Meteor Crater by SEM-EDX and micro-PIXE techniques

I. Uzonyi, Gy. Szöőr<sup>† a)</sup>, P. Rózsa<sup>a)</sup>, P. Pelicon<sup>b)</sup>, J. Simčič<sup>b)</sup>, C. Cserhádi<sup>c)</sup>, L. Daróczy<sup>c)</sup> and Á. Z. Kiss

Up to date (2008), 174 terrestrial impact craters have been explored on the Earth's surface. They were created by hitting asteroids, meteorites and/or comets. The most famous and well-preserved meteorite crater is the Barringer Meteor Crater in Arizona, USA which is approximately 50,000 years old. It was created by an iron meteorite.

In recent years, much effort has been devoted to the elemental characterization of various impact materials collected in its near environment by the leadership of the late Prof. Gyula Szöőr. Especially, their Fe-rich inclusions were studied supposedly originated from the projectile of the impacted meteorite [1]. In this report, results for some non-spherical, aggregate-like specimens are shown.

The application of Scanning Electron Microscope combined with Energy Dispersive X-ray Analysis (SEM-EDX) and a Scanning Nuclear Microprobe (SNM) is a powerful technique for the complex characterization of such materials. SEM provides the fine textural information and the concentration of the major elements. SNM with Particle Induced X-ray Emission (PIXE) method [2] serves for the determination of both the major constituents and the important minor and trace elements such as the Platinum Group Elements (PGEs): Ru, Rh, Pd, etc.

In this report analytical data are presented for S-Fe-Ni-Cu systems in order to feature the major characteristics of impact metamorphism of materials. A part of the work was presented in the 11<sup>th</sup> Int. Conf. on Nuclear Microprobe Technology and Applications (Hungary) and 71<sup>st</sup> Annual Meeting of the Meteoritical Society (Japan) conferences. Detailed results are under publication in a NIM B volume.

#### Acknowledgements

Support from the EU co-funded Economic Competitiveness Operative Programme GVOP-3.2.1.-2004-04-0402/3.0, the Hungarian-Slovenian intergovernmental S&T cooperation program (SLO-16/2005 GVOP) as well as from the Hungarian Research Foundation (OTKA) under contract No T046579 are acknowledged. The authors thank the Barringer Crater Company, Meteor Crater Enterprises and US Geological Survey (Flagstaff, AZ) for making the field-trip and collection of the samples possible. Special thanks to J.S. Kargel and A. Gucsik for their personal help.

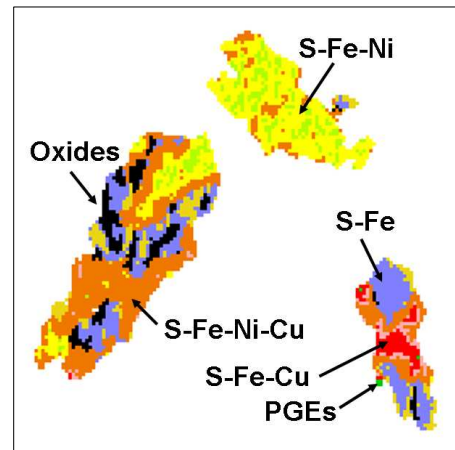


**Figure 1.** Compositional map of the impact materials. Identified minerals: chalcopyrite (S-Fe-Cu), pentlandite (S-Fe-Ni) and pyrrhotite (S-Fe). Enrichment of PGEs (Ru, Rh, Pd plus Ag) as well as Cl, Cr and Ti was detected in some border spots (PGEs). Scan size = 500 x 500  $\mu\text{m}^2$

- a) Department of Mineralogy and Geology, University of Debrecen, Debrecen, Hungary.
- b) Jožef Stefan Institute, Microanalytical Center, Ljubljana, Slovenia.
- c) Department of Solid State Physics, University of Debrecen, Debrecen, Hungary

[1] I. Uzonyi *et al.*: Spectrochimica Acta Part B - Atomic Spectroscopy **59** (2004) 1717.

[2] I. Uzonyi and Gy. Szabó: NIMB **231** (2005) 156.

## 6.4 Ion-beam analysis of a medieval glass bottle excavated in Győr

*I. Uzonyi, G. Tomka<sup>a)</sup>, Z. Szoboszlai, Zs. Kertész, A. Simon, Á. Z. Kiss*

To the east of the historical downtown of Győr on the place of the former Wagon Factory an archaeological excavation lead by P. Tomka and E. Szőnyi was carried out in the years 2004-2005. At the site remnants from the Roman Period (1<sup>st</sup> –2<sup>nd</sup> c.), and from various periods of the Middle Ages (10<sup>th</sup> -15<sup>th</sup> c.) came to light. [1]

From a storage pit (feature Nr. 259.) pieces of a glass bottle were saved. The bottle was completely restored. It is 18 cm tall, transparent: the well preserved material has a greenish tint (see fig. 1.).



**Figure 1.** Restored glass bottle excavated at Győr, Hungary.

Intact or complete pieces of medieval glass bottles are almost unknown in Hungary. Similar bottlenecks were unearthed in Buda not only on the territory of the former Royal Castle but also in the town. A depot-found, which could be a ware stock of a merchant perished in a fire, was saved in Fortuna Street, Buda. The sloping shoulder and biconical body of these bottles are different from the bottle from Győr [2]. The “goiter necked” glass bottles were spread in large areas of Southern and Central Europe. The closest parallels to the piece from Győr can be found in Austria (Vienna) [3] in Moravia (Brno) [4] and a piece with unknown provenience (Milano). Further analogies can be cited from the Balkan Peninsula (Panik in Bosnia, Korinthos in Greece),

from Italy (Cividale), from Germany (Landshut and Baunschweig) and from Switzerland (Basel) [5].

The find spots suggest that producing centres lay in Central Europe, but one has to keep in mind that luxury goods were transported pretty far in medieval times. According to the latest theories the predominance of early Byzantine glasses can be questioned and Italian production seems to be more important. The find from Győr can be dated with great probability to the 2<sup>nd</sup> half or to the end of the 13<sup>th</sup> century.

Analytical characterization of the glass bottle was performed in ATOMKI. For the determination of the elemental concentrations two non-destructive ion beam analytical (IBA) techniques: the particle induced X-ray emission (PIXE) and the particle induced gamma-ray emission (PIGE) were used. Measurements were carried out on a small glass piece from the present archaeological find which was not used for the restoration.

PIXE analysis was carried out at the Scanning Nuclear Microprobe facility. The sample was irradiated at five different spots by 2 MeV H<sup>+</sup> beam focused to 2x2  $\mu\text{m}^2$  spot size and applying scan size of 2x2 mm<sup>2</sup>. The accumulated charge at the sample was  $\sim 0.2 \mu\text{C}$ . Characteristic X-rays were detected by an ultra thin windowed and a Be windowed Si(Li) detectors, thus elements could be analyzed for the  $Z \geq 6$  atomic number region with high sensitivity. Characteristic X-ray spectra were evaluated with the PIXEKLM-TPI software package [6]. Efficiency calibration of detectors was based on the NIST 610 glass standard reference material.

In the case of the PIGE analysis the samples were irradiated in an isolated vacuum chamber with a 3.8 MeV proton beam of about 5 nA. The accumulated charge at the sample was  $\sim 3 \mu\text{C}$ . The gamma-rays were detected with a 40 % HPGe detector situated at 90° with respect to the beam direction and 20 cm

distance from the sample. To calculate the concentrations of Na, Al and Si the same NIST 610 glass standard was used.

The analysis revealed that the bottle was made from soda-lime glass. Comparing Na, Mg and Ca values with available literature data, “similarity” with Venice glass can be stated. However, considering the high Ti, Fe (and Al) concentrations it can be supposed that a relatively low quality vitrifying agent (siliceous material) was used excluding late medieval (15-16<sup>th</sup> c.) fine Venetian glass. The greenish tint attributable to the high Fe content indicates incomplete decolourization (by MnO) which is also characteristic for lower quality glass products. Therefore, the analytical results does not falsify the hypotheses that the artefact can be a 13<sup>th</sup> century (supposedly Venice) glass.

**Table 1.** Preliminary results on the composition of the Győr glass bottle. Concentrations and their Standard Deviations are expressed in wt.%. For comparison, chemical composition of Venetian glasses (V1: 11-14<sup>th</sup> c. [7]; V2:16<sup>th</sup> c. [7,8]; V3:15-16<sup>th</sup> c. [9]).

	Bottle	V-1	V-2	V-3
Na <sub>2</sub> O	15.7±1	14.0	13.0	15.4±2.4
MgO	2.3±0.2	2.30	3.30	1.1±0.3
Al <sub>2</sub> O <sub>3</sub>	4.5±0.5	4.00	0.90	1.7±1.2
SiO <sub>2</sub>	65.0±2	64.7	68.0	70.3±2.0
K <sub>2</sub> O	2.3±0.1	2.50	2.50	3.4±2.0
CaO	6.5±0.1	7.50	9.50	4.6±0.8
TiO <sub>2</sub>	0.23±0.01	0.24	0.06	-
MnO	1.1±0.1	1.90	0.60	0.12±0.07
Fe <sub>2</sub> O <sub>3</sub>	2.0±0.6	1.40	0.50	0.77±0.38

a) Hungarian National Museum, Múzeum krt. 14-16., 1088 Budapest, Hungary

[1] Bíró Sz., Molnár A., Nagy A. (ed.): A Vagongyár alatt-A Vagongyár előtt. Római temető és középkori település a győri Árkád területén. A Győr-Moson-Sopron Megyei Múzeumok Kiállításvezetői 2. Győr, 2007, 6-7, 94-99

[2] H. Gyürky K.: A Budapest I. Fortuna u. 18. számú lakóház régészeti kutatásából származó üvegleletek. In: Budapest Régiségei XXXVII. (2003) pp. 13-28

[3] K. Tarcsay: Zu den Rohstoffen und Rezepturen von Gläsern aus Wien - Materialanalytische Untersuchungen. In: Fundort Wien. Berichte zur Archäologie **8** (2005) 167, Taf. 3. 5

[4] H. Sedláčková: Typologie des Glases aus dem 13. und 14. Jahrhundert aus Brünn, Mähren. In: Auf gläsernen Spuren. Der Beitrag Mitteleuropas zur archäologisch-historischen Glasforschung. Beiträge zur Mittelalterarchäologie in Österreich **19** (2003) 129, Tafel 1 II.1.

[5] E. Baumgartner, I. Krueger: Phönix aus Sand und Asche. Glas des Mittelalters. München-Basel, 1988., 267, 271-272

[6] I. Uzonyi and Gy. Szabó: NIMB **231** (2005) 156.

[7] M. Verita. Some technical aspects of Venetian glass, Technique et Science Les Arts du Verre, Actes du Colloque de Namur oct 1989, Presse Universitaire de Namur, pp. 57-59.

[8] M. Verita and T. Toninato: Rivista della Staz. Sper. Vetro n. **4** (1990) 169.

[9] B. Gratuze et al.: Archaeolingua. Central European Series **1**, BAR International Series **1043** (II) (2002) 565.

## 6.5 Ion micro-beam analysis of single aerosol particles originating from Saharan dust episodes observed in Debrecen, Hungary

Z. Szoboszlai , Zs. Kertész , Z. Szikszai , I. Borbély-Kiss and E. Koltay

Mineral dust arising from deserts is one of the main contributions of the particulate matter in the atmosphere. Due to their wide range of environmental impact and their effect on the radiative forcing of the Earth's climate, study of sources and transport of desert dust is a hot field of atmospheric aerosol research.

Approximately 50 episodes of Saharan dust intrusion have been observed in the atmosphere of Debrecen since 1991 [1]. In order to separate dust particles of Saharan origin from local sources, and to follow the formation, ageing and evolution of particles originating from long range transport processes, individual aerosol particle analysis was carried out on the Debrecen nuclear microprobe.

The samples were collected at a rural site (Hortobágy-Nagyiván) 50 km from Debrecen, on 9th, 12th and 16th November 1996 when a Saharan sand plume reached Eastern Hungary and on 29th November 1997 when no Saharan effect occurred (control sample).

Combined off-axis STIM and PIXE-PIXE ion beam analytical techniques were used to determine the quantitative elemental composition of over 250 individual aerosol particles for elements with  $Z > 6$ . The influence of Saharan dust was shown through characteristic elemental ratios like Ti/Fe, Ti/Ca and Al/Ca (Table 1)

**Table 1.** Ti/Ca, Ti/Fe, Al/Ca elemental ratios

	Ti/Ca	Ti/Fe	Al/Ca
Saharan (Hortobágy-Nagyiván)	0.087	0.130	1.179
Saharan (Debrecen) [1]	0.07	0.10	0.73
Saharan (Italy) [1]	0.10	0.10	1.64
Non-Saharan (Hortobágy-Nagyiván)	0.018	0.035	0.962
Non-saharan (Deb.) [1]	0.05	0.07	0.47
Non-saharan (Italy) [1]	0.05	0.07	0.80

These tracer ratios were found to be higher in case of Hortobágy-Nagyiván than in the case of urban environments which were highly influenced by

local emissions, especially re-suspended soil dust due to urban traffic.

Hierarchical cluster analysis was performed on the obtained database to classify the particles. The overall composition was dominated by mineral dust. The conclusion have been drawn that the mineralogical composition of Saharan dust and the local soil was very similar, so Al, Si, Ca cannot be used as tracers of Saharan dust. However, particle classes characteristic to the Saharan samples were found. One of them is characterised by high Fe and Ti content, while the other by NaCl. The origin of this latter was most probably sea-salt from the Mediterranean Sea, and arrived here by long range transport processes together with the air body carrying the Saharan dust.

From individual particle analysis we have shown that aluminium-silicate particles with high Mg and K content were characteristic to the Saharan samples. Mg, besides Al, Ti and Fe can be used also as a tracer of Saharan dust. Through K we could observe the effect of biomass burning originating most probably from the equatorial Sahal region. Trace elements were also investigated, and it was found that most trace metals are strongly associated with iron and iron-rich aluminium-silicates.

Nuclear microscopy was proved to be a useful complementation to the bulk analytical techniques. Particles originating from long range transport processes were identified and separated from the local aerosol. With the help of ion beam microanalysis it became possible to get information about their formation, ageing and evolution during transport.

### Acknowledgements

This work was supported by the Hungarian Research Found (OTKA F60377), the EU co-funded Economic Competitiveness Operative Program (GVOP-3.2.1-2004-04-0402/3.0) and by the Coordinated Research Project of IAEA 13261/R).

[1] I. Borbély-Kiss *et al.*, J. Aerosol Sci. **35** (2004) 1205-1224

[2] Z. Szoboszlai *et al.*, Nucl. Instr. and Phys. Res. B. (2009) accepted for publication.

## 6.6 Atmospheric aerosol particle analysis at the Debrecen Nuclear Microprobe

Zs. Kertész, Z. Szikszai, Z. Szoboszlai, A. Angyal

Characterisation of atmospheric aerosol is in the focus of several national and international research programs due to their health impact and effects on the radiative balance of Earth. Bulk elemental analytical techniques, like macro-PIXE, are extensively used for analysing atmospheric aerosol. However more detailed and reliable data can be obtained if individual aerosol particles are analysed. Nuclear microscopy is a powerful tool which enables the quantitative determination of trace element distribution in complex samples with a sensitivity of  $\mu\text{g/g}$  on micrometer scale.

In the frame of an OTKA and a Coordinated Research Project of the IAEA, an experimental setup based on the simultaneous use of different ion beam analytical techniques was developed at the Debrecen scanning nuclear microprobe facility, which enables the total quantitative analysis of microparticles [1]. This measurement, data collection and evaluation setup was already applied successfully in various studies: (1) ion beam microanalysis of desert dust particles originating from Saharan dust intrusions [2], (2) characterization of urban aerosol sources by single particle analysis, (3) characterization of indoor aerosols [3].

As an example, nuclear microprobe study of indoor aerosol particles containing toxic metals is presented. Aerosol samples were collected in the IBA Lab of ATOMKI in the frame of a laboratory practice for undergraduate students. At the same time mechanical repair work was carried out on the heating system in the corridor outside the Laboratory. In order to demonstrate the monitoring of air pollution for the students, aerosol samples were collected with a 2-stage filter unit on Nucle-

pore polycarbonate filters. The samples were analysed by bulk-PIXE. Concentration of Zn, Cd and Pb were found to be exceeding the national air quality limit. Therefore single particle analysis was carried out on the coarse mode samples to find out the origin of the toxic elements. Some elemental maps are shown in Fig. 1. Most of the particles had a spherical shape with a diameter of 20-30  $\mu\text{m}$ . The main component was ZnO. The particles contained S, K, Cl, Fe, Cu, Pb and Cd too. The “usual” airborne aerosol particles (aluminium-silicates, sulphates, calcium-carbonates) were sitting on the surface of these spheres. Mg and Cd were found only inside the particles. The work on the heating system, namely cutting the radiator pipes was identified as a possible source. The heating system was  $\sim 40$  years old, and formerly a white coat of paint containing Pb and Cd was applied. Fe and Zn could originate from the pipe, while Cd and Pb from the stain.

With the help of ion microscopy the particle structure, the possible chemical composition, the deposition process and the aerosol source were identified.

### Acknowledgement

This work was supported by the Hungarian Research Found (OTKA F60377), the Economic Competitiveness Operative Program (GVOP-3.2.1-2004-04-0402/3.0) and the International Atomic Energy Agency (CRP 13261/R).

- [1] Zs. Kertész *et al.*, Proceedings of the 11<sup>th</sup> Int. PIXE Conference (2007) CD PI-12 1-4
- [2] Z. Szoboszlai *et al.*, Nucl. Instr. and Meth. B (2009) doi:10.1016/j.nimb.2009.03.019
- [3] Zs. Kertész *et al.*, Nucl. Instr. and Meth. B (2009) doi:10.1016/j.nimb.2009.03.050

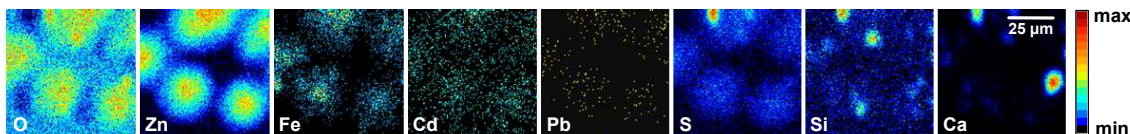


Figure 1. Elemental maps of indoor aerosol particles collected in the IBA Lab. on 05.11.2007.

## 7.1 Desorption and catalytic study of vanadium modified MCM-41 silica by $^{11}\text{C}$ radiolabeled methanol

É. Sarkadi-Pribóczy, T. Tsoncheva<sup>a)</sup>, M. Dimitrov<sup>a)</sup>

Vanadium modified MCM-41 (V-MCM-41) materials were prepared by solid state reduction technique with  $\text{V}_2\text{O}_5$  and catalytically tested in ethylacetate oxidation [1]. In the recent study,  $^{11}\text{C}$ -labeling methanol is introduced as a probe molecule for characterization of the state of various catalytic active sites, which were obtained after the V-MCM-41 treatment in oxidative (V-MCM-41\_o) or reductive (V-MCM-41\_r) atmosphere. Solid state vanadium modified mesoporous MCM-41 silica is characterised by XRD,  $\text{N}_2$  physisorption, FTIR and UV-Vis spectroscopies. Novel consecutive  $^{11}\text{C}$ - and  $^{12}\text{C}$ -methanol adsorption technique was used for the elucidation of the contribution of various vanadium species in methanol conversion.

The radiodetectors are placed in front of the reactor to follow the methanol desorption at different temperatures as well as for radio-GC analysis (including FID coupled on-line with radiodetector) of methanol conversion [2].

The rates of  $^{11}\text{C}$ -methanol desorption was negligible for V-MCM-41\_o, while a sharp increase is observed for V-MCM-41\_r in the temperature range of 160-180 °C, indicating the presence of various types of catalytic active sites for both materials. Radio-GC results also reveal different catalytic behaviour for these vanadium modifications. On V-MCM-41\_o, at lower temperature (250-280 °C) a small amount of dimethyl ether (DME) was registered. The selectivity to  $\text{CH}_4$ ,  $\text{CO}$ ,  $\text{CO}_2$ ,  $\text{HCHO}$  and methylal was strongly increased between 280-360 °C. On V-MCM-41\_r, no DME and only a negligible amount of methylal were detected. The process was carried out exclusively to  $\text{HCHO}$ , and similarly to V-MCM-41\_o, at higher temperatures - to  $\text{CO}$  formation. The desorption and catalytic measurements reveal that the variation in the pretreat-

ment medium provides the formation of catalytic centers with different redox and acidic activity. While the products of methanol decomposition ( $\text{CH}_4$ ,  $\text{CO}$ ,  $\text{HCHO}$ ,  $\text{CO}_2$ ) are typical of the presence of redox sites, the DME and methylal formation is possible only with the participation of the centers with acidic properties. Thus, the existence of centers with low acidic feature (probably of Lewis type) could be assumed for V-MCM-41\_o. They could be assigned to the presence of low coordinated vanadium oxide species. However, they significantly decrease after the sample pre-treatment in hydrogen. Thus, the pre-treatment atmosphere is an easy and powerful factor for the regulation of the catalytic behaviour of V-MCM-41.

Summarizing the solid state modification of MCM-41 with vanadia leads to the formation of grafted to the silica support vanadium species in different oxidative state and environment (isolated tetrahedral, polymeric,  $\text{V}_2\text{O}_5$  particles). They all exhibit catalytic activity in methanol conversion, but variations in the dehydration and dehydrogenation ability are found. Presence of stronger redox catalytic sites, containing  $\text{V}^{4+}$  ions are assumed for the reduced material.

### Acknowledgements

Financial support is by Bulgarian Academy of Sciences, the Bulgarian-Hungarian inter-academic exchange, Ministry of Education and Science (project BY-X-305/07), and by the Hungarian Scientific Research Fund No. T 048345.

a) Institute of Organic Chemistry, Bulgarian Academy of Science, Sofia, Bulgaria

[1] T. Tsoncheva, *et al.*, J. Colloid and Interface Sci. **321**, **342** (2008).

[2] É. Sarkadi-Pribóczy, *et al.*, Cat. Today, doi: 10.1016/j.cattod.2008.10.021.

## 7.2 X-ray Powder Diffraction and FTIR studies on Entacapone polymorphs

M. Kis-Varga, A. Bényei<sup>a)</sup>, T. Eszenyi<sup>b)</sup>

Entacapone, (*E*)-*N,N*-diethyl-2-cyano-3-(3,4-dihydroxy-5-nitrophenyl) acryl-amide is an inhibitor of catechol-*O*-methyl-transferase enzyme (COMT) and is used in the treatment of Parkinson disease. The structure was verified by single crystal X-ray diffraction study [1]. However, different crystalline phases of the compound *i.e.* polymorphic forms (*A* and *B*) were prepared by the Alkaloida R+D Ltd. and their extensive characterization was requested.

Traditional Fourier-transform infrared spectra (FTIR) in KBr pastille had failed to differentiate between the different phases presumably because at higher temperatures occurring during the pressing of the KBr pellet the most stable polymorph is formed. Using the attenuated total reflection technique (ATR-FTIR) the spectra were recorded in a diamond anvil cell and well documented difference of 10  $\text{cm}^{-1}$  was observed for several bands as seen in Fig. 1.

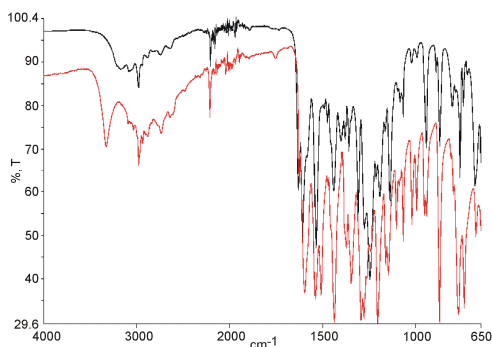


**Figure 1.** ATR-FTIR spectra of Entacapone polymorphs *A* (black) and *B* (red).

Quantitative X-ray powder diffraction (XRPD) studies made it possible to determine the polymorph composition of mixtures of the two forms down to the 0.1% limit. The calibration set of XRPD spectra are shown in Fig. 2. The structure of one form of Entacapone could be solved *ab initio* from the X-ray powder diffraction pattern measured in the ATOMKI

and using the DASH software package [2] (see Fig. 3).

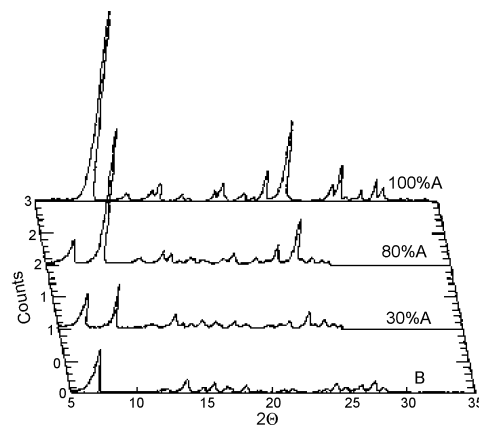


**Figure 2.** Calibration set of XRPD spectra for quantitative analysis of Entacapone *A-B* polymorph mixtures.

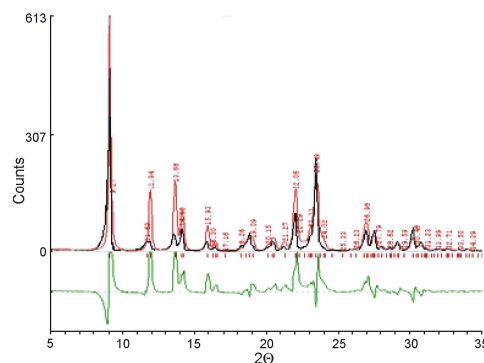


**Figure 3.** Measured (black) as well as calculated (red) and difference (green) XRPD patterns of one polymorph.

- a) University of Debrecen, Dept. of Chemistry, 1 Egyetem tér, Debrecen, Hungary H-4032
  - b) Alkaloida R+D Ltd, 2 Polgári Str., Tiszavasvári, Hungary H-4440
- [1] J. Leppanen, E. Wegelius, T. Nevalainen, T. Jarvinen, J. Gynther, J. Huuskonen, *J. Molecular Structure*, **562**, 129 (2001)
- [2] W. I. F. David, K. Shankland, J. van de Streek, E. Pidcock, W. D. S. Motherwell, J. C. Cole, *J. Appl. Cryst.*, **39**, 910 (2006)

### 7.3 Investigation of fish otoliths by combined ion beam analysis

*R. Huszánk, A. Simon, E. Szilágyi<sup>a)</sup>, K. Keresztessy<sup>b)</sup>, I. Kovács<sup>a)</sup>*

This work was implemented within the framework of the Hungarian Ion beam Physics Platform (<http://hipp.atomki.hu/>).

Otoliths are small structures, “the ear stones” of a fish, and are used to detect acceleration and orientation. They are composed of a combination of protein matrix and calcium carbonate ( $\text{CaCO}_3$ ) forming aragonite micro crystals. They have an annually deposited layered conformation with a microstructure corresponding to the seasonal and daily increments. Trace elements, such as Sr, Zn, Fe etc., are also incorporated into the otolith from the environment and the nutrition.

The elemental distribution of the otolith of fresh water fish burbot (*Lota lota L.*) collected in Hungary was measured with Elastic Recoil Detection Analysis (ERDA), Rutherford backscattering spectrometry (RBS) and Particle Induced X-ray Emission (PIXE) at the Nuclear Microprobe Facility of HAS ATOMKI.

The spatial 3D structure of the otolith could be observed with a sub-micrometer resolution. It is confirmed that the aragonite micro-crystals are covered by an organic layer and there are some protein rich regions in the otolith, too. By applying the RBSMAST code developed for RBS on macroscopic structure,

it was proven that the orientation of the needle shaped aragonite crystals is considerably different at adjacent locations in the otolith. The organic and inorganic component of the otolith could be set apart in the depth selective hydrogen and calcium maps derived by micro-ERDA and micro-RBS. Similar structural analysis could be done near the surface by combining the C, O and Ca elemental maps determined by micro-PIXE measurements. It was observed that the trace metal Zn is bound to the protein component.

#### *Acknowledgements*

This work was partially supported by the Hungarian OTKA Grant No. T046238 and the EU co-funded Economic Competitiveness Operative Programme (GVOP-3.2.1.-2004-04-0402/3.0).

a) KFKI Res. Inst. for Particle and Nuclear Physics, P.O. Box 49, H-1525, Budapest, Hungary

b) Dept. of Fish Culture, Institute of Environmental and Landscape Management, Szent István University, Páter K. u. 1, H-2103 Gödöllő, Hungary

[1] R. Huszánk, A. Simon, E. Szilágyi, K. Keresztessy, I. Kovács, *Micro-ERDA, micro-RBS and micro-PIXE techniques in the investigation of fish otoliths*, Nucl. Instr. and Meth. B (2009), doi:10.1016/j.nimb.2009.03.065

## 8.1 Status Report on Cyclotron Operation

*Z. Kormány, P. Kovács, I. Szűcs, I. Ander, F. Tárkányi, F. Ditrói*

The operation of the cyclotron in 2008 was concentrated to the usual 9 months; January, July and August were reserved for maintenance and holidays. The overall working time of the accelerator was 2302 hours; the time used for systematic maintenance was 312 hours. The breakdown periods amounted to 78 hours last year. The cyclotron was available for users during 1912 hours. The effectively used beam-on-target time is summarized in Table 1.

**Table 1.** Statistics of the irradiation time (beam-on-target) for different research groups.

Projects	Hours	%
Nuclear spectroscopy	471	38.0
Nuclear astrophysics	602	48.6
Nuclear data	15	1.2
Medical isotope production	36	2.9
Thin layer activation (TLA)	111	9.0
Target technology	4	0.3
<b>Total</b>	<b>1239</b>	<b>100</b>

A new project aiming the renewal of the nuclear magnetic resonance (NMR) based field stabilization system of the energy analyzing magnet has been started. First the parameters of the marginal oscillator in the external unit installed close to the magnet were improved. This is the only unit kept from the original ar-

rangement; the rest of the system has been rebuilt on a completely new design.

Instead of analogue signal processing used previously, the new system digitizes the low-frequency amplitude modulated signal of the marginal oscillator. The NMR-resonance is detected and the phase of the resonance signal is measured by a digital signal processing algorithm. The system hardware is built applying a C8051F041 mixed signal microcontroller, containing all the peripherals required for the measurement and the control of the different components. The prototype of the microcontroller program has been written and real tests with the magnet and the power supply will be started soon.

A second project for developing new power supplies for the low-current magnet coils of the cyclotron and the beam transport system has also been started. The new power supplies will be built with modern high-voltage tolerant IGBT components in their final stages. They will be cooled by forced air, so we can get rid of the water cooling circuits used for the old units. This results in major simplifications in the construction, operation and maintenance of the system. The design has been completed and the prototype of the new power supply is being built.

## 8.2 Activities at the Van de Graaff Accelerator Laboratory

*L. Bartha*

During 2008 the beam time of the VdG-1 machine amounted to 214 hours. The accelerator delivered protons only, as there was no request for other ion species. The proton beam was used for nuclear physics (210 hours, 98.1 %) experiments. Machine tests required 4 hours (1.9 %) beam time.

The 5 MV Van de Graaff machine was operating for 1009 hours during this period. Proton (81.3 %), and  $^4\text{He}^+$  (18.7 %) particles were accelerated.

The beam time was distributed among the following research subjects:

Analytical studies: 630 hours, 62.4 %

Micromachining: 336 hours, 37.6 %

### 8.3 Activities in the Electron Cyclotron Resonance (ECR) Laboratory

*S. Biri and R. Rácz*

The electron cyclotron resonance (ECR) ion source (ECRIS) has been operating since 1997. 2003 was the first year when we distributed the beamtime among the users. Between 2003 and 2008 the yearly operation time was around 500...600 hours.

Table 1 summarizes the beamtime we supplied in 2008 for the users. The “Hours” in the table actually mean the time when a plasma was made in the plasma chamber. In most cases a positive ion beam was extracted from the plasma so the ECRIS operated as particle accelerator. “Beam development” means our continuous effort to produce known or new plasmas and beams with better parameters: higher charge, higher intensity, better transport efficiency, wider ion choice, higher safety, etc.

It is already known for our users that the ATOMKI-ECRIS has two operation modes. The ECRIS-A is the original assembly to produce highly charged ion (HCI) beams. The ECRIS-B configuration forms large-size, low-

charged plasmas for some applications and for plasma investigations. In 2008 the ion source operated only 2 months in the “B” mode (March and April), 8 months in the “A” mode (January-February and May-October) while we did not operate it at all in the 2 last months of the year.

In November the ECRIS was stopped for 3 months to perform a major renewing and refurbishing of the laboratory. The ECR ion source is one of the facilities of ATOMKI which was designed and built entirely in our institute by institute people. The goal of the renewing was to establish an up-to-date laboratory at European standard which will be attractive place for foreign and domestic researchers, students and visitors. The following parts were exchanged or upgraded: furniture, floors, lights, cables, air conditioning system, floors painting. Some photos showing the new look of the laboratory will be put to our homepage [1] soon.

[1] <http://www.atomki.hu/atomki/ECR>

**Table 1.** Plasmas and ion beams produced in the ECR Laboratory in 2008.

The total energy of the beams is the product of the charge and the extraction voltage.

HCI: highly charged ion, DE: University of Debrecen, IEP: Institute of Experimental Physics, FD: Faculty of Dentistry, DAP: Division of Atomic Physics, ECR: ECR Group.

Research topic	User	Ion species	Extraction voltage (KV)	Hours	%
Ion guiding through capillaries	ATOMKI-DAP	Ne <sup>6+</sup> , Ne <sup>7+</sup> Ar <sup>9+</sup>	0.5 and 1.0	180	38
Production of new C60-based materials	ATOMKI-ECR	C <sub>60</sub> <sup>+</sup> , Fe <sup>+</sup>	0.4-10	20	4
Ti-coating with C60	DE-FD and ATOMKI-ECR	C <sub>60</sub> <sup>+</sup>	0.25 and 0.5	80	17
Interaction of HCIs with thin layers	DE-IEP	Ne <sup>4+...8+</sup>	15-30	110	24
Beam development & maintenance	ATOMKI-ECR	O <sup>1+...7+</sup> , Ar <sup>1+...16+</sup> Ne <sup>4+...9+</sup> , C <sub>60</sub> <sup>+</sup>	0.2-30	80	17
<b>Total</b>				<b>470</b>	<b>100</b>

## 8.4 New results from the improved $^{14}\text{C}$ AMS graphite target line in ATOMKI

*M. Molnár, L. Rinyu, É. Svingor, I. Futó, T. Nagy<sup>a)</sup>, M. Veres<sup>b)</sup>*

A Hungarian AMS graphite production facility was established in ATOMKI in 2005. After the first promising results [1], the complete vacuum system was upgraded and the hydrogen reduction based graphitization protocol was revised and improved. Also the whole lab building was completely renewed implementing an enhanced air filtration and conditioning system. Several sets of blanks and known-activity graphite samples were processed and tested in cooperation with the NSF Arizona  $^{14}\text{C}$  AMS facility in Tucson, Arizona, US.

The gas handling line is made of stainless steel with Swagelok valves and fittings. Using a newly installed Pfeiffer turbo molecular pump (TMU 071 P) we have a minimum pressure of  $< 1 \cdot 10^{-3}$  mbar at the connections for gas ampoules and graphitisation reaction rigs.

Graphite targets were prepared by reduction of carbon dioxide gas sample using Fe catalyst and hydrogen gas. The Fe powder we used was less than 325 meshes, 98 % purity (Alfa Aesar).

The reaction rig consists of a Hy-Lok plug valve, a Swagelok Vacuum Ultra-Torr Union Tee fitting, a quartz tube designed to limit carbon contamination, and a glass reusable water trap tube. The volume of the reaction rig is  $\approx 7.0 \text{ cm}^3$ .

Before the beginning of the graphitization process iron powder was activated by pre-reduction in 0.7 bar  $\text{H}_2$  atmosphere at  $450 \text{ }^\circ\text{C}$  for 90 min. The  $\text{H}_2:\text{CO}_2$  ratio was fixed at 2:1 according to our earlier results [1.], which suggest that this ratio avoids hydrocarbon formation during graphitisation. The initial pressure of a carbon dioxide gas sample was 300 - 500

mbar. The temperature of the water trap during the iron powder activation and the graphitization process was  $-5 \text{ }^\circ\text{C}$ . Minimum graphitization time was 300 minutes, however a typical sample was processed overnight.

The background of the gas handling line and the graphite target production system were tested by graphitization of C-14 free, old borehole carbon dioxide gas ( $\delta^{13}\text{C} = -3.4 \pm 0.2 \text{ } \text{‰}$  PDB, purity 4.5, Linde AG, Répcelak, Hungary). We also checked the reliability of the system by graphitizing gas produced from an intercalibration sample VIRI B (consensus  $^{14}\text{C}$  age value: 2820 yr BP) [2].

Most of the blank graphite targets produced in ATOMKI with hydrogen reduction gave good background results ( $^{14}\text{C}$  age  $> 50,000$  yrs BP) in comparison with zinc-reduced graphite blanks that are routinely produced in the NSF Arizona Lab.

Although all of the graphite samples from ATOMKI were processed in a completely different manner than is usual at the NSF Arizona Lab [3], the mean value of the VIRI B samples ( $2870 \pm 30$  yr BP) measured by the NSF Arizona AMS is consistent with measured by gas proportional counting technique in ATOMKI ( $2810 \pm 30$  yr BP) and with the consensus value for this sample (2820 yr BP) as published in the first report of the VIRI project [2].

a) University of Debrecen, Debrecen, Hungary

b) Isotoptech Zrt., Debrecen, Hungary

[1] L. Rinyu *et al.*, Radiocarbon **49** (2) (2007) 217.

[2] M. Scott *et al.*, Radiocarbon **49** (2) (2007) 409.

[3] P. J. Slota *et al.*, Radiocarbon **29** (2) (1987) 303.

## 8.5 Development of an atmospheric fossil fuel CO<sub>2</sub> monitoring station

*M. Molnár, É. Svingor, I. Futó, I. Major<sup>a)</sup>, M. Veres<sup>b)</sup>*

The aim of the project supported by Hungarian NSF (ref No. F69029) is determination of atmospheric fossil fuel CO<sub>2</sub> concentration in major cities or average industrial regions in Hungary using together measurement of CO<sub>2</sub> mixing ratio and radiocarbon (<sup>14</sup>C) content of the air.

For this aim we developed a high precision atmospheric CO<sub>2</sub> monitoring station in ATOMKI (Figure 1.). The station's measuring system is based on an Ultramat 6F (Siemens) infrared gas analyser. To help continuous, unattended run and autocalibration we built up an automatic gas handling line for the analyzer.



**Figure 1.** Developed mobile observation station for monitoring of atmospheric fossil fuel CO<sub>2</sub>.

For radiocarbon measurements we applied an integrating sampling system. One was installed in Debrecen station and two independent <sup>14</sup>CO<sub>2</sub> sampling line were installed 400 km far from Debrecen at Hegyhátsál station as

background references. During several tests of the measuring and sampling systems we demonstrated that uncertainty of individual CO<sub>2</sub> mixing ratio results is less than 0.5 ppm and the applied radiocarbon sampling system developed by ATOMKI works with good reproducibility.

In September and October of 2008 we measured the mixing ratio and radiocarbon content of atmospheric CO<sub>2</sub> at Debrecen and the far rural reference station (Hegyhátsál) simultaneously. It was concluded that trends in CO<sub>2</sub> mixing ratio variations in time are very similar at the three different sampling points (2 m above ground in Debrecen, 10 m and 115 m above ground in Hegyhátsál). Air quality in Debrecen during September of 2008 seemed to be relatively clear from the point of view of its CO<sub>2</sub> content at least. When winter came in October, with lower outside temperature and less sunshine hours the CO<sub>2</sub> content of air was increased in general at all the three sampling points, but this effect was more intensive closer to the ground level.

According our radiocarbon observations it was clearly indicated that there was not significant amount of fossil fuel CO<sub>2</sub> in the air of Debrecen during September in 2008. But in October of 2008 the  $\Delta^{14}\text{C}$  value of atmospheric CO<sub>2</sub> of Debrecen decreased with more than 40 ‰ relative to September's results, and according our calculations it was caused by about 20 ppm fossil fuel CO<sub>2</sub> which appeared as a surplus amount in the air above the previous months carbon dioxide level.

Using the developed mobile and high-precision atmospheric CO<sub>2</sub> monitoring station we plan to determine the atmospheric fossil fuel CO<sub>2</sub> trend in the whole 2008/2009 winter in Debrecen.

a) University of Debrecen, Debrecen, Hungary

b) Isotoptech Zrt., Debrecen, Hungary

## 8.6 Testing automatic groundwater sampling unit by the help of isotope analytical and dissolved ion investigations

*R. Janovics<sup>a)</sup>, M. Molnár, É. Svingor, M. Veres<sup>b)</sup>, I. Somogyi<sup>c)</sup>, M. Braun<sup>a)</sup>, Zs. Stefánka<sup>d)</sup>*

Automatic water sampling unit was developed in Hertelendi Ede Laboratory of Environmental Studies of MTA ATOMKI for monitoring the radioactive emission from nuclear facilities into the groundwater (Figure 1.).



**Figure 1.** Picture of automatic ground-water sampling unit.

The efficiency of existing and renewed geometry units and the reproducibility of survey data have been examined in the course of this work. A testing method was developed for this purpose, and ion binding efficiencies of ion exchange resins were analysed for different ion concentrations. These efficiencies have to be taken into consideration when we estimate the amount of the contamination got into the groundwater on the basis of the proportion of ions gained back from the resin.

The model tests were executed under controlled laboratory circumstances. These circumstances were tried to be formed into facts true to nature.

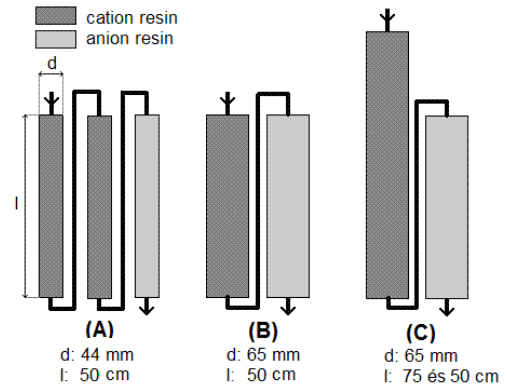


**Figure 2.** Schematic drawings of the tested three different resin geometries.

It has been found during the chain of tests that the sampling unit is suitable for well reproducible sampling. It can be told that all the tested different geometrical lay-outs (A, B, C in Figure 2.) are utilizable and work with proper efficiency in small/low range of concentration as well. The “A”-lay-out showed some ion loss in the last period but this phenomenon hardly has an influence on the effective and valid applicability of the existing system in the intended task. Taking the different efficiencies into consideration the activities can be corrected in the case of every element if it is necessary. A correcting factor should be introduced for the  $^{14}\text{C}$  anion exchanging sampling because samples show systematically lower radiocarbon content than the real values. We are working on continuing the tests. The gamma activity measurement of existing gained back cation samples and giving the exact value of  $^{14}\text{C}$  correction can give more reliable picture and direction to developing existing and possibly new systems.

a) University of Debrecen, Debrecen, Hungary

b) Isotoptech Zrt., Debrecen, Hungary

c) Iontech Kft., Litér, Hungary

d) Institute of Isotopes, Budapest, Hungary

## 8.7 PDMS patterning by proton beam

*S. Z. Szilasi, R. Huszánk, C. Cserhádi<sup>a)</sup>, A. Csik and I. Rajta*

In this paper the poly-(dimethylsiloxane) (PDMS) is introduced as a resist material for proton beam writing. We were looking for a biocompatible micropatternable polymer in which the chemical structure changes significantly due to proton beam exposure making the polymer capable of proton beam writing.

PDMS is a commonly used silicon-based organic polymer, optically clear, and generally considered to be inert, non-toxic biocompatible polymer. PDMS is also notably hydrophobic, meaning that water cannot easily penetrate its surface. This property has led extended use of PDMS in microfluidics too. PDMS is a cross-linkable polymer, it acts like a rubbery solid when it is cross-linked. In this state, the polymer does not deform permanently under stress or strain.

Up to now the PDMS has been used as a casting or replicating material in microfabrication to form microchannels, micromolding, or creating microstamps, etc. PDMS has not been used as a resist material for direct write techniques. In this work we investigated the surface topography of the irradiated regions of PDMS under and without stress (on the cut surface and on the original fluid surface, respectively). In the samples wherein stress was not developed, noticeable *compaction* was observed. In case of those samples wherein stress was developed, noticeable *swelling* occurred.

During the irradiation around the actual position of the beam spot we experienced significant swelling that reduced in time. To determine the large scale remaining changes in the surface topography at the cut edges of the samples we used Scanning Electron Microscope (SEM).

After numerous profilometer measurements we experienced that the irradiated areas became harder, so the probe could move on it without sinking. The unirradiated areas of

the PDMS were so soft, that the probe sank in the medium even with the smallest load ( $5 \cdot 10^{-7}$  N). Because of this phenomenon the irradiated areas seem to be higher than the unirradiated ones so the accurate measurement is impossible. The SEM images confirmed our assumptions on the faults of the profilometer measurements.

In the SEM images taken from the cut side of the samples noticeable compaction of the PDMS can be seen at the irradiated but originally stress-free areas. We found, that the rate of compaction does not depend strongly on the delivered fluence in the 400-1600 nC/mm<sup>2</sup> range. We found that the compaction is about 3-4  $\mu\text{m}$  ( $\sim 5\%$ ) in all cases. The measurements along the cut-surface of the sample where stress was developed have shown noticeable swellings of 15-20  $\mu\text{m}$  heights.

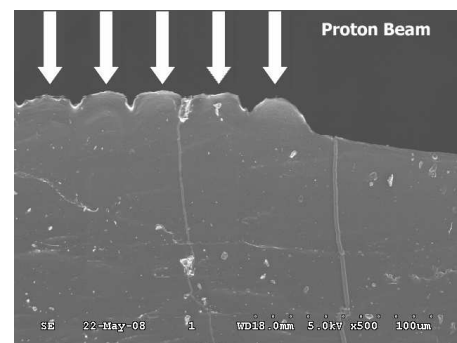


**Figure 1.** SEM image of another PDMS sample from the direction of the surface at a different magnification. Significant swelling can be observed at the irradiated pattern perpendicular to the surface.

### *Acknowledgements*

The support of the Hungarian National Research Found (OTKA) via grants A080, M041939, M36324; and EU co-funded Economic Competitiveness Operative Programme (GVOP-3.2.1.-2004-04-0402/3.0) is gratefully acknowledged.

- a) Uni. Debrecen, Dept. of Solid State Physics, H-4010 Debrecen, P.O. Box 2, Hungary

## 8.8 First Experiments on a Microreactor Created by Proton Microbeam

*R. Huszánk, S. Z. Szilasi, K. Vad and I. Rajta*

Microreactors are innovative and promising tools in technology nowadays because of their advantages compared to the conventional-scale reactors. These advantages include vast improvements in surface to volume ratio, energy efficiency, reaction speed and yield, and increased control of reaction conditions, to name a few examples.

In this work we present the design of a prototype micro-electrochemical cell of  $1.5 \mu\text{L}$  volume ( $2.5 \times 2.5 \times 0.240 \text{ mm}$ ) created with a 3 MeV proton microbeam. We deposited gold electrodes on the bottom and top sides of the chamber. The cell can be separated into two half-cells with a suitable membrane applicable to galvanic or fuel cells as well. We used a polycapillary film (also made by PBW ourselves) to separate the two half-cells, hindering the mixing of the anolyte and catholyte solutions. Fig. 1. shows the 3D model of the designed structure. Fig. 2. shows the assembled microreactor with the attached pipes.

Measuring a detectable current driven between the two electrodes in this micro-electrochemical cell containing a simple electrolyte solution demonstrates an operating device. As a result of the minimal mixing caused by the polycapillary film, this cell design can be suitable for electro-synthesis. At 1 V potential the measured current was about  $150\text{-}200 \mu\text{A}$ , at 2 V it was about  $250\text{-}400 \mu\text{A}$ . After charging the cell with direct current for a while, it was found to act as a micro battery due to the changes of the starting concentration of the NaOH electrolyte and the formation of products in the anolyte and catholyte solutions. After five minutes of charging with 1 V, the measured voltage potential of electrodes was about 20 mV for a few minutes with slowly decreasing current.

Due to the micromachining technique's high resolution, further reduction of the dimensions of this kind of microreactor is also planned.

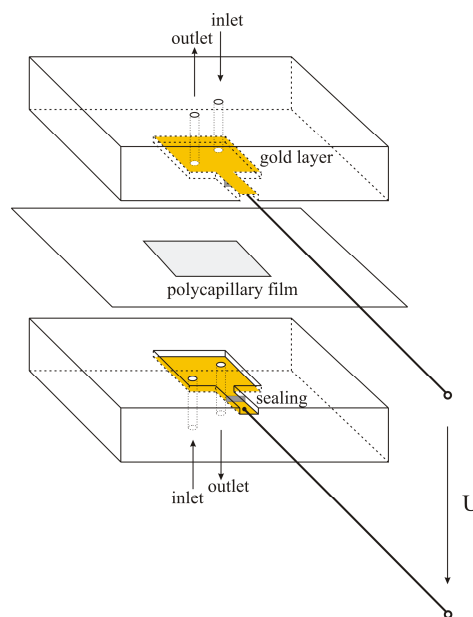


**Figure 1.** Assembly scheme of the microreactor with the polycapillary film and the two chambers containing deposited gold electrodes.

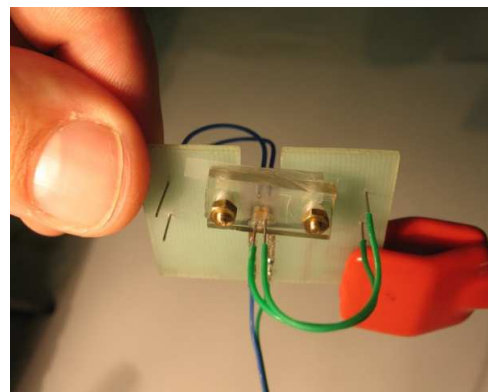


**Figure 2.** The assembled microreactor.

### *Acknowledgements*

The technical assistance of the Van de Graaff accelerator operating staff at HAS ATOMKI is gratefully acknowledged. The work was supported by the EU co-funded Economic Competitiveness Operative Programme (GVOP-3.2.1.-2004-04-0402/3.0).

## 8.9 Si Micro-turbine by Proton Beam Writing and Porous Silicon Micromachining

*I. Rajta, S. Z. Szilasi, P. Fürjes<sup>a)</sup>, Z. Fekete<sup>b)</sup> and Cs. Dűcső<sup>a)</sup>*

A 3D Si micro-turbine characterized by high aspect ratio vertical walls was formed by the combination of proton beam writing (PBW) and subsequent selective porous Si (PS) etching. Crystal damages generated by the implanted protons result in increased resistivity, thereby limit or even prevent the current to flow through the implanted area during electrochemical etching.

Characteristic feature of the proposed process is that the shape of the micro electro-mechanical (MEMS) components is defined by two implantation energies. A higher energy is applied for defining the housing of the device while the lower energy is used to write the moving components. The implantation energies were selected such as to result appropriate difference between the two projected ranges, thereby providing structures with different height after development. The thickness of the walls of the moving component and the isotropic etching profile of the electrochemical PS formation was also taken into consideration. The electrochemical etching is driven until the sacrificial PS layer completely underetches the moving components, but the etch-front does not reach the bottom of the housing. Therefore, the dissolution of PS results in a ready-to-operate device with a released moving component embedded in the cavity of the housing.

The operation of the encapsulated device fabricated by the two-energy implantation is successfully demonstrated (Fig. 1). Rotation speed of the device is estimated in the range of thousands rpm, however, further analysis of the novel structure optimized for performance and MEMS compatible assembly will be done and precise characteristics will be determined by adequate optical read-out method.

The feasibility of Proton Beam Writing combined with Porous Si Micromachining and conventional Si processing steps was successfully demonstrated by fabricating Si micro-turbine chip. The aligned, two-energy pro-

ton beam implantation can provide high aspect ratio, completely or partially released microelements embedded in a cavity or a channel, thereby enabling us to form mobile components in the microfluidic MEMS. Although the process opens a new way in micromachining, the widening of the implanted regions around the projected range limits the dimensions and the geometry of the processed devices. The described technique can be exploited in fabrication of various MEMS with embedded mobile elements.

This work is the first demonstration of a silicon device containing a moving part made by proton beam writing.

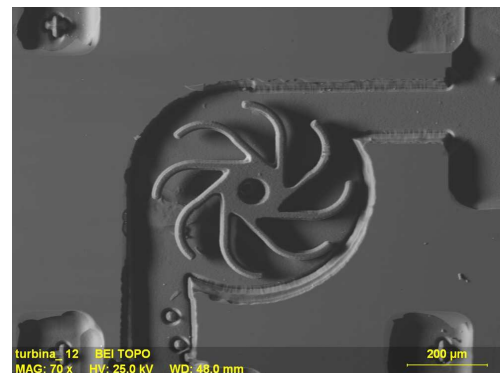


**Figure 1.** The processed micro-turbine chip with still rotor (the video showing the movement of the rotor can be seen at <http://iba.atomki.hu/video/>).

### *Acknowledgements*

The support of the Hungarian National Research Found (OTKA) via grants T047002, A080, M041939, M36324 and F042474; and EU co-funded Economic Competitiveness Operative Programme (GVOP-3.2.1.-2004-04-0402/3.0) is gratefully acknowledged. The authors also thank the contribution of Dr. A.L. Tóth with SEM analysis and Mr. B. Forgács with design and fabrication of plastic encapsulation of the microturbine chip.

- a) Res. Inst. for Techn. Phys. and Mat. Sci. - MFA, H-1525 Budapest P.O. Box 49, Hungary
- b) Budapest Uni. of Techn. and Econ., Budafoki st.8., H-1111 Budapest, Hungary

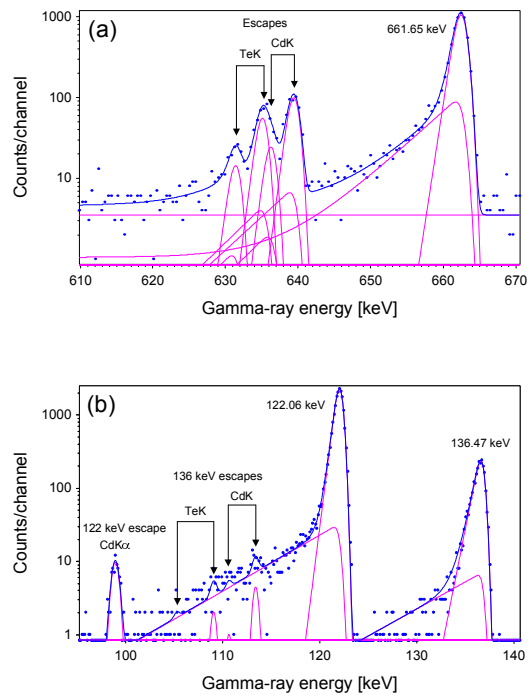
## 8.10 Analog and digital pulse shape discrimination of planar CdTe detector signals

*T. Papp\**, *G. Kalinka*, *J. Gál*

Compound semiconductors have high detection efficiency for higher energy photons, but suffer from poor collection efficiency, especially for holes. Since in common planar detectors the contribution of electrons and holes to the induced signal are equal, impaired performance is expected if all signals are processed. There are techniques whereby the contribution of the holes are reduced: (i) unipolar charge sensing: only signals induced by electrons are picked up in the detector by appropriately designed electrode system, or (ii) pulse shape discrimination: selecting only electron induced signals later in the signal processing system, (iii) combining (i) and (ii). Unipolar sensing includes the application of the small pixel effect, coplanar anodes, Frisch grid, hemispherical cathode, drift-strips [1]. Signal pulse shape discrimination distinguishes and then either simple rejects or “restores”, as well, signals with recognizable contribution due to slow holes. Since simple rejection causes drop of efficiency, sophisticated methods for restoration (or correction) has been developed.

This latter aim was beyond the scope of the present work, where we simply tested the discrimination capability of our analog and digital systems. The detector used was a  $3 \times 3 \times 1$  mm<sup>2</sup> diode type CdTe (produced by ACRO-RAD) operated at -20 °C and 400 V. The analog system included a NE-805 Pulse Shape Discriminator (ATOMKI),[2] based on leading edge CFD. A Cs-137 gamma-spectrum acquired with the narrowest time-pass window of 2.5 ns resulted in a tenfold peak to Compton ratio, and a fivefold, 10.5 to 1.97 keV FWHM improvement with 90 % rejection ratio. This resolution is close to the best result ever reported (1.5 keV), [3], achieved with a smaller and much better quality detector. Note that a Fano factor value of 0.1 would mean 1.28 keV contribution at that energy. The photopeak together with the well resolved CdK and TeK escape peaks can be seen in Fig.a. Very similar results were obtained with a CSX4

digital signal processor (Cambridge Scientific, Canada),[4], where the discrimination criteria are: noise, rise time, pulse shape and pile up. Its performance is illustrated here for Co-57. The corresponding photopeak region is shown in Fig.b. Despite a 350 eV electronic noise contribution the 700 eV FWHM at 122 keV is also among the best ones ever achieved with CdTe detectors. Although much better quality spectra can be achieved applying stringent criteria for rejection, here a compromise was made using the least but justified rejections only. It is clear from the figures, that electron trapping remaining after the removal of hole trapping, still causes significant tailing at these energies.



\* T.P. acknowledges support from the Marie Curie International Reintegration Grant within the 7th European Community Framework Programme.

- [1] Z. He, NIMA **463** (2001) 250, and references therein
- [2] J. Gál, Thesis, Debrecen University, 1976
- [3] V. I. Ivanov *et al.*, IEEE Trans. Nucl. Sci. **NS-45** (1998) 390
- [4] T. Papp *et al.*, Anal. Sci. **21** (2005) 737

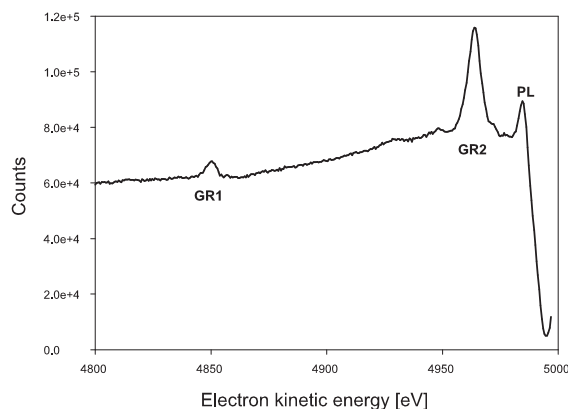
## 8.11 From the crystal structure to the light emission properties of GSO and LSO scintillators

*T. Papp\*, Zs. Jánosfalvi, G. Kalinka, J. Molnár, M. Novák, A. Orbán, J. Tóth and D. Varga*

Recently developed scintillators like GSO and LSO will be an important scintillators for positron emission tomography (PET) scanners in the future [1]. Various crystal production methods of LSO have yielded inconsistencies in both decay time and light output [2]. To optimize the consistency of decay time and light output, several crystal modification and standardization approaches have been developed. One of them, the heat treatment in oxygen atmosphere, is reported to improve the performance. We have started an ambitious project to quantify the crystals via the detailed study of the energy transport processes, and the energy level diagrams. The methods we have used are the high energy REELS (Reflection Electron Energy Loss Spectroscopy) and XPS. They are ideally suited to determine the band gap, the niveau level energies and the energy and magnitude of the intrinsic trapping sites. Beside the properties of the band gap and energy level structure, our interest is focused on the significance of collective excitations, and their role in the energy transport processes. The observed collective excitations already indicate the need to rethink the details of the energy transport processes. We have made a large set of measurements on GSO, LSO and LYSO crystals, pristine and heat treated in oxygen atmosphere. We have measured the REELS spectra of them, and fabricated scintillation detectors [3] then measured the scintillation detector spectra and light yields. A 5 keV REELS spectrum of a GSO sample measured at high energy resolution [4] is displayed in the Figure. Giant resonance peaks, GR1 and GR2, at 149 and 35 eV, and the plasmon peak at 14 eV energy losses, respectively, are indicated in the spectrum.

The effect of the treatment was very forthcoming in the REELS spectra. We are making theoretical calculations to derive the REELS spectra. Varying the crystal structure we intend to match the calculated to the measured REELS spectra and niveau energies. After

specifying the crystal structure, an ab initio calculation is made using WIEN2K code [5] for determining the dielectric functions of rare-earth orthosilicates. From the calculated dielectric function the REELS spectra can be derived and compared with the experimental ones. Therefore based on the trial failure method, we can determine the possible crystal structures based on the agreement with the experimental data. The greater challenge is to extend the method for actinides based scintillators, where the collective excitation is expected even more significant, and versatile.



\* T.P. acknowledges support from the Marie Curie International Reintegration Grant within the 7th European Community Framework Programme.

- [1] J. S. Karp, *Eur. J. Nucl. Med.* **29**(2002)1525
- [2] C. L. Melcher, M. Schmand, M. Eriksson, L. Eriksson, M. Casey, R. Nutt, J. L. Lefaucheur, B. Chai, *IEEE Transactions on Nuclear Science*, **47**(2000)965
- [3] J. Imrek, Gy. Hegyesi, G. Kalinka, J. Molnár, D. Novák, I. Valastyán, J. Végh, L. Balkay, M. Emri, S. Kis, L. Trón, T. Bükki, Z. Szabó, A. Kerek, *IEEE Nuclear Science Symposium Conference Record* 5(2006)3037
- [4] L. Kövér, D. Varga, I. Cserny, J. Tóth, K. Tőkési, *Surface and Interface Analysis* **19** (1992)9
- [5] P. Blaha, K. Schwarz, G. Madsen, D. Kvasnicka, J. Luitz: *WIEN2K An Augmented Plane Wave Plus Local Orbital Program for Calculating Crystal Properties*, November 2001, Technische Universität Wien, <http://www.wien2k.at/>

## 8.12 A new generation of PET scanners for small animal studies

*G. Hegyesi, J. Imrek, G. Kalinka, J. Molnár, D. Novák, I. Valastyán, L. Balkay<sup>a)</sup>, M. Emri<sup>a)</sup>, S. Kis<sup>a)</sup>, L. Trón<sup>a)</sup>, I. Bagaméri<sup>b)</sup>, Z. Szabó<sup>c)</sup> and A. Kerek<sup>d)</sup>*

Research on small animal PET scanners has been a hot topic in recent years. These devices are used in the preclinical phases of drug tests and during the development of new radiopharmaceuticals. They also provide a cost efficient way to test new materials, new design concepts and new technologies that later can be used to build more efficient human medical imaging devices. The development of a PET scanner requires expertise on different fields, therefore a consortium was formed that brought together Hungarian academic and industrial partners: the Nuclear Research Institute (which has experience in the development of nuclear detectors and data acquisition systems), the PET Center of the University of Debrecen (which has clinical experience in the application of nuclear imaging devices and background in image processing software), Mediso Ltd. (which has been developing, manufacturing, selling and servicing medical imaging devices since 1990) and other academic partners. This consortium has been working together since 2003: the knowledge base acquired during the development of our small animal PET scanners (miniPET-I and miniPET-II) is now being utilized to build a commercial multimodal human PET scanner.

The operation of a PET scanner is based on the simultaneous detection ("coincidence") of two gamma photons originating from a positron annihilation. In traditional PET scanners coincidence is detected by a central unit during the measurement. In our system there is no such central module: all detected single gamma events are recorded (list mode data acquisition), and the list of events are processed using a computer cluster (built from PCs). The usage of independent detector modules and commercial components reduce both development and maintenance costs. Also, this mode of data acquisition is more suitable for development purposes, since once the data is collected and stored it can be used many times

to test different signal processing algorithms, or the same method with different parameters.

The miniPET-II small animal PET scanner consists of 12 independent detector modules. The inner diameter of the scanner is 206 mm. On each module there is a segmented scintillator block (35 x 35 crystals of 1.27 mm x 1.27 mm x 12 mm) coupled to a Hamamatsu H9500 position sensitive photomultiplier tube (PSPMT) which detects the incoming gamma photons. The timing, energy and position signals of the PSPMT are digitized by four channel ADC running at 50 MHz, and analyzed by a Digital Signal Processing (DSP) block. The DSP block and a "System-on-Module" embedded system are implemented in a Field Programmable Gate Array (FPGA, Virtex-4 FX12) based small piggyback card. The System-on-Module runs a custom embedded Linux operating system. This Linux provides a convenient platform for application development, debugging and for system integration. The collected data are sent to the computing cluster for further processing via a gigabit Ethernet link. The miniPET-II detector module can also be used independently from the PET scanner as a general purpose physics measurement device.

- a) University Medical School of Debrecen, PET Center, University of Debrecen, Debrecen, Hungary
  - b) MEDISO Ltd, Budapest, Hungary
  - c) Institute of Experimental Physics, University of Debrecen, Debrecen, Hungary
  - d) Royal Institute of Technology, Stockholm, Sweden
- [1] J. Imrek, Gy. Hegyesi, G. Kalinka, J. Molnár, D. Novák, I. Valastyán, J. Végh, L. Balkay, M. Emri, S. Kis, L. Trón, T. Bükki, Z. Szabó, A. Kerek: Development of an improved detector module for miniPET - II., IEEE Nuclear Science Symposium Conference Record 5(2006)3037
- [2] Hamamatsu H9500 PSPMT data sheet available online:  
[http://www.sales.hamamatsu.com/assets/pdf/parts\\_H/H9500\\_H9500-03\\_TPMH1309E01.pdf](http://www.sales.hamamatsu.com/assets/pdf/parts_H/H9500_H9500-03_TPMH1309E01.pdf)

## 8.13 A little sonochemistry again

*I. Török*

In 2005 I realized that our director-founder Prof. A. Szalay really was a forerunner of sonochemistry with his first internationally published paper: Die Zerstörung von hoch polymeren Molekülen mittels Ultraschallwellen [1]. I published my findings in Hungarian [2] and in a shorter form in English [3].

Later I studied the second work of Szalay: Intesitätsbestimmungen zur Erklärung der depolymerisierende Wirkung der Ultraschallwellen [4]. In this paper Szalay tried to find the mechanism of the chemical effect of ultrasound. He found, that the energy of oscillation is not enough to split the chemical bonds. He calculated the energy obtained by water, as he worked with aqueous solutions. Then he thought, that may be, the polymer molecules, many orders larger than the water molecule, can get enough energy, but there was not proof. Anyhow it is seen, that he started to find the mechanism of the chemical effect of the ultrasound. It is sorrowful, that because the lack of foundations, they abandoned the subject [5]. Perhaps, if they could continue the work, they could reach to the mechanism of cavitation, which now is regarded to be the searched mechanism, and become the founder-fathers of the sonochemistry, instead of to be only a forerunner.

### *References*

- [1] A. Szalay, Zeitschr. f. phys. Chem. A **164** (1933) 234.
- [2] Török I., Természet Világa **138** (2007) 172.
- [3] I. Török, Annual Report of ATOMKI 2006 (2007) 10.
- [4] A. Szalay, Physikalische Zeitschr. **35** (1934) 293.
- [5] A. Szent-Györgyi, Nature **131** (1933) 278.

## 9.1 International conference on radiation damage in biomolecular systems

*K. Tókési and B. Sulik*

The 5th international conference on Radiation Damage in Biomolecular Systems (RADAM08) was held in Debrecen, Hungary, on June 13-15 2008. The conference was jointly organized by the Institute of Nuclear Research of the Hungarian Academy of Sciences (ATOMKI) Debrecen, the University of

Debrecen, Centre of Arts, Humanities and Sciences, and Faculty of Medicine. The conference focused on a detailed understanding of the fundamental interaction processes initiated by the deposition of various types of radiation in biological material.



**Figure 1.** Conference photo.

The main topics of the program were: electrons and biomolecular interactions, ions and biomolecular interactions, radiation in physiological environments, theoretical developments for radiation damage, track structures in cells.

The conference program included 28 talks (invited and contributed) in 10 sessions and 23 poster presentations. 26 papers have been accepted and published in the conference proceedings [1]. The meeting brought together 67 registered participants from 14 countries.

The organizers express their thanks for the support of the sponsors of the conference: European Science Foundation within the framework of the Activity: Electron Induced Processing at the Molecular Level, the Hungarian National Office for Research and Technology, the Hungarian Academy of Sciences, and the Program of Apponyi Albert.

[1] AIP Conference Proceedings, 1080, Eds: K. Tókési and B. Sulik (2008)

## 9.2 International conference on elementary processes in atomic systems

*K. Tórkési and L. Nagy<sup>a)</sup>*

The 4th Conference on Elementary Processes in Atomic Systems (CEPAS08) was held in Cluj-Napoca, Romania, on June 18-20, 2008. The conference was jointly organized by the Faculty of Physics of the Babeş-Bolyai University and the Institute of Nuclear Research of the Hungarian Academy of Sciences

(ATOMKI) Debrecen, Hungary. The conference focused on all aspects of processes and phenomena stimulated by interactions of electrons, positrons, ions, atoms, molecules, photons and other constituents of matter with gaseous, liquid, and condensed matter at low and intermediate energy.



**Figure 1.** Conference photo.

The main topics of the program were: kinematically complex investigations, investigation of charged particle interaction with nano-, micro-, and macro- capillaries, interferences in electron emission, interaction of intense laser pulses with matter, investigation of surfaces and nanostructures, experiments with biomolecules, exotic particle collisions, status report of the Stored Particles Atomic Physics Research Collaboration (SPARC).

The conference program included 35 talks (invited and contributed) and 87 poster presentations in two sessions. 68 papers have been

accepted and published in the conference proceedings [1]. The meeting brought together 107 registered participants from 21 countries.

The organizers express their thanks for the support of the sponsors of the conference: Ministry of Education, Research and Youth, Romania, Babeş-Bolyai University, Cluj-Napoca, European Physical Society.

a) Babeş-Bolyai University, Faculty of Physics, 400084 Cluj-Napoca, str. Kogălniceanu nr. 1, Romania

[1] Nucl. Instr. and Meth. Phys. Res. B. Volume 267, Issue 2, Pages 181-456 (January 2009).

### 9.3 Organization of ICNMTA2008

*I. Rajta, Á.Z. Kiss, A. Simon, Zs. Kertész, Z. Szikszai,  
I. Uzonyi, S.Z. Szilasi, R. Huszánk, Z. Szoboszlai,  
A. Angyal, L. Csedreki, G.A.B. Gál, I. Major*

The 11<sup>th</sup> International Conference on Nuclear Microprobe Technology and Applications & 3<sup>rd</sup> International Workshop on Proton Beam Writing [1] have been organized by HAS-ATOMKI in co-operation with the International Atomic Energy Agency. The conference took place in Debrecen, Hungary between 20-25 July 2008.

Authors presented their original and unpublished work in the following areas in microbeam technology: microprobe facilities, beam optics, analytical and imaging techniques, quantitative analysis, beam effects, proton beam writing and modification, complementary techniques; and a wide range of applications in: materials science, microelectronics, biology, medicine and botany, earth and planetary sciences, art and archaeology, environmental sciences.

In addition to *PBW* two other workshops have been organized: *3D tomography* and *Software & Database*. These workshops proved to be extremely useful places for discussion.

The number of participants was 142, they represented 26 countries from all over the world. There were 4 review, 7 invited, 4 technical invited, 36 contributed talks and 2 poster sessions with 94 posters. 90 manuscripts have been submitted to the conference proceedings, which will be published by Elsevier as a special issue of Nuclear Instruments and Methods B.

We feel honored to have hosted many old friends as well as first-time visitors. We are hoping that the event we organized will be memorable to many participants.

#### *Acknowledgements*

We are grateful for the sponsors: HAS-ATOMKI, International Atomic Energy Agency (IAEA), High Voltage Engineering, National Electrostatics Corp., Oxford Microbeams Ltd., ORTEC, Spektrum Mérés-technika Kft., National Instruments, NKTH (Mecenatúra), MTA, Paksi Atomerőmű Zrt., Spektrum-3D Kft., Carl Zeiss Technika Kft., DKV Zrt., Molcomp System Kft.

[1] <http://icnmta.atomki.hu/>



**Figure 1.** The official group photo of the participants

## 9.4 Report on the 4th Conference on Environmental Science of the Carpathian Basin

*Á.Z. Kiss*

The main organizers of the conference were the Faculty of Science and Technology of the University of Debrecen and the Sapientia - Hungarian University of Transylvania, Faculty of Science and Art, Cluj-Napoca, Romania (the proposer of this series of conferences). The Institute of Nuclear Research of the Hungarian Academy of Sciences (ATOMKI) took part in the organization as its Hertelendi Ede Environmental Research Laboratory and the Ion Beam Application Laboratory are engaged in the study of the environment of the Carpathian Basin. Moreover the Department of Environmental Physics, run jointly by the University of Debrecen and ATOMKI, plays an important role in teaching environmental physics at the university.

The conference was held on 28-29 March, 2008, in the building of the Regional Committee of the Hungarian Academy of Sciences (HAS) in Debrecen.

The aim of the conference was to bring together scientists and students from different countries, involved in various aspects of environmental science and technology, since the common environmental problems of the Carpathian Basin to be solved make necessary the cooperation between them, living and working in different parts of the basin. The conference gave an opportunity to show the lat-

est results in these fields, and in the same time it was an occasion for the young scientists to be introduced and to exchange experience. The scientific sections were the followings: environmental science and education, environmental chemistry, environmental physics, environmental geography, environmental protection and environmental technology, environmental biology and nature protection, landscape ecology and urban ecology [1].

The number of registered participants (161) was the largest since the beginning (2005) of the conference series. They arrived from five countries (Hungary, Rumania, Slovakia, Croatia and Serbia), several institutions from 27 towns of the Carpathian Basin. The number of oral talks was 110, and the posters presented were close to 40. The conference proceedings contains 126 papers and the participants obtained the two volumes at the beginning of the conference [2]. A selected part of the talks was published after the conference in ref. [3]. The official languages of the conference were Hungarian and English.

The conference was sponsored by the Ministry of Environment and Water, Budapest, the Regional Committee of the HAS in Debrecen and the Centre of Arts, Humanities and Sciences of the University of Debrecen.

[1] <http://geo.science.unideb.hu/taj/page/kornykonf2008.html>

[2] IV. Kárpát-medencei Környezettudományi Konferencia, Debrecen, Ed.: Z. Orosz, et al. REXPO Kft., 2008, Vol. **I.-II.** (in Hungarian with abstracts in English).

[3] Presentations of the 4th Carpathian Basin Conference on Environmental Sciences, Ed.: G. Lakatos, *Acta Pericemonologica Debrecenina*, **3** (2009) 1- 194.

## 10.1 Events

### **29th Physicist Days**

3-7 March 2008

### **KKK-2008** 4th Carpathian-basin Environmental Science Conference

28-29 March 2008

### **4th Hungarian SPM Meeting**

11 April 2008

### **3rd Workshop** on Strengthening of regional R&D collaborations between Hungary and Ukraine

18-20 May 2008

### **RADAM 2008** Conference on Radiation Damage in Biomolecular Systems

13-15 June 2008

### **CEPAS 2008** 4th Conference on Elementary Processes in Atomic Systems

18-20 June 2008

### **ICNMTA 2008** 11th International Conference on Nuclear Microprobe Technology and Applications

20-25 July 2008

### **JVC-12 / EVC-10 / AMDVG-7** Joint Vacuum Conference

22-26 September 2008

### **Researchers' Night**

26 September 2008

### **Physicist Students' Weekend**

10-12 October 2008

### **Science on Stage**

23-26 October 2008

### **Hungarian Science Celebration 2008**

3-7 November 2008

### **Young Entrepreneur's Week**

17-23 November 2008

### **Dénes Berényi 80:** Meeting of the Section of Physical Sciences of the HAS in honour of Dénes Berényi academician's 80th birthday

26 November 2008

### **Synchrotron and Free Electron Laser Radiation Applications School**

26-27 November 2008

## 10.2 Hebdomadal Seminars

January 17

Dark matter, the dominant substance of the Universe  
T. Fényes

January 25

First physics at LHC  
L. Dobrzynski (*Laboratoire Leprince-Ringuet, Palaiseau, IN2P3*)

January 31

Charged particle induced reactions and the astrophysical p-process  
N. Özkan and R.T. Güray (*Kocaeli University, Kocaeli, Turkey*)

February 22

Recent results of the PHENIX experiment at RHIC: fluidity of the quark-gluon plasma  
T. Csörgő (*Research Institute for Particle and Nuclear Physics /RMKI/, Budapest*)

March 13

Beyond the Born-Oppenheimer approximation: the role of degenerate states  
in processes of molecular dynamics and photo physics  
Á. Vibók (*University of Debrecen*)

March 18

Experimental study of the hyperdeformation of nuclei in the actinide region  
M. Csatlós

March 20

Photonic nanoarchitectures of biological origin: what can we learn of it  
L.P. Bíró (*Research Institute for Technical Physics and Materials Sciences /MFA/, Budapest*)

March 27

Plans of research and development at the Debrecen isotope separator  
M. Hunyadi

April 3

Vibrating mirrors at the border of quantum and classical  
T. Geszti (*Eötvös Loránd University, Budapest*)

April 17

Development of neutronanalytical methods  
R. Dóczy

April 24

State of affairs  
M. Pálinkás, Zs. Fülöp

May 8

Correlation measurements in heavy ion collisions with particles of large transversal momentum  
G. Veres (*Eötvös Loránd University, Budapest*)

May 15

Elliptical fluidity and the fluctuations of excentricity in heavy ion collisions  
G. Veres (*Eötvös Loránd University, Budapest*)

May 22

Nuclear energy renaissance and globalization  
J. Rónagy (*Hungarian Atomic Energy Authority, Budapest*)

- May 29  
 Future of particle physics in Europe  
 R-D. Heuer (*Research Director of DESY*)
- June 5  
 Landau, the mysterious  
 Gy. Radnai (*Eötvös Loránd University, Budapest*)
- June 9  
 Ion beam analytical study of the properties and effects of atmospheric aerosol  
 Zs. Kertész
- June 12  
 Layer preparation from laser induced carbon plasma in vacuum, hydrogen and metan  
 J. Budai (*University of Szeged*)
- June 24  
 Determination of the electron states of the valence-shell of MoS<sub>2</sub>  
 Zs. Jánosfalvi
- June 26  
 Multi-cluster decays of the actinide nuclei  
 D. Kamanin (*JINR, Dubna*)
- September 11  
 A new type electrostatic analyzer of large viewing angle  
 L. Tóth
- September 25  
 Nuclei far from the stability line; perspectives of international research  
 T. Fényes
- November 6  
 Cooperation in systems with many participants  
 A. Szolnoki (*Research Institute for Technical Physics and Materials Sciences /MFA/, Budapest*)
- November 7  
 Inclusive jet production cross section measurement in photon-photon collisions  
 at OPAL and muon trigger efficiency measurements at ATLAS  
 A. Krasznahorkay Jr.
- November 13  
 Introduction of new colleagues in Atomki  
 O. Bak, R. Bartók, G. Gál, R. Janovics, Z. Köllő, I. Kuti, L. Papp, R. Rác, G. Tóth
- December 4  
 Collective excitations in atoms, detector materials and biological tissues  
 T. Papp
- December 17  
 In the wake of the lost symmetry - the Nobel prize 2008 in Physics  
 Z. Trócsányi

### 10.3 Awards

Dénes Berényi

Commander's Cross Order of Merit of the Republic of Hungary

Doctor Honoris Causa Babeş-Bolyai University, Cluj-Napoca, Romania

Kálmán Szily Memorial Award

Honorary Medal of the University of Debrecen

The Smithsonian Astrophysical Observatory named the (5694)3051 P-L Minor Planet "Berényi"

Sándor Biri

Visiting Researcher Toyo University, Japan (until 2013)

János Gál

HAS-ATOMKI Sándor Szalay Award

Beáta Király

HAS-ATOMKI Young Scientist Award

István Rajta

Roland Eötvös Physical Society: Imre Bródy Award

László Sarkadi

Member of the European Academy

Béla Sulik

HAS Section of Physical Sciences: Physics Prize

Fellow of the American Physical Society

Károly Tőkési

Roland Eötvös Physical Society: Sándor Szalay Award

Zoltán Trócsányi

Roland Eötvös Physical Society: György Marx Award

László Végh

Roland Eötvös Physical Society: Prometheus Award

## 10.4 List of Publications

The list of the Institute's publications can be found on-line at:

<http://www.atomki.hu/p2/years/yea02008.htm>

## Author index

- Achouri N.L., 21  
Aleksandrov A.A., 24  
Aleksandrova I.A., 24  
Algora A., 23  
Ander I., 61  
Andersen H.H., 30, 31  
Angélique J.C., 21  
Angyal A., 57, 76  
Aoi N., 19  
Arbó D.G., 27, 28, 29  
Aumayr F., 42, 43  
Azaiez F., 20, 21
- Bagaméri I., 72  
Balkay L., 72  
Bartha L., 62  
Batist L., 23  
Beke D.L., 49, 50  
Bényei A., 59  
Belleguic M., 20, 21  
Bereczky R.J., 42–45  
Bernabeu J., 23  
Biri S., 34, 39, 63  
Bódog M., 48  
Borbély S., 26, 27  
Borbély-Kiss I., 1, 56  
Borcea C., 20, 21  
Bourgeois C., 20, 21  
Braun M., 66  
Brown B.A., 20, 21  
Bučar K., 32  
Burgdörfer J., 45–47  
Burkard K., 23
- Cano D., 23  
Charlton M., 30, 31  
Chesnel J.-Y., 37  
Csatlós M., 24  
Csedreki L., 76  
Cserháti C., 53, 67  
Cserny I., 36  
Csige L., 24  
Csik A., 48–50, 67
- Daróczi L., 50, 53  
Das S., 44  
Dassanayake B.S., 44  
de Châtel P.F., 41  
Dimitrov M., 58  
Ditrói F., 61  
Dlouhy Z., 20, 21  
Dombrádi Zs., 19–21  
Donzaud C., 21  
Döring J., 23  
Duprat J., 21
- Elekes Z., 19–22  
Emri M., 72  
Erdélyi Z., 49  
Erdélyi G., 50  
Estevez M.E., 23  
Eszenyi T., 59
- Farkas J., 22  
Fekete Z., 69  
Frémont F., 37  
Frigeri C., 49  
Fülöp Zs., 18–20, 22  
Futó I., 64, 65  
Fürjes P., 69
- Gadea A., 23  
Gál G.A.B., 76  
Gál J., 70  
Gierlik M., 23  
Grévy S., 20, 21  
Guillemaud-Mueller D., 20, 21  
Gulyás J., 24  
Gulyás L., 33  
Gyürky Gy., 17, 18, 22
- Hajaji A., 37  
Hakl J., 41, 48  
Hegyesi G., 72  
Hunniford C.A., 30, 31  
Huszánk R., 1, 60, 67, 68, 76  
Hüller W., 23

Ibrahim F., 20, 21  
 Ichioka T., 30, 31  
 Imao H., 30, 31  
 Imrek J., 72  
 Iván I., 39

Jánosfalvi Zs., 36, 71  
 Janovics R., 66  
 Juhász Z., 37, 39

Kalinka G., 70–72  
 Kamanin D.V., 24  
 Katona G.L., 50  
 Kavčič M., 32  
 Kerek A., 20, 72  
 Keresztessy K., 60  
 Kertész Zs., 1, 54, 56, 57, 76  
 Kirchner R., 23  
 Kis S., 72  
 Kis-Varga M., 48, 59  
 Kiss Á.Z., 1, 53, 54, 76, 77  
 Kiss G.G., 18, 22  
 Knudsen H., 30, 31  
 Koltay E., 1, 56  
 Kondratyev N.A., 24  
 Kormány Z., 61  
 Kovács I., 60  
 Kovács P., 61  
 Kowarik G., 42, 43  
 Kövér L., 36  
 Krasznahorkay A., 20, 24  
 Kristiansen H.-P.E., 30, 31  
 Kruppa A.T., 25  
 Kuroda N., 30, 31  
 Kuznyecova E.A., 24

Lakatos A., 50  
 Langer G.A., 48–50  
 Leenhardt S., 21  
 Lemell C., 45–47  
 Lévai G., 15, 16  
 Lewitowicz M., 20, 21  
 Lopez-Jimenez M.J., 21  
 Lukyanov S.M., 20, 21

Major I., 65, 76  
 Major Z., 51

Mandal S., 20  
 Mátéfi-Tempfli M., 39  
 Mátéfi-Tempfli S., 39  
 McCullough R.W., 30, 31  
 Mészáros S., 41, 48  
 Miraglia J.E., 28, 29  
 Mittag W., 21  
 Moller S.P., 30, 31  
 Molnár J., 71, 72  
 Molnár M., 52, 64–66  
 Motobayashi T., 19  
 Mrazek J., 20, 21  
 Mukha I., 23

Nacher E., 23  
 Nagata Y., 30, 31  
 Nagy L., 26, 27, 75  
 Nagy T., 64  
 Nándori I., 41  
 Naqvi F., 24  
 Negoita F., 20, 21  
 Nemcsics A., 49  
 Novák D., 72  
 Novák M., 45, 71

Orbán A., 35, 71

Palásthy B., 32  
 Palcsu L., 51, 52  
 Pálincás J., 39  
 Pallinger Á., 48  
 Papp L., 51  
 Papp T., 70, 71  
 Paripás B., 32  
 Pelicon P., 53  
 Penionskhevitch Y., 20, 21  
 Plettner C., 23  
 Podolyak Zs., 20, 21  
 Porquet M.G., 21  
 Pougheon F., 21  
 Pyatkov Yu.V., 24

Rác R., 34, 63  
 Rajta I., 1, 67–69, 76  
 Rauscher T., 18  
 Rinyu L., 64  
 Roeckl E., 23

Roussel-Chomaz P., 20, 21  
 Rózsa P., 53  
 Rubio B., 23

Saint-Laurent M.G., 20, 21  
 Sakurai H., 19  
 Salamon P., 25  
 Sarkadi L., 35  
 Sarkadi-Pribóczki É., 58  
 Savajols H., 20, 21  
 Schiessl G., 45  
 Schiessl K., 46  
 Serényi M., 49  
 Simčič J., 53  
 Simon A., 1, 18, 49, 54, 60, 76  
 Sletten G., 20, 21  
 Sobolev Y., 21  
 Sohler D., 20, 21  
 Solleder B., 47  
 Somogyi I., 66  
 Somorjai E., 18, 22  
 Sorlin O., 20, 21  
 Stanoiu M., 20, 21  
 Stefánka Zs., 66  
 Stodel C., 21  
 Sulik B., 33, 37, 39, 74  
 Svingor É., 64–66  
 Szöőr Gy., 53  
 Szűcs I., 61  
 Szabó Gy., 1  
 Szabó Z., 72  
 Szikszai Z., 1, 56, 57, 76  
 Szilágyi E., 60  
 Szilasi S.Z., 1, 67–69, 76  
 Szoboszlai Z., 1, 54, 56, 57, 76

Tain J.L., 23  
 Takács E., 34, 39

Tanis J.A., 44  
 Tárkányi F., 61  
 Thomsen H.D., 30, 31  
 Timár J., 20, 21  
 Timis C., 20  
 Tomka G., 54  
 Torii H.A., 30, 31  
 Tornyi T., 24  
 Tóth J., 50, 71  
 Tőkési K., 26, 27, 28–33, 39, 42–44,  
 45, 46, 47, 74, 75  
 Török I., 73  
 Trón L., 72  
 Tsoncheva T., 58

Uggerhoj U.I., 30, 31  
 Uzonyi I., 1, 53, 54, 76

Vad K., 41, 48, 50, 68  
 Valastyán I., 72  
 Valiente J.J., 23  
 Varga D., 45, 71  
 Varsányi I., 52  
 Veres M., 64–66  
 Vertse T., 25  
 Vikor Gy., 39

Yalçın C., 22  
 Yamamoto A., 20  
 Yamazaki Y., 30, 31

Zhuchko V.E., 24  
 Zouros T.J.M., 33  
 Žitnik M., 32